ON

SPECTRA AND COLOURS

OF

SYNTHETIC STELLAR POPULATIONS

Inaugural Thesis

for the Laureateship
of Doctor of Philosophy
presented to the Faculty of Sciences
of the University of Basel

Erich Wenger

from Blumenstein BE

Basel

March 22, 2005

Approved by the Faculty of Sciences
on request of:

Prof. Dr. Roland Buser (Supervisor)
Prof. Dr. Bruno Binggeli
Prof. Dr. Eva Grebel

Basel
February 8, 2005

Prof. Dr. Hans-Jakob Wirz (Head of Faculty)

Abstract

We compiled a library of integrated properties of stellar populations called BLoIS (Basel Library of Integrated Spectra) with the help of evolutionary synthesis algorithms developed by Gustavo Bruzual and Stéphane Charlot, using the theoretical stellar spectral library called BaSeL, which was constructed by François Cuisinier, Thibault Lejeune, and Pieter Westera.

By building up BLoIS we were able to study the effects of the different input parameters on the integrated properties (mainly spectra and colours) of synthetic stellar populations. We find that the slope of the Initial Mass Function (IMF) produces the largest effects, followed by the SFR, and the mass range of the IMF. Different stellar evolutionary tracks and different spectral libraries have only moderate effects.

The analysis of BLoIS showed that all population spectra and most of the population colours are unique, because the metallicity characterizes the spectra in a unique way. Comparisons amongst model populations confirmed that the IMF affects the integrated spectra and colours in the most sensitive way.

Furthermore, there is no absolute degeneracy between age and metallicity in BLoIS, but certain combinations of these parameters can lead to similar spectra and colours. However, we can confirm that these similarities are more pronounced at older ages and we can state that the degree of similarity depends on the position in the age-metallicity plane.

As a theoretical application we developed a least-squares algorithm to derive subpopulations from a composed population spectrum. In the framework of model populations this algorithm is able to recover the individual contributions of subpopulations to the total spectrum.

To put constraints on observations we developed Monte Carlo simulation programmes. Using those we found that the observations of old populations must be more accurate than observations of young populations in order to achive the same confidence level in recovering the correct population.

Contents

1 **Introduction** 1

2 **Evolutionary Synthesis** 3
- 2.1 Stellar Evolutionary Tracks . . . 3
- 2.2 Stellar Spectral Libraries . . . 5
- 2.3 Initial Mass Function (IMF) . . . 7
- 2.4 Star Formation Rate (SFR) . . . 8
- 2.5 Age-Metallicity Relation (AMR) . . . 9
- 2.6 Synthesis Algorithm . . . 9

3 **The Basel Library of Integrated Spectra BLoIS** 15
- 3.1 Simple Stellar Populations (SSPs) . . . 15
  - 3.1.1 Initial Mass Function (IMF) . . . 16
  - 3.1.2 Stellar Evolutionary Tracks . . . 30
  - 3.1.3 Stellar Spectral Libraries . . . 34
  - 3.1.4 Consequences for BLoIS 1.1 . . . 41
- 3.2 Composite Stellar Populations (CSPs) . . . 41
  - 3.2.1 Constant SFR . . . 42
  - 3.2.2 Short Burst SFR . . . 42
  - 3.2.3 Linearly decreasing SFR . . . 44
  - 3.2.4 Exponentially decreasing SFR . . . 48
  - 3.2.5 Delayed SFR . . . 51
  - 3.2.6 Consequences for BLoIS 1.1 . . . 51
- 3.3 Samland-models . . . 54
- 3.4 File structure of BLoIS 1.1 . . . 54

4 **Fitting Methods** 59
- 4.1 Chi-Square Fitting . . . 59
- 4.2 Least-Squares Adjustment (LSA) . . . 63
- 4.3 Software . . . 66
  - 4.3.1 SPECFIT, SPECFITSIM, COLFIT, COLFITSIM . . . 66
  - 4.3.2 SPECLSA, COLLSA, SPECSUBPOP, COLSUBPOP . . . 75

5 **Results** 83
- 5.1 Characteristics of BLoIS 1.1 . . . 83
  - 5.1.1 Uniqueness . . . 84
  - 5.1.2 Sensitivity with respect to parameters . . . 87
- 5.2 Age-Metallicity Degeneracy (AMD) . . . 92
- 5.3 Deriving Subpopulations . . . 97

5.4 Monte Carlo Simulations 101

6 Summary, Conclusions, Outlook **111**

A Publications **115**
A.1 The Age of M3 115
A.2 BLoIS: The Basel Library of Integrated Spectra 121

GISSEL User Manual **125**

Bibliography **215**

Declaration **217**

Curriculum Vitae **219**

Acknowledgements **221**

List of Figures

2.1 Geneva tracks 4
2.2 Completed Geneva tracks 4
2.3 BaSeL spectra 6
2.4 Different IMFs 9
2.5 Sandage's SFRs 10
2.6 SFRs in GISSEL 10
2.7 AMR and SFR by Samland 11
2.8 Samland models 11
2.9 Principle of evolutionary synthesis 12
2.10 Convolution 14
2.11 SFRs of Subpopulations 14

3.1 Spectra for different IMF-slopes (low metallicity) 17
3.2 Colours for different IMF-slopes (low metallicity) 18
3.3 Spectra for different IMF-slopes (high metallicity) 19
3.4 Spectra for different upper IMF mass limits $\mathcal{M}_{\rm u}$ 22
3.5 Colours for different uppper IMF mass limits $\mathcal{M}_{\rm u}$ 23
3.6 Spectra for different lower IMF mass limits $\mathcal{M}_{\rm l}$ 24
3.7 Colours for different lower IMF mass limits $\mathcal{M}_{\rm l}$ 25
3.8 Spectra for different $\mathcal{M}_{\rm l}$ and $\mathcal{M}_{\rm u}$ 27
3.9 Culours for different $\mathcal{M}_{\rm l}$ and $\mathcal{M}_{\rm u}$ 28
3.10 Spectra for two segmented IMF 29
3.11 Spectra for bimodal IMF 31
3.12 Spectra for different tracks (high metallicity) 32
3.13 Colours for different tracks (high metallicity) 33
3.14 Spectra for different tracks (low metallicity) 35
3.15 Colours for different tracks (low metallicity) 36
3.16 Spectra for different stellar libraries (high metallicity) 37
3.17 Colours for different stellar libraries (high metallicity) 38
3.18 Spectra for different stellar libraries (low metallicity) 39
3.19 Colours for different stellar libraries (low metallicity) 40
3.20 Spectra for constant and short burst SFRs 43
3.21 Colours for constant and short burst SFRs 45
3.22 Spectra for linearly decreasing SFRs 46
3.23 Colours for linearly decreasing SFRs 47
3.24 Spectra for exponentially decreasing SFRs 49
3.25 Colours for exponentially decreasing SFRs 50
3.26 Spectra for delayed SFRs 52
3.27 Colours for delayed SFRs 53
3.28 Scd-model by Samland 55

3.29 Directory structure of BLoIS 56

4.1 Obervational situation 61
4.2 Flow chart of SPECFIT 68
4.3 Probability density function 70
4.4 Example of noised spectrum 71
4.5 Flow chart of COLFIT 73
4.6 Example of noised colours 74
4.7 Flow chart of SPECLSA 77
4.8 Contributions of subpopulations 79
4.9 Flow chart of SPECSUBPOP 80

5.1 Identical spectra 85
5.2 Identical colours 86
5.3 Important parameters for low resolution spectra 88
5.4 Important parameters for high resolution spectra 90
5.5 Important parameters for colours 91
5.6 Age-metallicity degeneracy (AMD) for spectra 93
5.7 χ^2-values for AMD 95
5.8 Example of AMD 95
5.9 AMD for colours 96
5.10 χ^2-values for AMD 97
5.11 Subpopulations 98
5.12 Recovery probabilities for SSP spectra 103
5.13 Recovery probabilities for SSP colours 104
5.14 Recovery probabilities for CSP spectra 104
5.15 Recovery probabilities for CSP colours 105
5.16 Recovery probabilities for low resolution spectra 106
5.17 Recovery probabilities for high resolution spectra 107
5.18 Recovery probabilities for colours 108

List of Tables

2.1 Evolutionary tracks in GISSEL 5
2.2 Stellar spectral libraries 7

3.1 Selection of filters in "bc03" 20
3.2 Properties of SSPs in BLoIS 1.1 41
3.3 Properties of CSPs in BLoIS 1.1 54

4.1 Programmes performing χ^2 fitting 75
4.2 Programmes performing least-squares adjustment 81

5.1 χ^2-fit for spectra 89
5.2 Sensitivity respecting parameters for spectra 92
5.3 Sensitivity respecting parameters for colours 92
5.4 Estimated AMD parameters for spectra 94
5.5 Estimated AMD parameters for colours 96
5.6 Derived subpopulations 100
5.7 Input for "evochem" 101
5.8 Derived subpopulations for "evochem" spectrum 102

1 Introduction

Research taught us that stars are born in groups and that stars live in groups. This lead to the concept of stellar populations, such as associations, open and globular clusters, population I and II stars, and the whole variety of galaxies. Since instrumental progress enormously improved the observations of stellar populations over the last decade, it's theory's turn to develop more refined models and more efficient methods for the analysis of stellar populations. This thesis is dedicated to synthetic stellar populations.

In the seventies of the last century astronomers (e.g., Spinrad & Taylor 1971; Faber 1972; O'Connell 1976; Turnrose 1976; Pritchet 1977) came up with the method of population synthesis, which composed the properties of stellar populations by building linear combinations of stellar properties. In a trial-and-error sense the models then were tested on the observations. Others (e.g., Renzini 1981; Renzini & Buzzoni 1983; Buzzoni 1990) used the fuel consumption theorem to put the models on a more physical basis. But it was Bruzual & Charlot 1993 who introduced evolutionary synthesis, which assumes stellar evolutionary tracks, a star formation rate, and an initial mass function to evolve the properties of stellar populations temporally. In addition, one needs empirical or theoretical stellar spectra. The latter are provided by BaSeL (Basel Spectral energy distribution Library) developed by our research group. The method of evolutionary synthesis is briefly explained in Chapter 2.

The first goal of this thesis consists in studying the effects of different parameters on the integrated properties (mainly spectra and colours) of synthetic stellar populations. As we can take advantage of the evolutionary synthesis code from Bruzual and Charlot the first step is to build up a library of these properties by using this code. The library should be as complete as possible but with as few redundancies as possible. Thus, its compilation goes along with the study of the different effects of the parameters on the integrated properties. The library is called "BLoIS", which stands for "Basel Library of Integrated Spectra", and is presented in Chapter 3.

The second goal of this thesis is the analysis of the theoretical library BLoIS, again focussing on integrated spectra and integrated colours. Apart from the uniqueness and the parameter sensitivity in the library we treat the age-metallicity degeneracy, derive subpopulations from composed model populations, and put constraints on observations by Monte Carlo simulations. To achieve this we have to develop different methods. Those methods along with the corresponding software are described in Chapter 4. The results and the conclusions are compiled in Chapter 5 and Chapter 6, respectively.

To define the scope of this thesis we would like to mention that building up a library of integrated properties of stellar populations by varying all the input parameters in a systematic way (as we have done for BLoIS) leads to primary applications that lie in the theoretical framework. Based on the results of this thesis one will be able to treat questions concerning the realism of these models.

2 Evolutionary Synthesis

The integrated light of a stellar population is composed of the contributions of the single stars. In the 1970's one tried to derive e.g. the integrated spectrum of galaxies by combining individual stellar spectra. This technique was called *population synthesis*. By trial and error, a weighted mix of stellar spectra of various types were calculated such as to obtain a model that fitted the observations the best. This method contained only a limited amount of physics and was far from producing unambiguous results.

In the 1980's one tried to overcome these inadequacies by the so-called *evolutionary synthesis*. In this approach, assumptions of stellar evolutionary tracks, Initial Mass Function, Star Formation Rate, and stellar spectra lead to the computation of an age-dependent integrated spectrum of a stellar model population.

In this chapter we shall briefly recapitulate the basics of evolutionary synthesis of stellar populations. The necessary ingredients as well as the principle of the method is presented.

It is to be mentioned that at the Astronomical Institute of the University of Basel we can take advantage of an evolutionary synthesis software package called GISSEL (Galaxy Isochrone Synthesis Spectral Evolution Library) developed by Prof. Dr. Gustavo A. Bruzual and Dr. Stéphane Charlot. This code is presented in a separate chapter called "GISSEL User Manual" after Appendix A.

2.1 Stellar Evolutionary Tracks

The first ingredients to evolutionary synthesis are the so-called evolutionary tracks. Based on evolutionary models of the stellar interior the basic goal is to describe the path of a star in the theoretical Hertzsprung-Russell-Diagramme (HRD) during its lifetime.

In **Figure 2.1** we give an example of a set of evolutionary tracks published by the Geneva group. At every grid point in the theoretical HRD a set of the following stellar properties is provided: chemical composition Z, effective temperature T_{eff} , mass $\mathcal{M}$, age t, and luminosity L. Apart from the Geneva group there are evolutionary tracks by the Padova and the Yale groups. For details see e.g. Schaller et al. 1992 (Geneva), Girardi et al. 1996 (Padova) or Kim et al. 2002 (Yale).

In the context of evolutionary synthesis (dealing with the calculation of integrated spectra up to ages of 20 Ga) the tracks have to be completed for post-AGB phases of the stars because they are not included in the original tracks. For details see Charlot & Bruzual 1991 or Bruzual 2003. In **Figure 2.2** we show the same Geneva tracks as in Figure 2.1

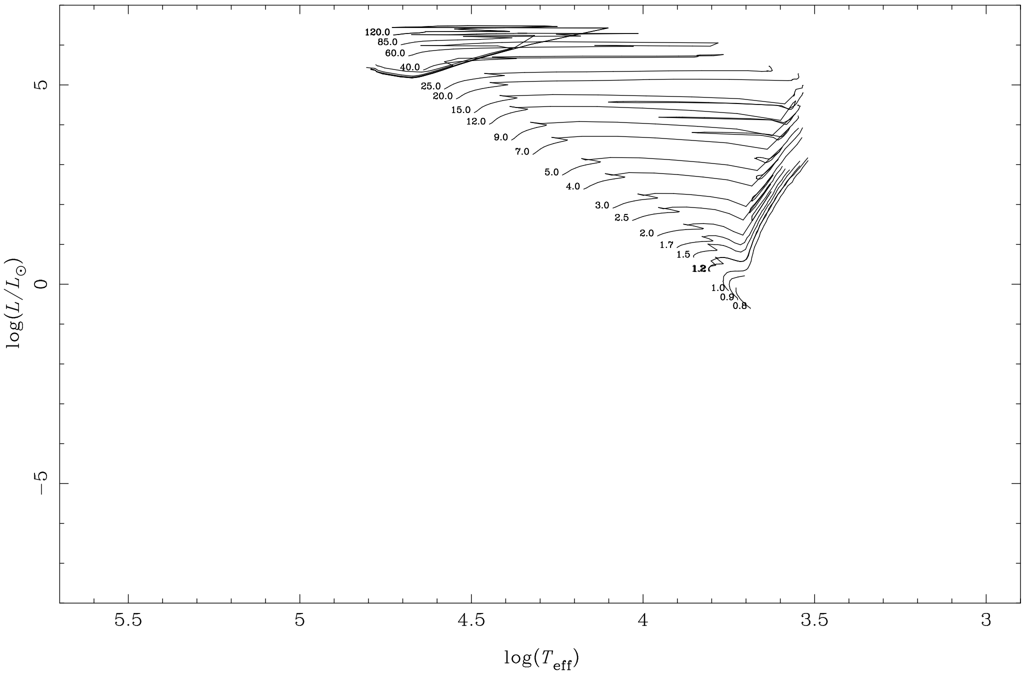

Figure 2.1: Stellar evolutionary tracks for different stellar masses published by the Geneva group

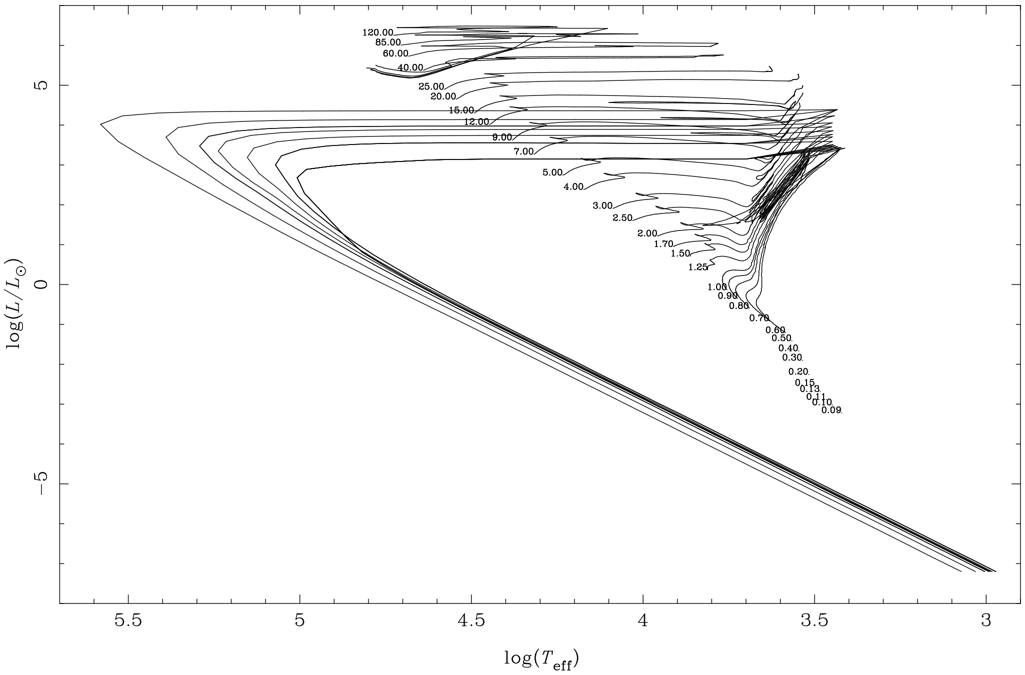

Figure 2.2: Geneva tracks as in Figure 2.1 but completed for post-AGB phases

Name	Z	**[Fe/H]**
Geneva 1992	0.02	0.1060
Padova 1994	0.0001	–2.2490
	0.0004	–1.6464
	0.004	–0.6329
	0.008	–0.3300
	0.02	0.0923
	0.05	0.5595
	0.1	1.0090
Padova 2000	0.0004	–1.6464
	0.001	–1.2486
	0.004	–0.6329
	0.008	–0.3300
	0.019	0.0660
	0.03	0.2883

Table 2.1: Different stellar evolutionary tracks implemented in the GISSEL code.

but this time completed with all the known stellar evolutionary phases.

As stellar evolutionary codes are far from being identical the tracks in **Table 2.1** are all implemented in the GISSEL code to allow for comparison (see Appendix C in the chapter "GISSEL User Manual").

2.2 Stellar Spectral Libraries

The second ingredients are the stellar spectra. Basically, they can either be observed or theoretical. For the latter there are several libraries compiled at the Astronomical Institute of the University of Basel. One example is shown in **Figure 2.3**. They are based on stellar atmosphere models and can be either purely theoretical or so-called semi-empirical if the models have been calibrated. For a general discussion on such libraries see Buser & Kurucz 1992. For details on the Basel libraries see Appendix A in chapter "GISSEL User Manual"; Lejeune 1997; Lejeune et al. 1997, 1998; Westera 2001; Westera et al. 2002.

Empirical libraries for their part can either stem from a single survey or can be compiled from different sources. Generally speaking the advantage of empirical spectra is their higher resolution whereas the theoretical spectra cover a larger parameter range. For the empirical libraries see e.g. Le Borgne et al. 2002 (STELIB) or Pickles 1998 (Pickles).

The libraries implemented in the GISSEL code are listed in **Table 2.2** along with their properties. As the two observational libraries cover a shorter wavelength range compared to the theoretical models, the former can be extended to shorter and longer wavelengths using the BaSeL 3.1 library. This allows for a consistent modelling of spectral properties.

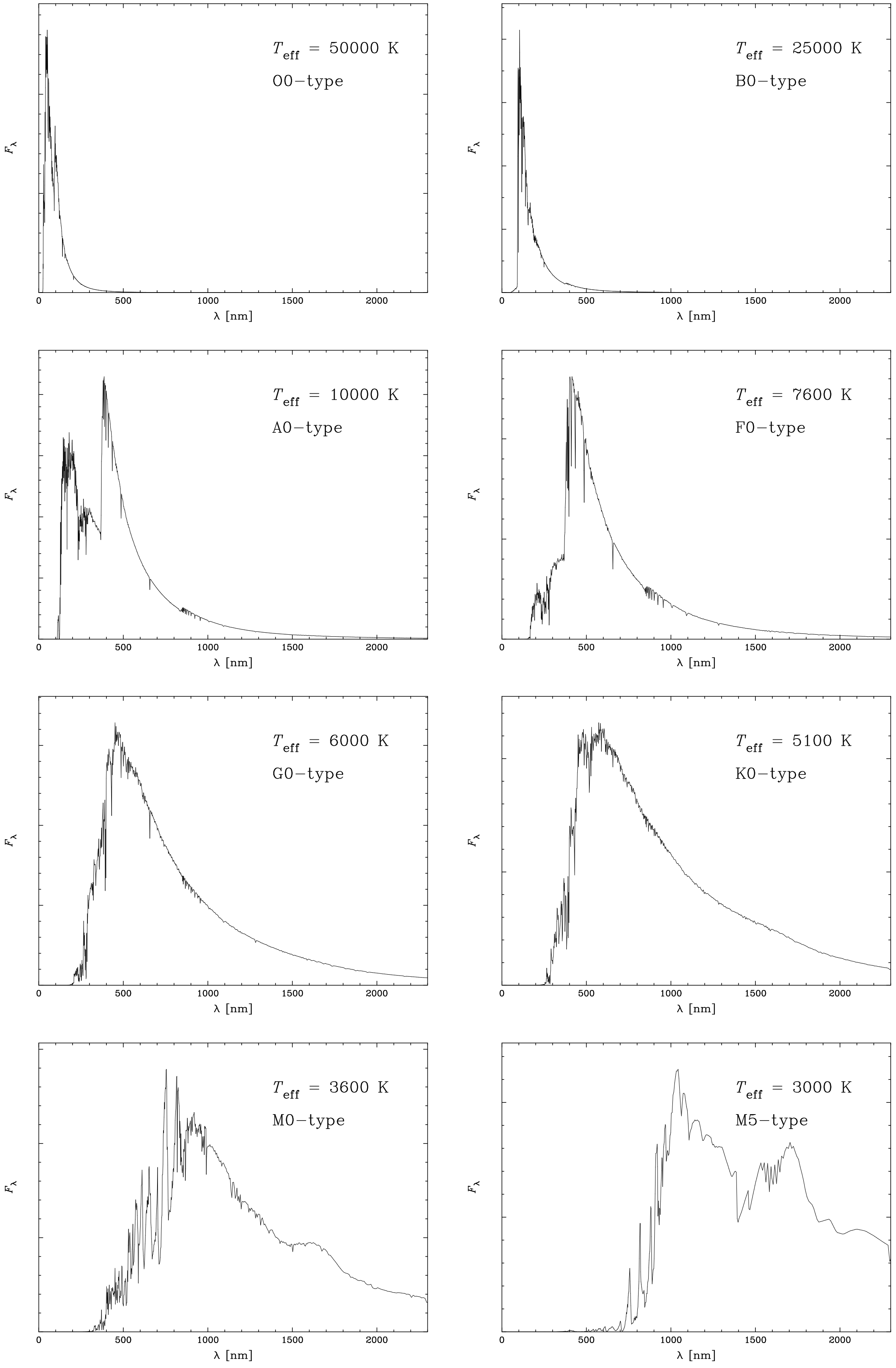

Figure 2.3: Stellar spectra for different $T_{\rm eff}$ from the Basel Spectral Energy Distribution Library BaSeL 3.1 (main sequence spectral types at $Z = Z_\odot$).

Name	**Type**	**λ-range** [nm]	**Res$_{\text{max}}$** [nm]	**# Fluxpoints**	**Met.-range** [$Z_\odot$]
BaSeL 1.0	theoret.	9.1 – 160 000	2.0	1 221	0.0001 – 10
BaSeL 2.2	semi-empir.	"	"	"	"
BaSeL 3.1	"	"	"	"	"
STELIB	observ.	320 – 950	0.3	6 900	0.01 – 3
Pickles	"	120.5 – 2 500	"	"	1

Table 2.2: Different stellar spectral libraries implemented in the GISSEL code

2.3 Initial Mass Function (IMF)

The IMF gives us the number of stars per mass interval at the birth of a stellar population. In principle it can be derived from the luminosity function LF and the mass-luminosity relation. We define the IMF $\xi(\mathcal{M})$ as:

$$dN = \xi(\mathcal{M})\, d(\ln \mathcal{M}) \tag{2.1}$$

where dN : number of stars in a logarithmic mass interval
$\mathcal{M}$: mass of stars (in $\mathcal{M}_\odot$)
$\xi(\mathcal{M})$: IMF

Thus, the total number of stars N_{tot} can be written as:

$$N_{\text{tot}} = \int \xi(\mathcal{M})\, d(\ln \mathcal{M}) = \int \frac{1}{\mathcal{M}}\, \xi(\mathcal{M})\, d(\mathcal{M}) \tag{2.2}$$

The total mass $\mathcal{M}_{\text{tot}}$ is calculated by:

$$\mathcal{M}_{\text{tot}} = \int \mathcal{M}\, \xi(\mathcal{M})\, d(\ln \mathcal{M}) = \int \xi(\mathcal{M})\, d(\mathcal{M}) \tag{2.3}$$

According to Salpeter 1955, the IMF can be written as follows:

$$\xi(\mathcal{M}) = c\, \mathcal{M}^{-x} \tag{2.4}$$

where c : constant

x : slope of IMF

Salpeter gives $c = 0.03$ and $x = 1.35$ as an approximation. Note that positive values for x result in negative slopes. This nomenclature is consistent with the one in the GISSEL code. The constant c can be used for the normalisation (total mass = 1 $\mathcal{M}_\odot$) of the IMF. It's calculated by the following equation, which gives us the total amount of mass $\mathcal{M}_{\mathrm{tot}}$ between the upper and the lower mass limits in a stellar population.

$$\mathcal{M}_{\mathrm{tot}} = \int_{\mathcal{M}_{\mathrm{l}}}^{\mathcal{M}_{\mathrm{u}}} c\,\mathcal{M}^{-x}\, d(\mathcal{M}) = 1\,\mathcal{M}_\odot \tag{2.5}$$

where $\mathcal{M}_{\mathrm{l}}$: lower mass limit of the IMF

$\mathcal{M}_{\mathrm{u}}$: upper mass limit of the IMF

This normalisation is used in the GISSEL code. All stellar populations calculated there are normalized to 1 $\mathcal{M}_\odot$.

The different IMF types available in the GISSEL code are presented in **Figure 2.4**. Here are the corresponding references: Chabrier 2001, Kroupa 2001 (universal and present day), Salpeter 1955, Scalo 1998, Scalo 1986, Miller and Scalo 1979, Kennicutt 1983, Lequeux 1979, Ferraro et al. 1997, Piotto et al. 1997. The characteristics of these IMFs are listed in Appendix D in the chapter "GISSEL User Manual".

Note that the IMFs are derived from different observed stellar populations as e.g. the solar neighbourhood or Globular Clusters. Furthermore, the slope of the IMF is $x = 2.35$ if we define dN in Equation 2.1 as the number of stars in a *linear* instead of a *logarithmic* mass interval, i.e., $dN = \xi(\mathcal{M})\, d\mathcal{M}$.

2.4 Star Formation Rate (SFR)

The SFR provides the amount of stars that are born at a certain age of a stellar population. In complex populations we can more generally speak of the so-called star formation history (SFH).

In **Figure 2.5** we reproduce the famous compilation of SFRs from Sandage 1986. Note that these SFRs are analytic functions that describe in a qualitative way the stellar birth activity of different galaxy types.

In **Figure 2.6** we show the different SFR types that are implemented in the GISSEL code. The corresponding analytic functions are explained in Section 3.2 below.

If we are interested in calculated SFHs we have to look for galaxy models as e.g. by Samland 2003 (see next section).

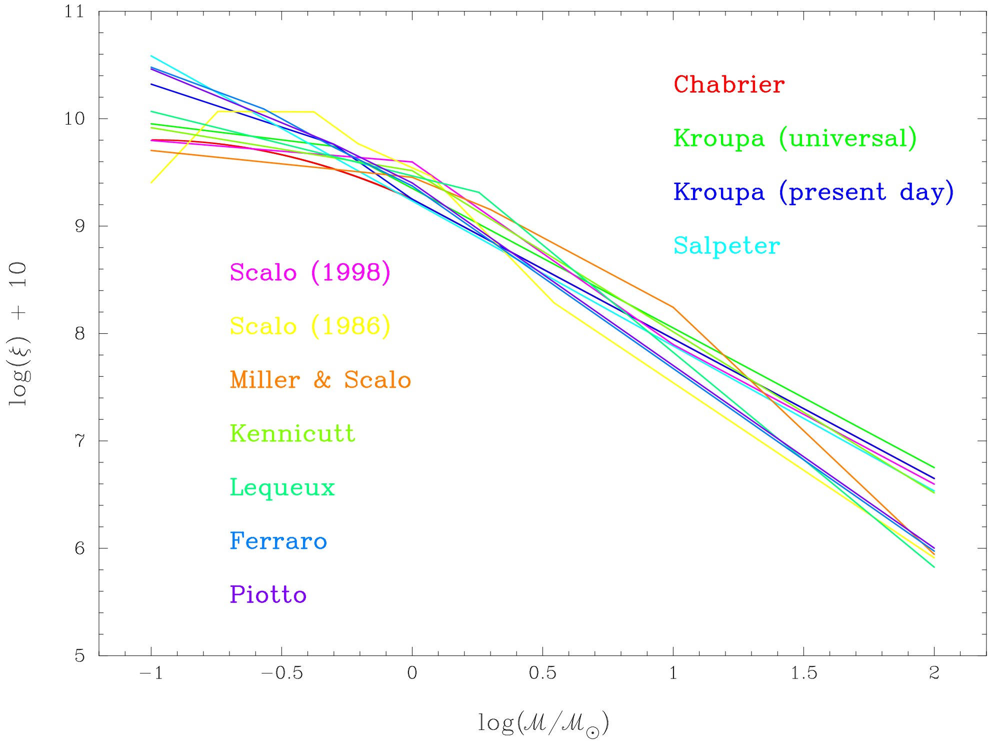

Figure 2.4: Different IMFs used in the GISSEL code (see Appendix D in chapter "GISSEL User Manual"). The IMFs are normalized to 1 $\mathcal{M}_\odot$.

2.5 Age-Metallicity Relation (AMR)

The last ingredient needed for evolutionary synthesis is the knowledge of the chemical evolution of a stellar population. Like the SFR we can simply assume analytic functions to describe this evolution. But for a more realistic description of the AMR chemical models have to be calculated.

One possibility is to use the chemo-dynamical galaxy models by Markus Samland. For details see Samland 2003. An example of such a model AMR is shown in **Figure 2.7**. In this particular case the stars of the galaxy are represented by 650 000 stellar particles which are evolved both dynamically and chemically. In **Figure 2.8** we can see the basic processes and interplays considered in these galaxy models.

2.6 Synthesis Algorithm

Evolutionary synthesis tries to calculate the properties of a model population along its temporal evolution. In **Figure 2.9** we explain the principles of evolutionary synthesis for the example of spectra. So the goal in this case is to derive the integrated spectra of a model population for a certain number of time steps. We start with the tracks providing Z, T_{eff} , $\mathcal{M}$, L, and t of the stars. If we join the points of equal ages in the theoretical HRD we get the so-called isochrones, one per time step. For each metallicity we can thus calculate a set of isochrones.

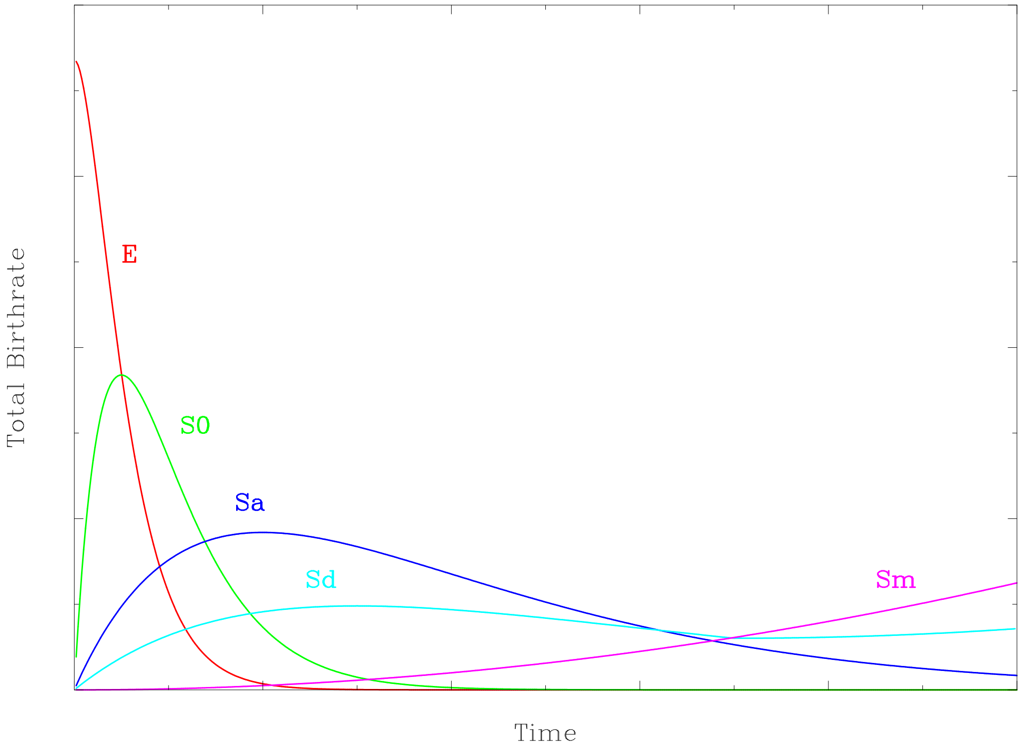

Figure 2.5: Total stellar birthrate in galaxies of different Hubble-types according to Sandage 1986.

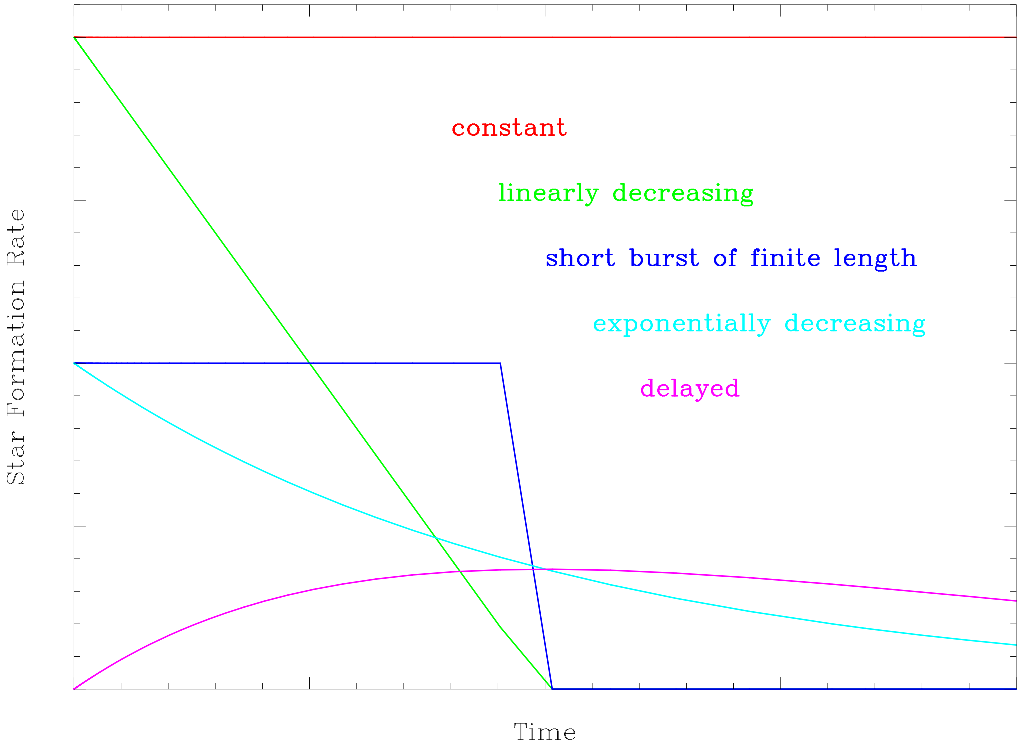

Figure 2.6: Different types of SFRs implemented in the GISSEL code (see Section 3.2)

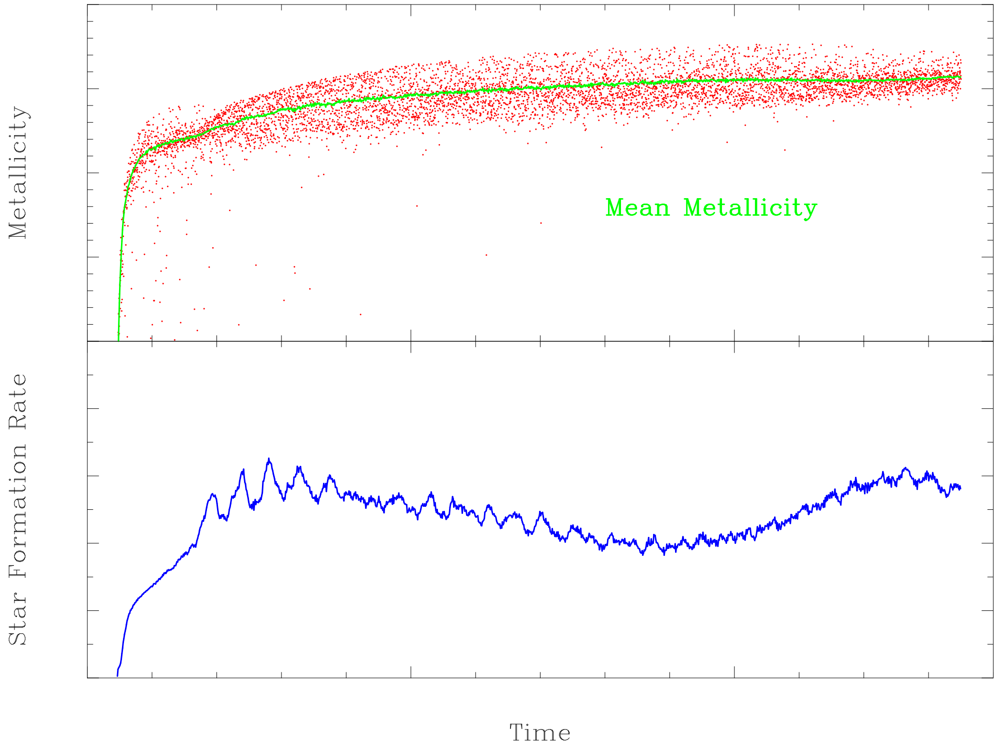

Figure 2.7: AMR and SFR calculated by chemo-dynamical galaxy models of Samland 2003.

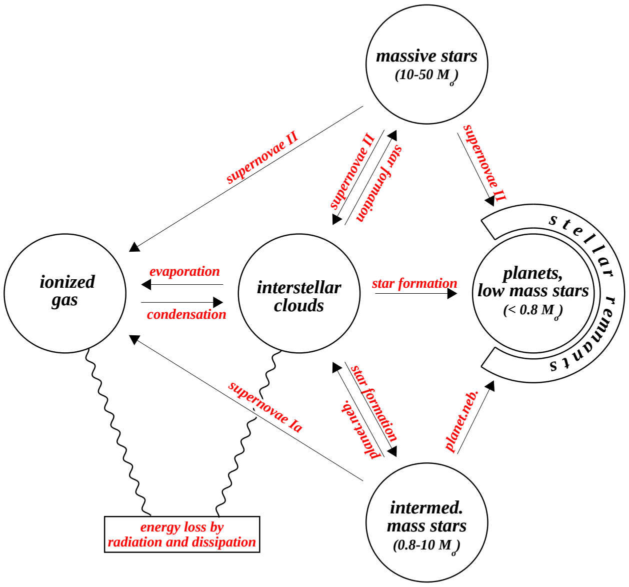
massive stars
(10-50 M☉)
supernovae II
supernovae II
star formation
supernovae II
ionized gas
evaporation
condensation
interstellar clouds
star formation
planets, low mass stars
(< 0.8 M☉)
stellar remnants
supernovae Ia
star formation
planet.neb.
planet.neb.
intermed. mass stars
(0.8-10 M☉)
energy loss by radiation and dissipation

Figure 2.8: Processes considered by the chemo-dynamical galaxy models of Samland 2003.

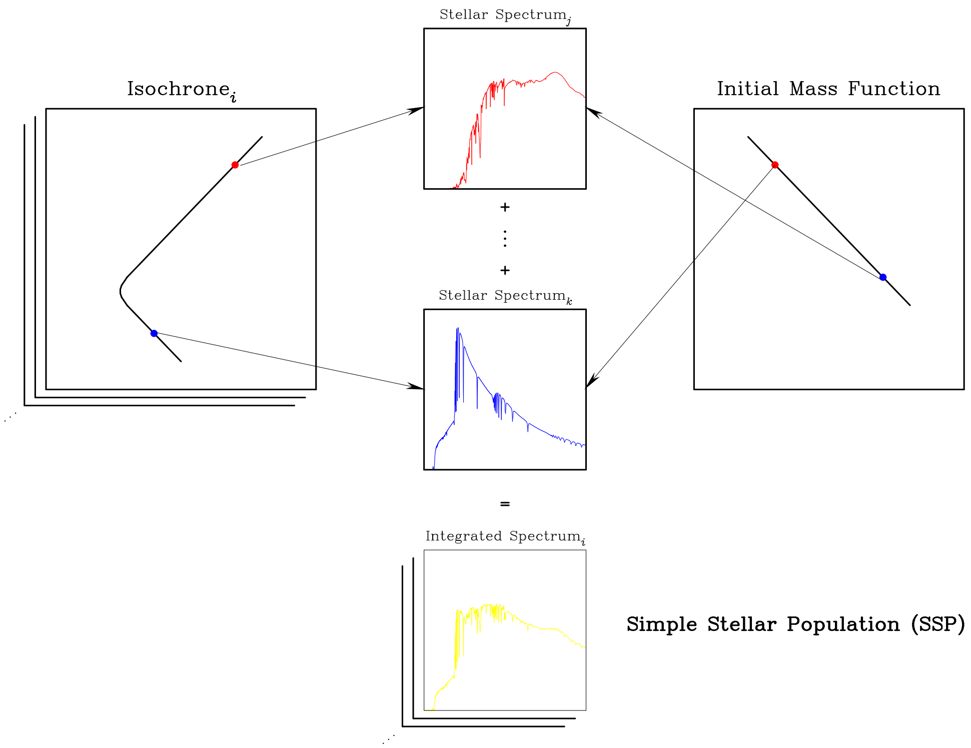

Figure 2.9: The principle of evolutionary synthesis

From each grid point in these isochrones we know the values for Z, T_{eff}, $\mathcal{M}$, and L. Z can be transformed to [Fe/H] and T_{eff}, $\mathcal{M}$, and L are used to derive $\log g$. With the triple ([Fe/H], T_{eff}, $\log g$) we can then search the library of stellar spectra in order to assign a proper spectrum to each of these grid points. This has to be done for each isochrone.

So we know what *type* of stars we have to consider. The IMF then tells us about their *number*. Assuming that the IMF is time independent, which is still a matter of debate, we can weight the different spectra. So we end up with building the sum of the mass-weighted stellar spectra for each isochrone which represent the integrated spectra of the model population at the time steps given by the isochrones. This set of integrated spectra is called a simple stellar population (SSP) because we assume that the star formation took place in an initial instantaneous burst; a so-called δ-burst.

The programme that performs this evolutionary synthesis is called "bc03" (see Section 3.1 in chapter "GISSEL User Manual"). Amongst others it calculates the following properties of a stellar population for 221 ages between 0 and 20 Ga:

- integrated spectra (of total - and partial populations)
- integrated colours (of total - and partial populations)
- bolometric magnitude
- absolute magnitudes in different passbands
- amplitude of the 912 Å (Lyman) discontinuity
- amplitude of the 4000 Å break

- mass to light ratio in different colour bands
- total mass in stars, gas and remnants
- star formation rate
- different spectral line indices
- supernova and planetary nebula birth rate
- number of black holes, neutron stars and white dwarfs
- percentage of the light in different colour bands
- isochrones in parameters and colours

If we want to take a different SFH into account we can select the spectra of an SSP and convolve them with a chosen SFR as follows:

$$F_{\mathrm{CSP}}\,(t) = \int_0^t \mathrm{SFR}\,(t-\tau)\,F_{\mathrm{SSP}}\,(\tau)\,d\tau \tag{2.6}$$

where $F_{\mathrm{CSP}}\,(t)$: integrated spectra of the CSP at time t
$\mathrm{SFR}\ (t-\tau)$: Star Formation Rate
$F_{\mathrm{SSP}}\,(\tau)$: integrated spectra of the SSP at age τ

If we convolve an SSP with an SFR in this manner we get a so-called composite stellar population (CSP). Schematically this procedure is shown in **Figure 2.10**. The programme that performs this convolution is called "csp" (see Section 4.1 in chapter "GISSEL User Manual").

Now if we'd like to consider the chemical evolution of the model population we first have to build several SSPs, each for a different metallicity. According to a given AMR we create individual SFRs for each metallicity as shown in **Figure 2.11**. Then we convolve these individual SFRs with the corresponding SSPs as described above, resulting in as many CSPs as we have metallicities. Now we take the first two CSPs and add them considering the different burst strengths calculated from a given over all SFR. This leads to a new CSP which can be added to the third CSP. We repeat this procedure until the last CSP is added and one single CSP is generated. Note that this procedure does not calculate the chemical evolution of a model population in a self consistent way. It just takes the SFR and the AMR as analytic input functions. The programme that performs this procedure is called "evochem" (see Section 4.3 in chapter "GISSEL User Manual").

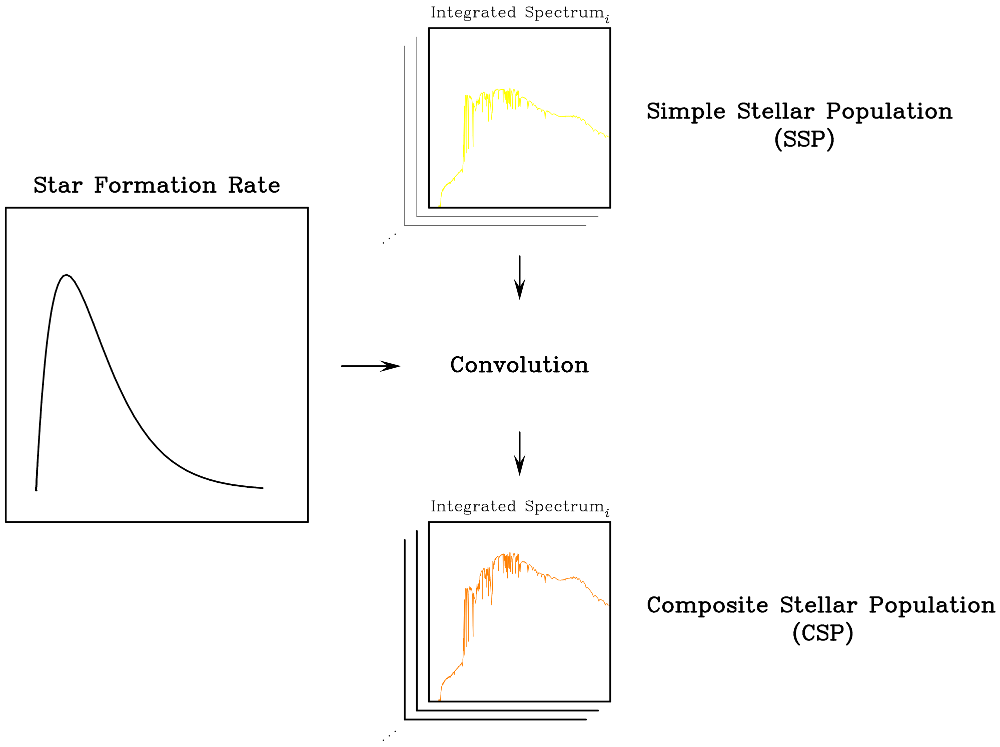
Integrated Spectrum$_i$
Simple Stellar Population
(SSP)
Star Formation Rate
Convolution
Integrated Spectrum$_i$
Composite Stellar Population
(CSP)

Figure 2.10: Convolution of an SSP with an SFR leading to a CSP

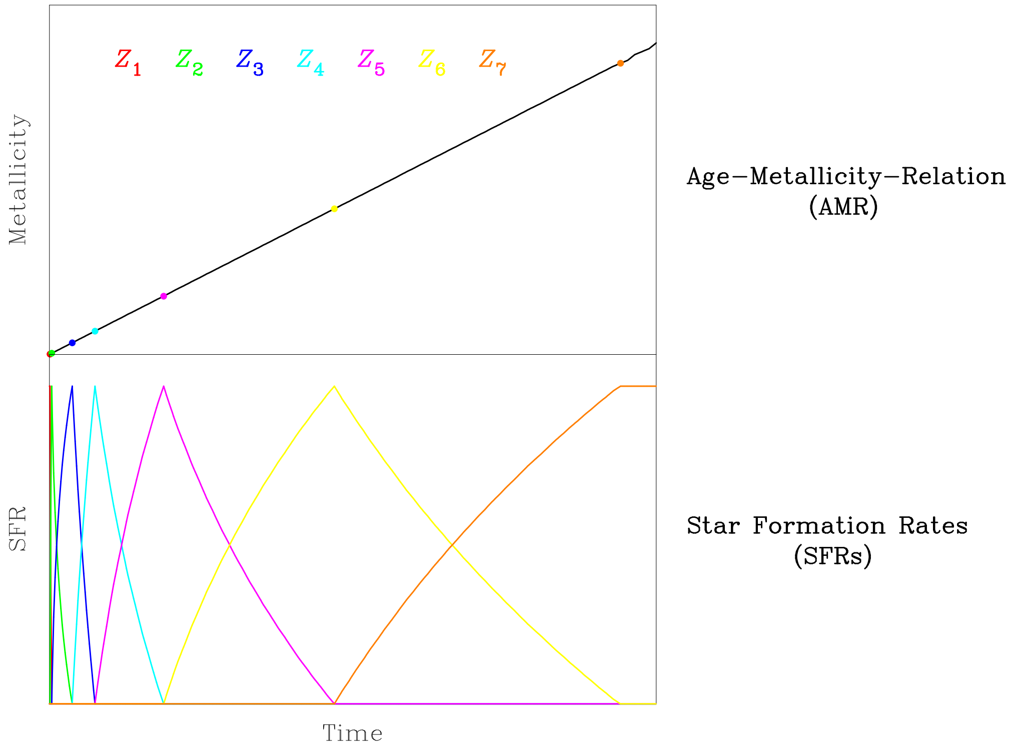

Figure 2.11: SFRs of subpopulations according to a given AMR

3 The Basel Library of Integrated Spectra BLoIS

One main output of evolutionary synthesis is the integrated spectrum of an evolved stellar population. In order to study the effects of the different input parameters (like IMF or SFR) on these integrated properties, to treat the Age-Metallicity degeneracy (AMD), to derive subpopulations from composed model populations, and to put constraints on observations by Monte Carlo simulations, we built up a library of integrated properties called BLoIS, which stands for Basel Library of Integrated Spectra. It does not only contain spectra but all the properties listed in Section 1.1 of the chapter "GISSEL User Manual".

On the one hand we'd like to make this library as complete as possible, i.e., we should consider every combination of input parameters to the evolutionary synthesis. On the other hand, we don't want to keep redundant data. So the aim is to reduce parameter space without losing information, thus to rule out those parameter ranges that have either no or only negligible effects on the spectra and the colours. Moreover, we can build certain spectra by combining or interpolating other spectra. This reduces the number of possible parameter combinations, too.

In the first section we show the effects of the different input parameters on Simple Stellar Populations (SSPs) and on Composite Stellar Populations (CSPs) in the second section. The third section is dedicated to an example of the chemo-dynamical galaxy models by Markus Samland and the last to the file structure of BLoIS.

3.1 Simple Stellar Populations (SSPs)

We have seen in Section 2.6 that an SSP is defined as a stellar population that built all its stars at the very beginning of its life in one single, instantaneous burst of star formation. The SFR is described as a so-called δ-burst. Then we assume that the population evolves passively, i.e., neither dynamical nor chemical evolution.

3.1.1 Initial Mass Function (IMF)

The IMF gives us the number of stars per mass interval at the birth of a stellar population (see Section 2.3).

Slope of the IMF

First of all we'd like to investigate the effects on the integrated spectra and the integrated colours caused by different slopes of the IMF. For this purpose we took the BaSeL 3.1 stellar spectral library and the Padova 2000 tracks at a metallicity of $Z = 0.0004$. We selected the maximum mass range of 0.1 to 100 $\mathcal{M}_\odot$ for the IMF and, according to the definition of the IMF in Equation 2.4, we chose the following slopes:

$$x \in \{0.0, 0.5, 1.0, 1.5, 2.0, 2.5, 3.0, 3.5, 4.0, 4.5, 5.0\}$$

The effects on the integrated spectra and their temporal evolution is shown in **Figure 3.1**. Note that these are rest-frame spectra. As the absolute flux values can differ up to seven orders of magnitude, we normalized them by dividing all flux values by the mean of all flux values (see Equation 4.25), in order to be able to compare the spectra. Besides, the letters in the upper part of each panel indicate the central wavelengths λ_c of the passbands that were used to calculate the synthetic colours (see below). Furthermore, the ages of the spectra are indicated in the panels in a.

The results show that there are four distinctive groups of slopes that have approximately the same effect on the integrated spectra: $\{0.0, 0.5, 1.0, 1.5, 2.0, 2.5, 3.0\}$, $\{3.5\}$, $\{4.0\}$, and $\{4.5, 5.0\}$. For clarity reasons we display only one spectrum of a representative of these groups. Note that the spectrum of the steep slopes do not show a significant temporal evolution. The reason for this is that at such high slope values red low luminosity stars – which evolve only very slowly – dominate the integrated light from the very beginning.

Now we'd like to know in which way the integrated colours of these very same populations are affected. To do so, we took advantage of the fact that the evolutionary synthesis code "bc03" can derive the colours by synthetic photometry (see Section 3.1 in chapter "GISSEL User Manual") using the filters listed in **Table 3.1**. Note that this is only a selection of filters (for the full list see Appendix F in chapter "GISSEL User Manual") and in principle, it is possible to choose any known photometric system.

The integrated colours of the spectra in Figure 3.1 are shown in **Figure 3.2**. Note that these are rest-frame colours. We can confirm two of the conclusions we drew for the integrated spectra, i.e., (a), there are some minor changes between slopes from 0.0 to 2.0 and (b), steep slope populations don't evolve much. For steeper slopes however, the integrated colours can differ as much as 1 mag, depending on the colour and on the age of the population. We'd like to mention the trend that steeper slopes lead to redder colours and the over-all trend of most of the colours turning red during the temporal evolution of the populations. There are exceptions to the latter statement: the distinctive uprise towards bluer colours between 4 and 6 Ma and the sudden decrease towards redder colours at around 100 Ma (for some colours only). The former is due to hot O- and B-stars developing a maximum in luminosity at 100 nm and the latter to the sudden decrease of the 4 000 Å break at 100 Ma.

For comparison the same investigation has been executed at a high metallicity $Z = 0.03$. The result is shown in **Figure 3.3**. Comparing Figures 3.1 and 3.3, there are no qualitative

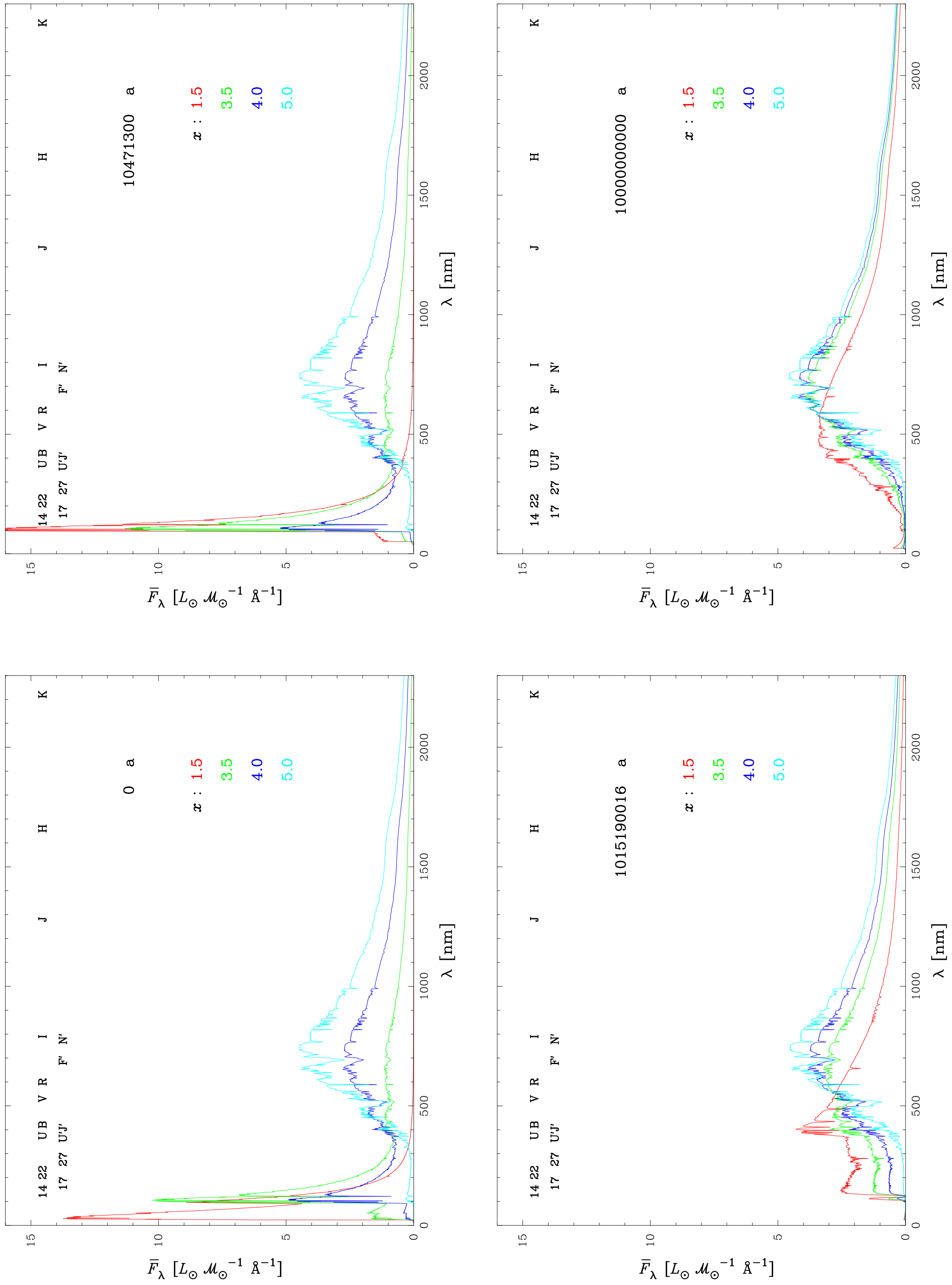

Figure 3.1: Temporal evolution of normalized integrated spectra calculated for different IMF-slopes x at $Z = 0.0004$ (Padova 2000 tracks, BaSeL 3.1 stellar library). Corresponding colours in Figure 3.2.

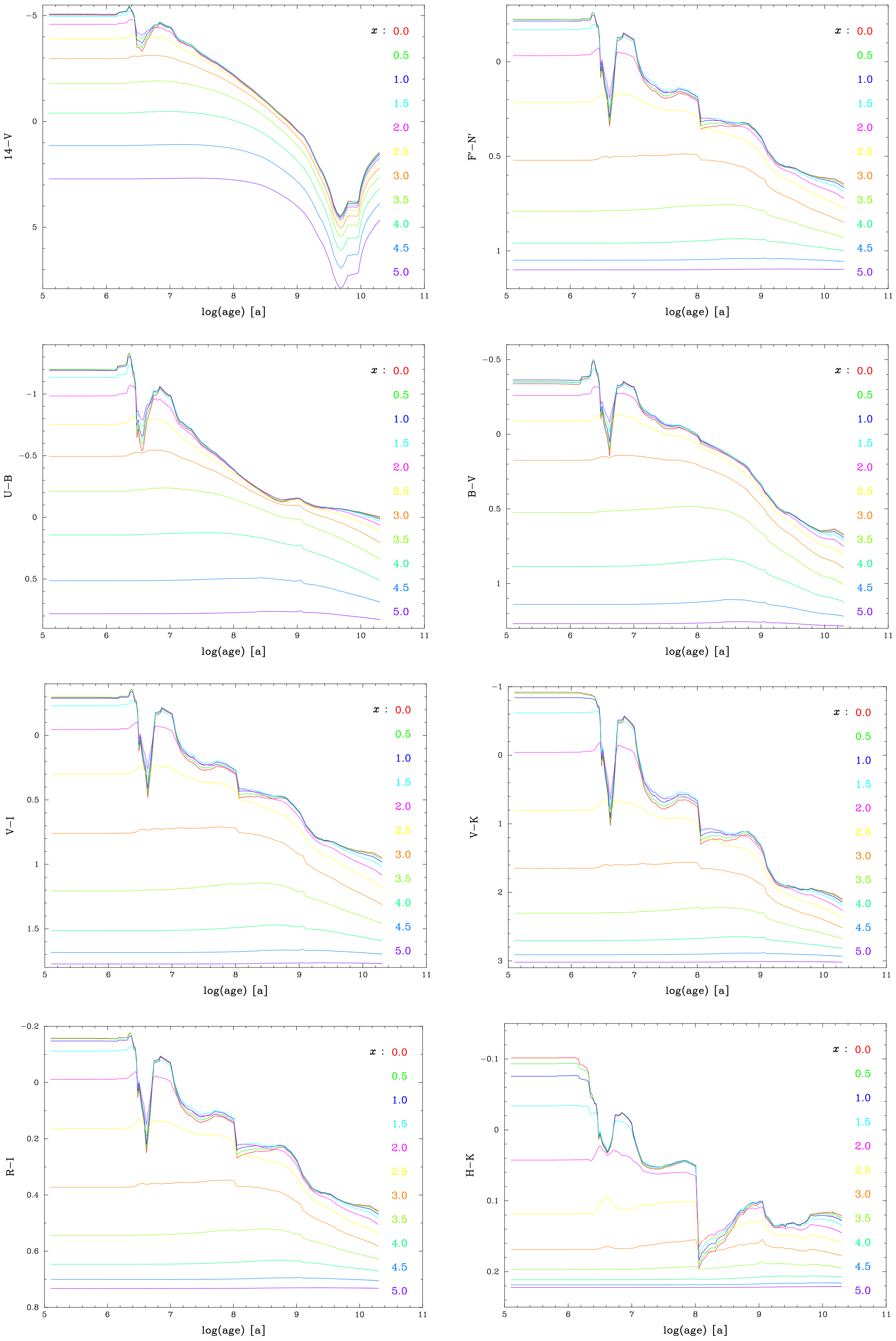

Figure 3.2: Temporal evolution of integrated colours calculated for different IMF-slopes x at $Z = 0.0004$ (Padova 2000 tracks, BaSeL 3.1 stellar library). Corresponding spectra in Figure 3.1.

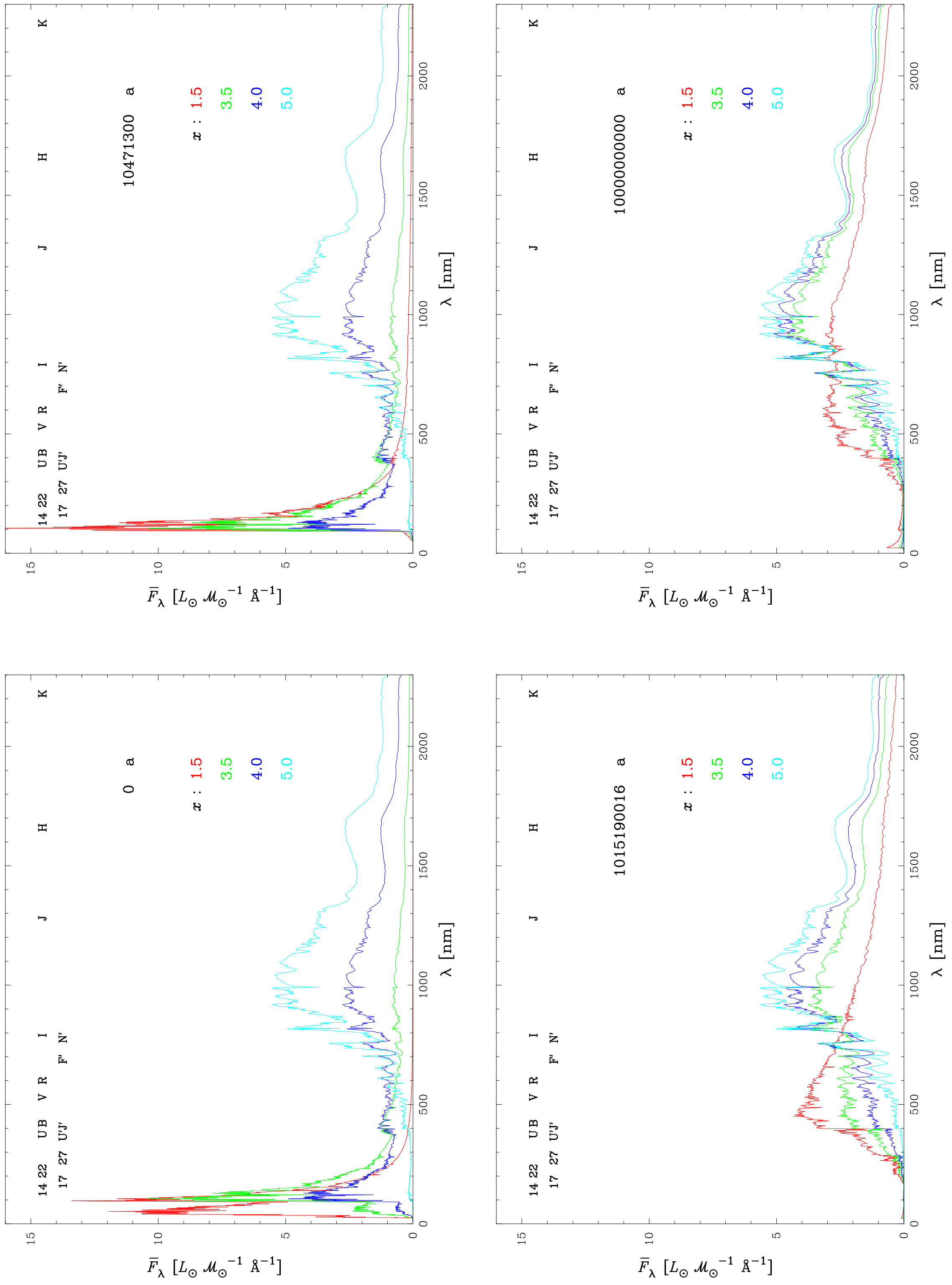

Figure 3.3: Same as Figure 3.1 but for $Z = 0.03$.

Name	λ_c	**Remarks**
14	141 nm	ST-UV14 filter (STFOC)
17	174 nm	ST-UV17 filter (STFOC)
22	221 nm	ST-UV22 filter (STFOC)
27	276 nm	ST-UV27 filter (STFOC)
U'	370 nm	Koo-Kron U+ filter (Koo's thesis)
J'	410 nm	Koo-Kron J+ filter (Koo's thesis)
F'	690 nm	Koo-Kron F+ filter (Koo's thesis)
N'	780 nm	Koo-Kron N+ filter (Koo's thesis)
U	375 nm	Buser's U filter (R. Buser)
B	421 nm	Buser's B filter (R. Buser)
V	530 nm	Buser's V filter (R. Buser)
R	600 nm	Cousins R filter (Bessell 1983, PASP, 95,480)
I	790 nm	Cousins I filter (Bessell 1983, PASP, 95,480)
J	1 280 nm	IR J filter + Palomar 200 IR detectors + atmosphere.55
H	1 660 nm	IR H filter + Palomar 200 IR detectors + atmosphere.56
K	2 220 nm	IR K filter + Palomar 200 IR detectors + atmosphere.57

Table 3.1: Selection of filters in the evolutionary synthesis code "bc03" along with the corresponding central wavelengths λ_c. For the full list see Appendix F in chapter "GISSEL User Manual".

differences between the low and the high metallicity set of spectra. This holds true for the integrated colours, too; so we shall not display them.

For completeness we calculated the spectra and the colours for positive slopes, i.e.:

$$x \in \{0.0, -1.0, -2.0, -3.0, -4.0, -5.0\}$$

The results are very much the same as if we'd take a bimodal IMF with a positive slope until 1 $\mathcal{M}_\odot$ and a negative slope from there on. This will be shown later. Thus the resulting figures do look quite similar to Figure 3.4 where the upper mass limit has been altered.

As for the negative slopes above we calculated spectra and colours for positive slopes at high metallicity $Z = 0.02$. As there were no significant differences compared to the low metallicity case we skip those plots.

For the different slopes of the IMF we conclude that:

- Slope values between 0.0 and 2.0 affect the integrated spectra and the integrated colours only mildly (0.1 mag for extreme cases).
- Slope values higher than 2.0 do show distinctive differences up to 8 mag, depending on colour and age of the population.
- Steeper slope values result in redder colours.

- Positive slopes result in similar effects as IMFs with different upper mass cut-offs (see below).
- There are no substantial differences to these conclusions as far as different metallicities are concerned.

Upper and lower mass limits of the IMF ($\mathcal{M}_u$, $\mathcal{M}_l$)

Now we investigate the influence of different mass ranges of the IMF on the integrated spectra; first for the upper mass limits $\mathcal{M}_u$. We chose the following values:

$$\mathcal{M}_u \in \{100, 75, 50, 25, 20, 10, 5, 2\}$$

The lower mass limit $\mathcal{M}_l$ remained at 0.1 $\mathcal{M}_\odot$, the metallicity was set to $Z = 0.0004$ (Padova 2000 tracks), we chose the BaSeL 3.1 stellar library, and for the slope we took $x = 1.35$, the value of the Salpeter IMF.

The effects of the different upper mass limits on the integrated spectra are shown in **Figure 3.4**. First of all we can see that all the spectra look the same after about 1 Ga, so changing the upper mass limit affects young stellar populations. The further evolution of the spectra is the same as for low-slope populations in Figure 3.1. In Figure 3.4 we show 4 distinctive values for the upper mass limit which correspond to the 4 groups of similar effects on the spectra: {100, 75, 50}, {25, 20, 10}, {5}, and {2}. At the beginning the 2 $\mathcal{M}_\odot$ cut-off population is dominated by A-stars simply because there are no earlier stars. Again there are no substantial differences when we look at other metallicities.

So we check the integrated colours of the population from Figure 3.4 in **Figure 3.5**. With this figure we can confirm that there are literally no differences in the colours after 1 Ga. Apart from H–K the colours are nearly identical between upper cut-offs of 100 to 50 $\mathcal{M}_\odot$. Other than for spectra each cut-off step between 2 and 25 $\mathcal{M}_\odot$ can be distinguished quite well. The constant (red) colours for low upper mass limits at early ages are due to the non-existing hot (blue) stars. In general, lower values of the upper mass limit result in redder colours.

Now we go for the lower mass limits $\mathcal{M}_l$. All the input parameters were the same as for the investigation about the lower mass limit. The upper mass limit was set to 100 $\mathcal{M}_\odot$, whereas the values for the lower mass limit were assumed as:

$$\mathcal{M}_l \in \{0.1, 0.2, 0.4, 0.6, 0.8, 1.0, 1.2, 1.4, 1.6, 1.8, 2.0\}$$

The influence on the integrated spectra is seen in **Figure 3.6**. Contrary to the upper mass limit, the change in the lower mass limit affects the spectra of old populations, since the spectra look the same up to an age of nearly 1 Ga. Here we can distinguish 2 groups of cut-off values, namely 0.1 to 0.6 and 0.8 to 2.0 $\mathcal{M}_\odot$. The first group is characterized by mild variations, i.e., some minor differences at old ages. All the values from the second group each have their distinctive effect on the spectra. After 1 Ga the population with 2.0 $\mathcal{M}_\odot$ cut-off reaches the phase of White Dwarfs. Those can dominate the integrated spectra since there are no red low mass stars. With higher cut-off mass the populations reach the White Dwarf phase earlier, i.e., 1 Ga for the 2.0 $\mathcal{M}_\odot$ cut-off and 14 Ga for the 0.8 $\mathcal{M}_\odot$ cut-off.

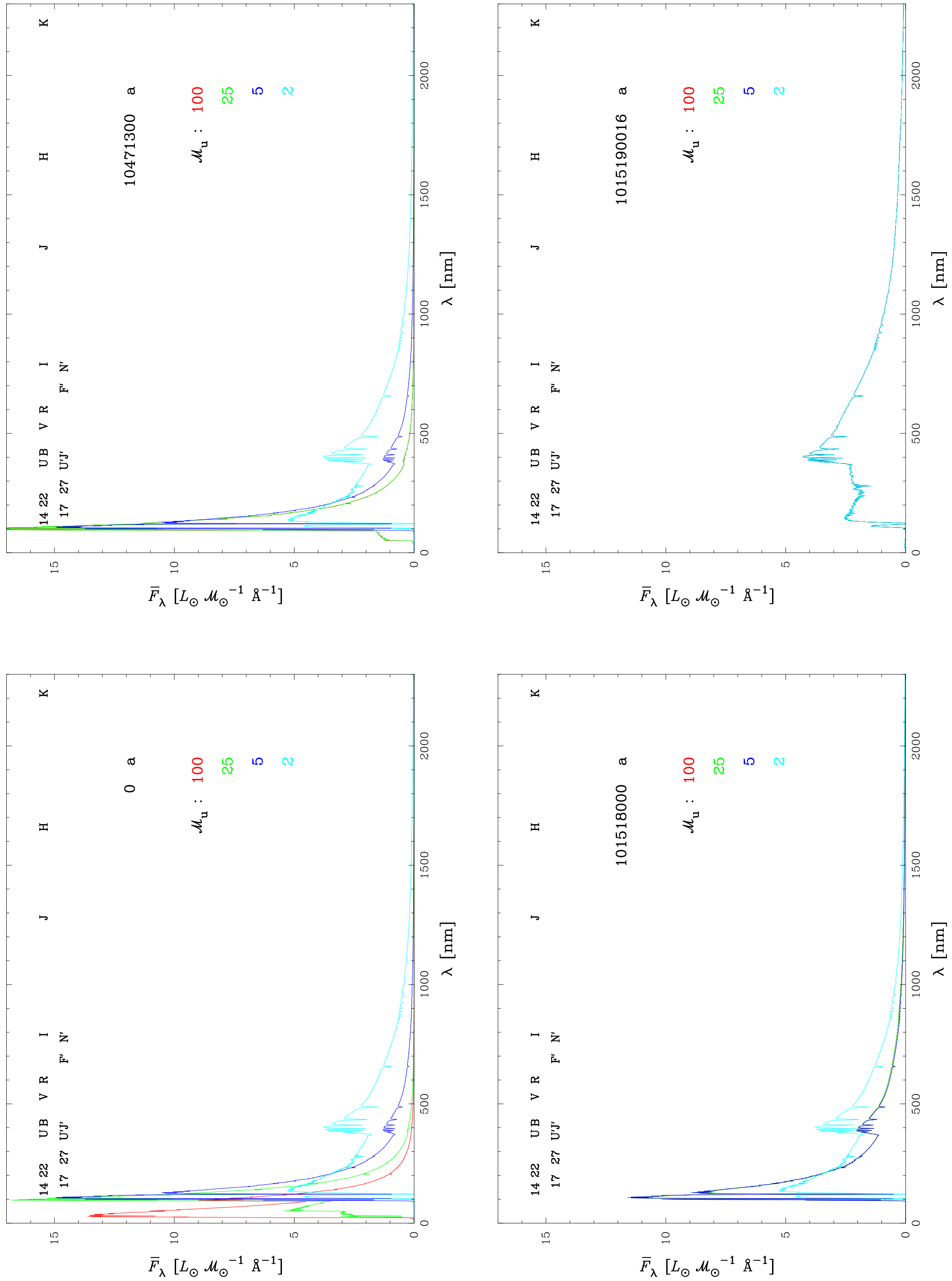

Figure 3.4: Temporal evolution of normalized integrated spectra for different upper mass limits $\mathcal{M}_u$ of the IMF (Salpeter IMF, Padova 2000 tracks, $Z = 0.0004$, BaSeL 3.1 stellar library). Corresponding colours in Figure 3.5.

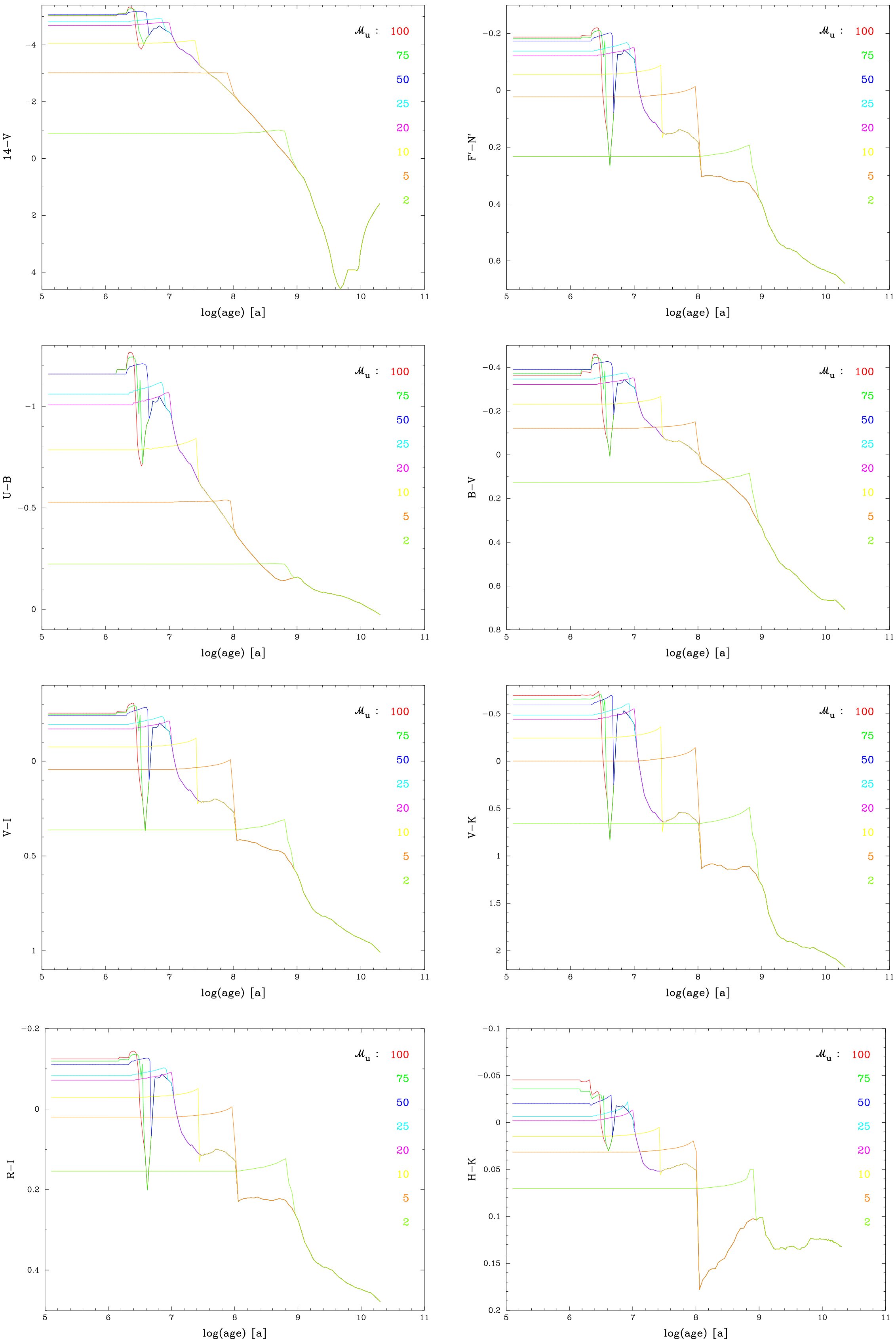

Figure 3.5: Temporal evolution of integrated colours for different upper mass limits $\mathcal{M}_u$ of the IMF (Salpeter IMF, Padova 2000 tracks, $Z = 0.0004$, BaSeL 3.1 stellar library). Corresponding spectra in Figure 3.4.

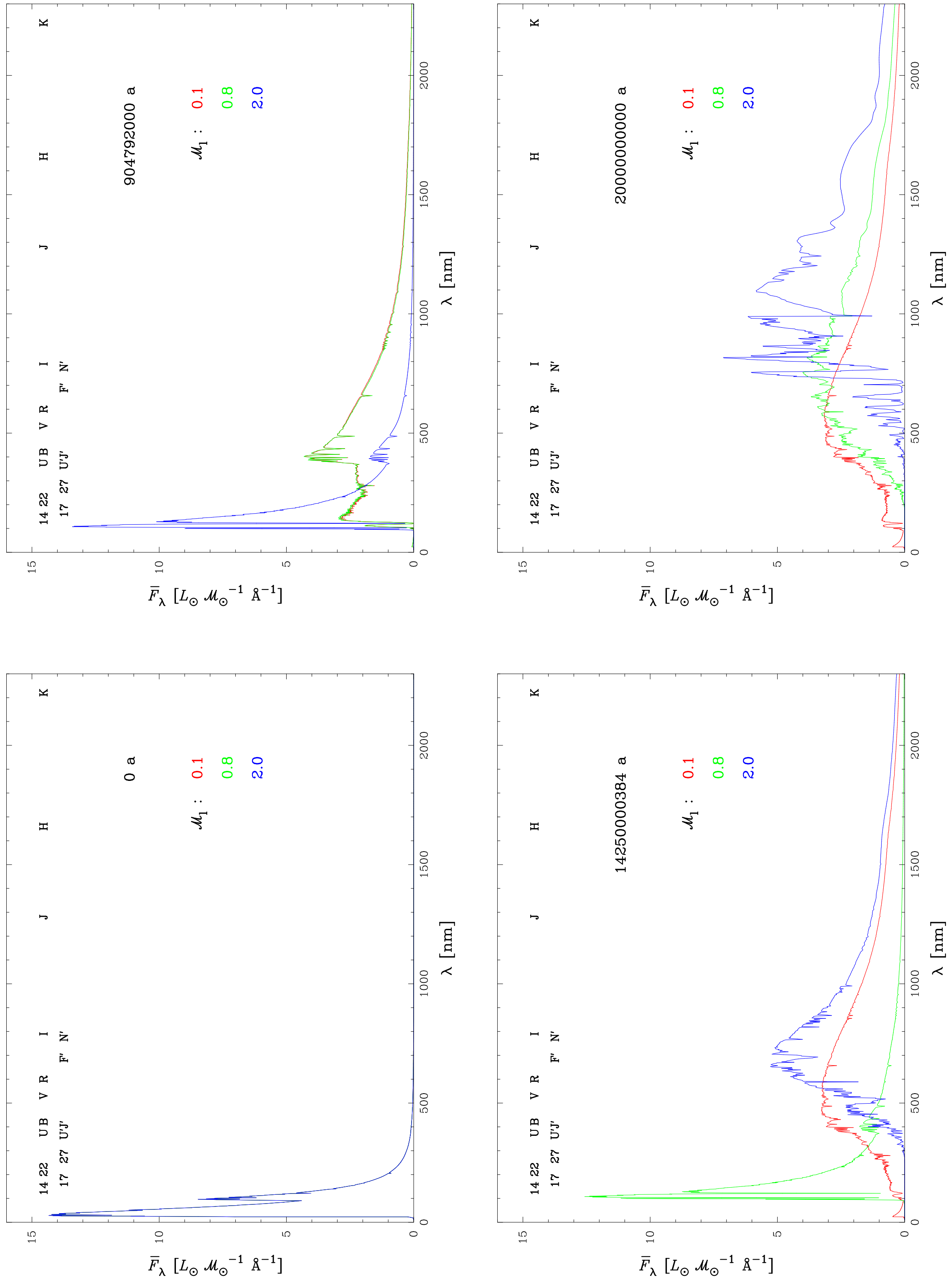

Figure 3.6: Temporal evolution of normalized integrated spectra for different lower mass limits $\mathcal{M}_1$ of the IMF (Salpeter IMF, Padova 2000 tracks, $Z = 0.0004$, BaSeL 3.1 stellar library). Corresponding colours in Figure 3.7.

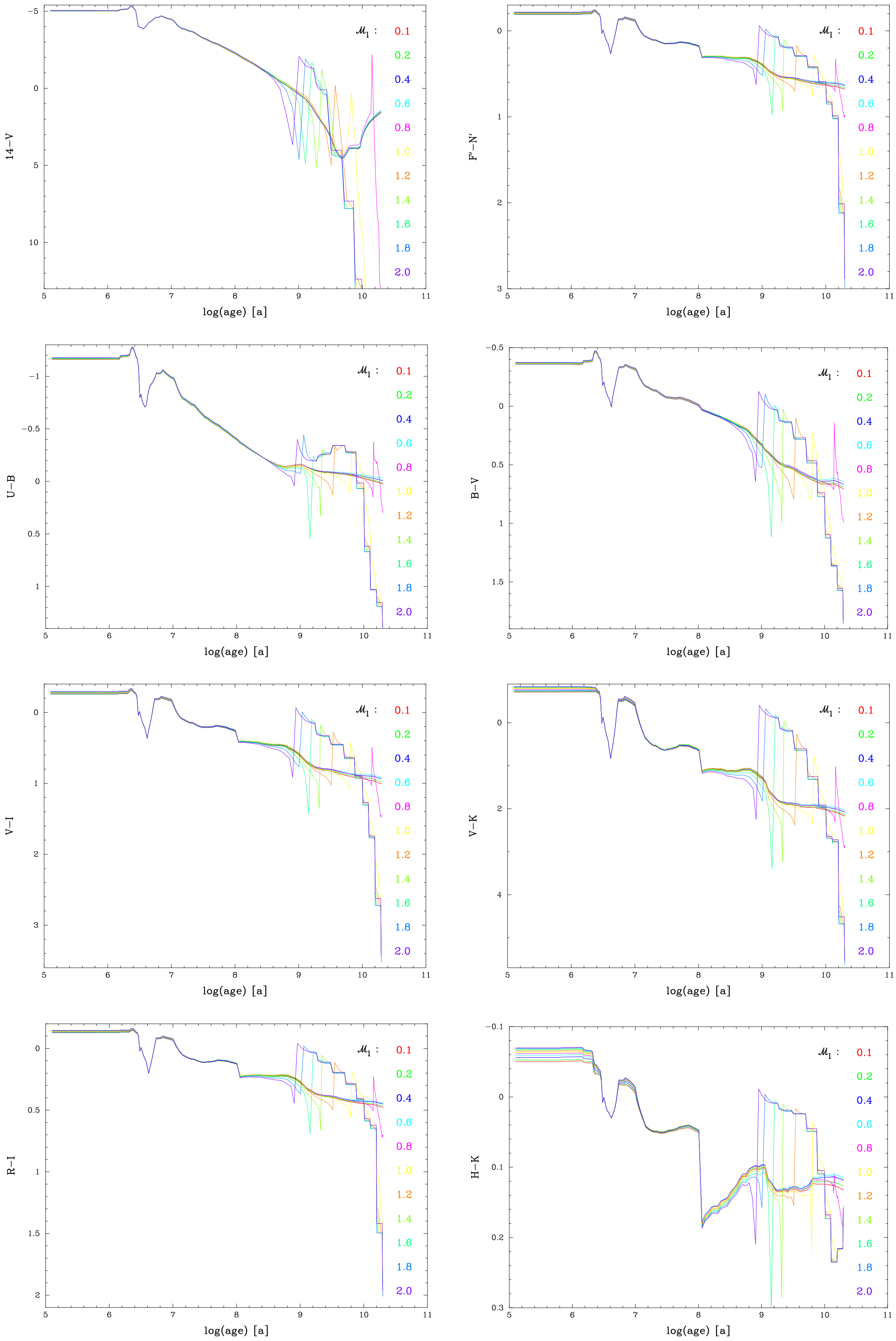

Figure 3.7: Temporal evolution of integrated colours calculated for different lower mass limits $\mathcal{M}_l$ of the IMF (Salpeter IMF, Padova 2000 tracks, $Z = 0.0004$, BaSeL 3.1 stellar library). Corresponding spectra in Figure 3.6.

All the statements for the spectra can be confirmed by looking at the integrated colours in **Figure 3.7**. The dramatically increasing colours to the blue can be explained by the sudden entry into the White Dwarf phase. The step-shaped decrease afterwards is due to the cooling sequence being represented by only a few points in the evolutionary tracks. Generally, higher values of the lower mass limits result in slightly (< 0.01 mag) bluer colours.

And now we'd like to see the effect caused by changes of both the upper and lower mass limits. The other input parameters were again the same as above. For the different IMF mass-ranges we took:

$$\mathcal{M}_\mathrm{l} - \mathcal{M}_\mathrm{u} \in \{0.1-100, 0.4-75, 0.6-50, 0.8-25, 1.0-20, 1.2-10, 1.4-5, 1.6-2\}$$

First we analyse the influence on the integrated spectra in **Figure 3.8**. Over all, we can describe the spectra as a combination of Figure 3.4 and Figure 3.6; the change of the upper and the lower mass limit affects the spectra of young and old stellar populations, respectively, whereas the intermediate aged populations remain untouched. At young ages, the spectra look similar to the spectra with upper mass cut-off in Figure 3.4. According to the cut-off value, hot O- and B-stars dominate the spectra more or less. After 800 Ma there are no differences amongst the spectra. Then White Dwarfs begin to dominate the spectra of populations with lower mass cut-offs as seen in Figure 3.6.

Now for the effects on the integrated colours in **Figure 3.9**. The above statement that the spectra can be seen as a combination of populations having different upper or lower mass limits, can be confirmed for the colours. Note that the scales of the colour axis in Figures 3.5, 3.7, and 3.9 are all different.

For the different cut-offs of the IMF we conclude that:

- The upper mass limit affects young stellar populations (< 1 Ga).
- Upper mass limits between 100 and 50 $\mathcal{M}_\odot$ have few effects on colours (< 0.01 mag).
- Lower values of the upper mass limits result in redder colours (< 4 mag).
- The lower mass limit affects old stellar populations (> 1 Ga).
- Lower mass limits between 0.1 and 0.6 $\mathcal{M}_\odot$ have few effects on colours (< 0.01 mag).
- Higher values of the lower mass limits result in bluer colours (< 4 mag).
- Changing both limits doesn't affect intermediate age populations (0.1 to 1 Ga).
- There are no substantial differences to these conclusions as far as different metallicities are concerned.

Two segmented IMF

In this subsection we'd like to investigate the effects of a two segmented IMF. For the spectra in **Figure 3.10** we took IMFs where the slopes between 0.1 and 1 $\mathcal{M}_\odot$, defined as x_a, are all 1.0 whereas the ones between 1 and 100 $\mathcal{M}_\odot$, defined as x_b, are taken as 1.0, 3.0, and 5.0. For comparison we show the spectra of a population with a slope 1.0 IMF which has a lower and an upper mass limit of 0.1 and 2.0 $\mathcal{M}_\odot$, respectively. The other input parameters were the same as above.

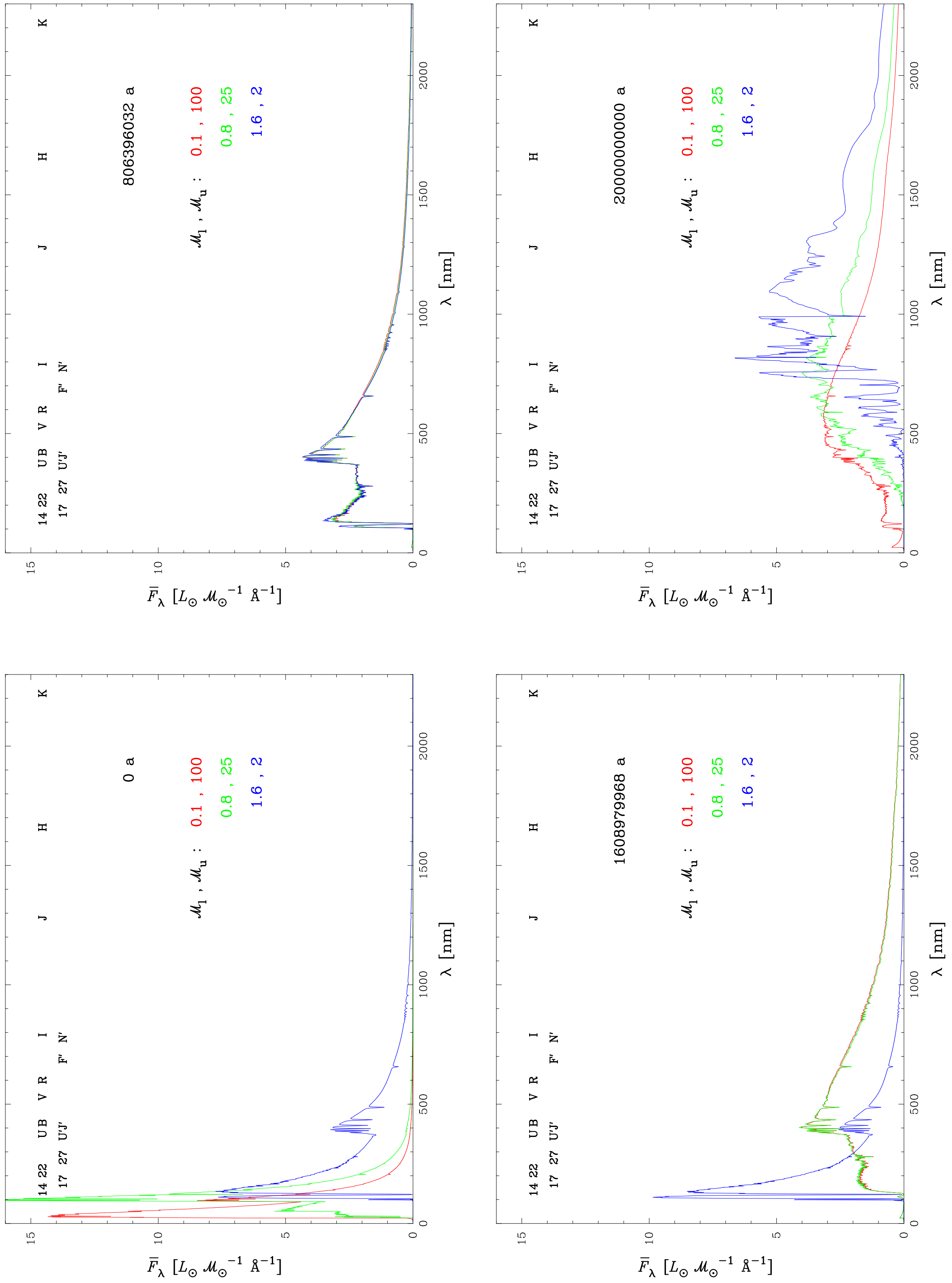

Figure 3.8: Temporal evolution of normalized integrated spectra for different lower $\mathcal{M}_l$ and and upper $\mathcal{M}_u$ mass limits of the IMF (Salpeter IMF, Padova 2000 tracks, $Z = 0.0004$, BaSeL 3.1 stellar library). Corresponding colours in Figure 3.9.

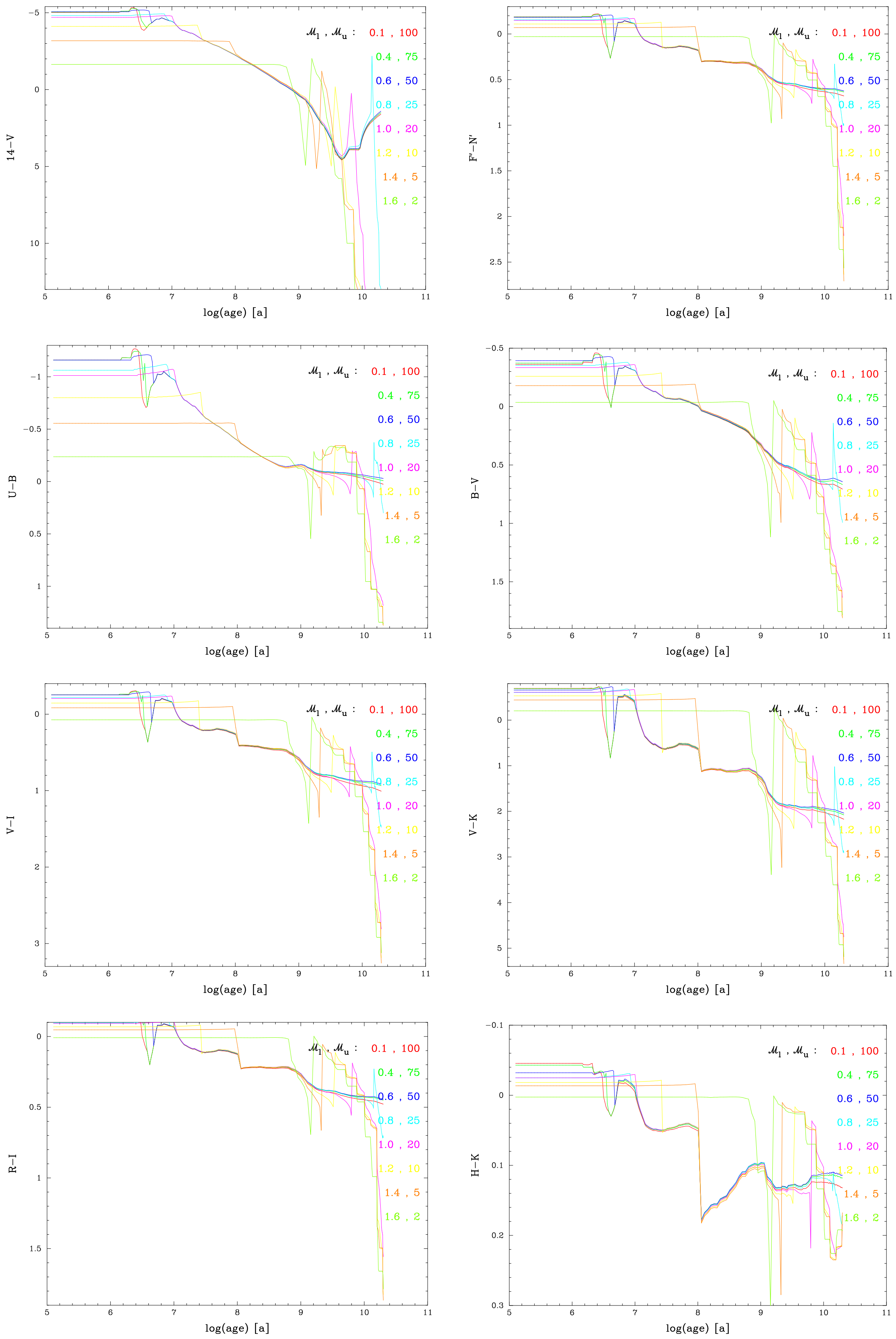

Figure 3.9: Temporal evolution of integrated colours for different lower $\mathcal{M}_\mathrm{l}$ and and upper $\mathcal{M}_\mathrm{u}$ mass limits of the IMF (Salpeter IMF, Padova 2000 tracks, $Z = 0.0004$, BaSeL 3.1 stellar library). Corresponding spectra in Figure 3.8.

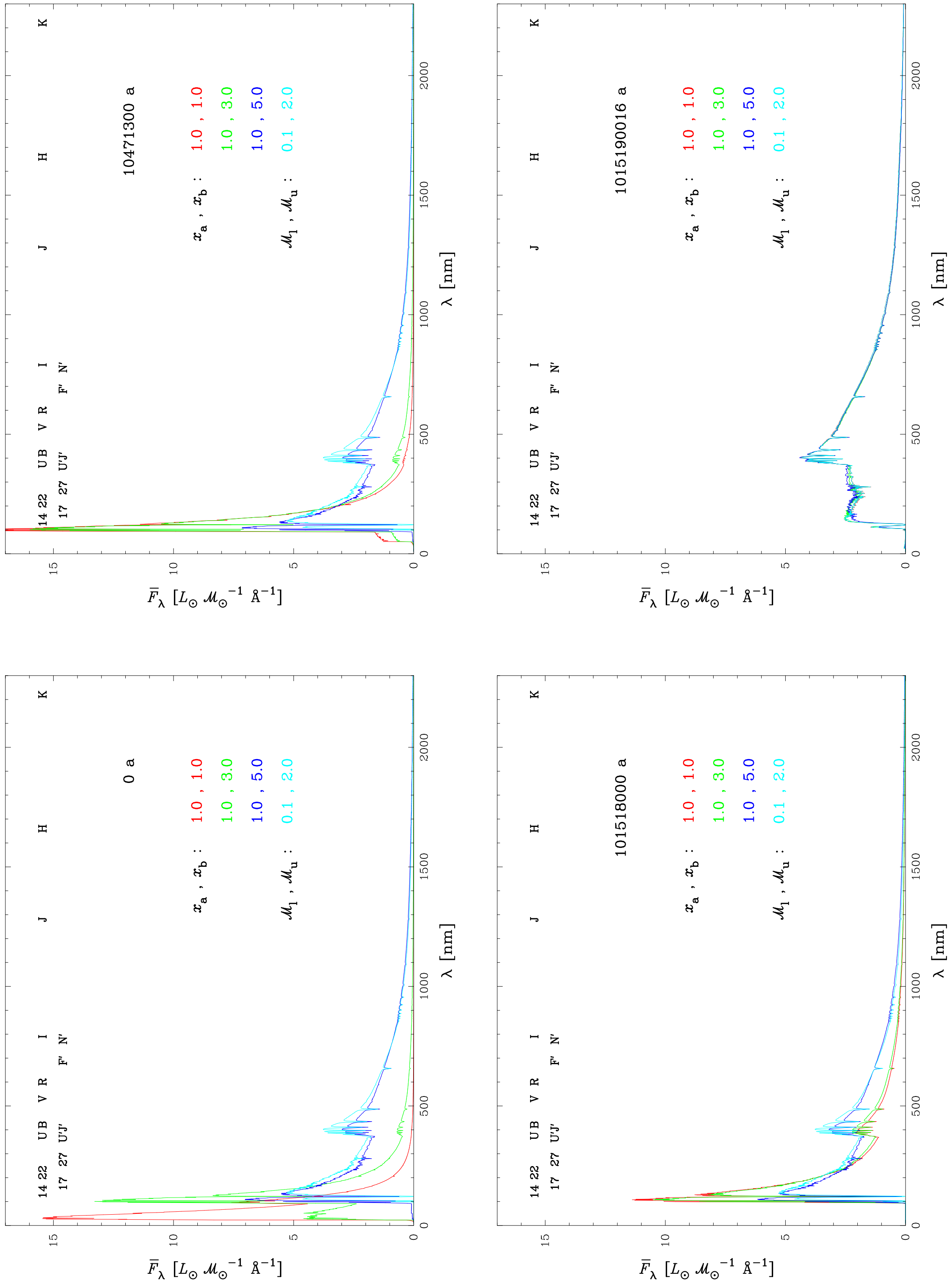

Figure 3.10: Temporal evolution of normalized integrated spectra calculated for IMFs segmented at 1.0 $\mathcal{M}_\odot$ with slopes x_a and x_b compared to a population with $\mathcal{M}_\mathrm{l} = 0.1$ and $\mathcal{M}_\mathrm{u} = 2.0$. (Padova 2000 tracks, $Z = 0.0004$, BaSeL 3.1 stellar library).

Comparison to Figure 3.4 shows that a two segmented IMF can be seen as a combination of a non segmented IMF with the full mass range and an IMF with a cut-off at roughly the same point where the former is segmented. As Figure 3.4 and 3.10 do look very similar we skip the effects of segmented IMFs on integrated colours.

For the two segmented IMF we conclude that:

- The effects of a segmented IMF are similar to the ones of a non segmented IMF with a full mass range combined with an IMF with an upper cut-off.
- No changes to this statement can be made at other metallicities.

Bimodal IMF

We calculated the spectra for a bimodal IMF segmented at 1.0 $\mathcal{M}_\odot$. Here the slopes have different signs from 0.0 to 5.0, i.e., a negative slope x_a between 0.1 and 1 $\mathcal{M}_\odot$ and a positive slope x_b between 1 and 100 $\mathcal{M}_\odot$. The resulting spectra are shown in **Figure 3.11**. They look quite similar to the ones calculated for different lower mass limits $\mathcal{M}_\mathrm{l}$ (see Figure 3.6). So the statements made for the spectra with lower cut-offs can be applied to this situation. Again the effects on the integrated colours are suppressed here.

For curiosity we generated spectra for the same bimodal IMFs as above but for a positive slope until 1 $\mathcal{M}_\odot$ and a negative slope afterwards ($x_a = -x_b$). The results are very similar to the cut-off of the upper mass limit $\mathcal{M}_\mathrm{u}$ in Figure 3.4.

For the bimodal IMF we conclude that:

- An IMF with a negative and a positive slope interval result in spectra and colours similar to the cases of lower mass cut-offs.
- An IMF with a positive and a negative slope interval result in spectra and colours similar to the cases of upper mass cut-offs.
- There are no differences to these conclusions at other metallicities.

3.1.2 Stellar Evolutionary Tracks

To investigate on these effects we chose the three evolutionary track types that are currently available in the GISSEL code (see Table 2.1): Geneva 1992, Padova 1994, and Padova 2000 tracks. The results are presented in **Figure 3.12** for solar metallicity $Z = 0.02$. There are some minor differences between the Geneva and the Padova tracks especially at younger ages. The two sets of Padova tracks nearly look the same, however.

Now we show same picture for the integrated colours in **Figure 3.13**. First, we can see that the two Padova tracks are quite similar. They can differ up to 0.1 mag for some intermediate ages. The Geneva tracks however show larger differences compared to the Padova tracks. At 10 Ma the former can be 0.4 mag redder than the latter, depending on which colour. At 20 Ma Geneva tracks can be 0.3 mag bluer than the Padova tracks. Nevertheless, between 0 and 2.5 Ma and between 0.1 and 20 Ga the differences are moderate (< 0.1 mag) for most colours. Of course these effects are due to the different schools of stellar evolutionary models.

For comparison we calculated the same for a low metallicity value, i.e., for $Z = 0.0004$. For this metallicity, the Geneva tracks are not implemented in the code, so we compare just

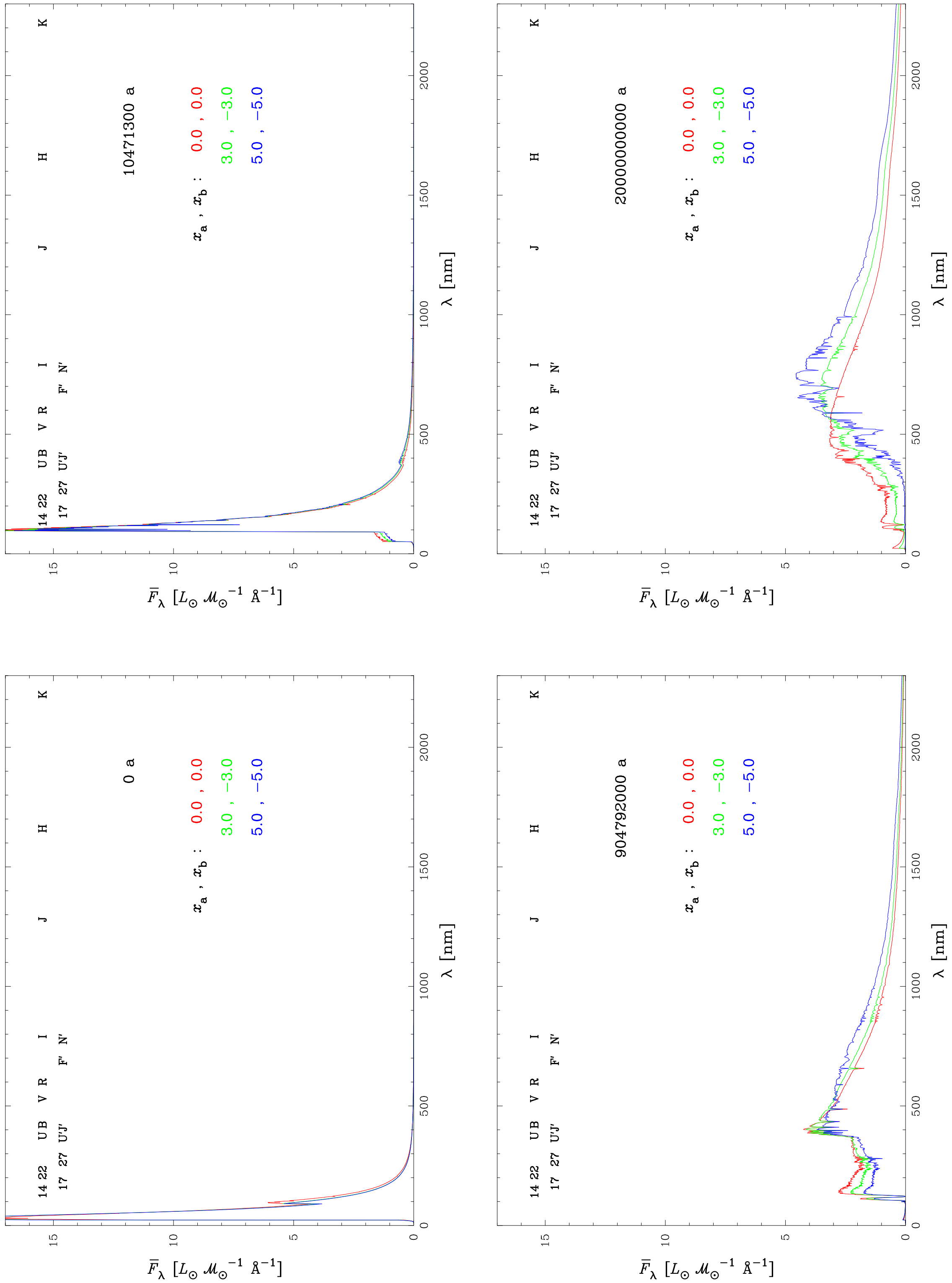

Figure 3.11: Temporal evolution of normalized integrated spectra calculated for bimodal IMFs segmented at 1.0 $\mathcal{M}_\odot$ with slopes x_a and $-x_b$ (Padova 2000 tracks, $Z = 0.0004$, BaSeL 3.1 stellar library).

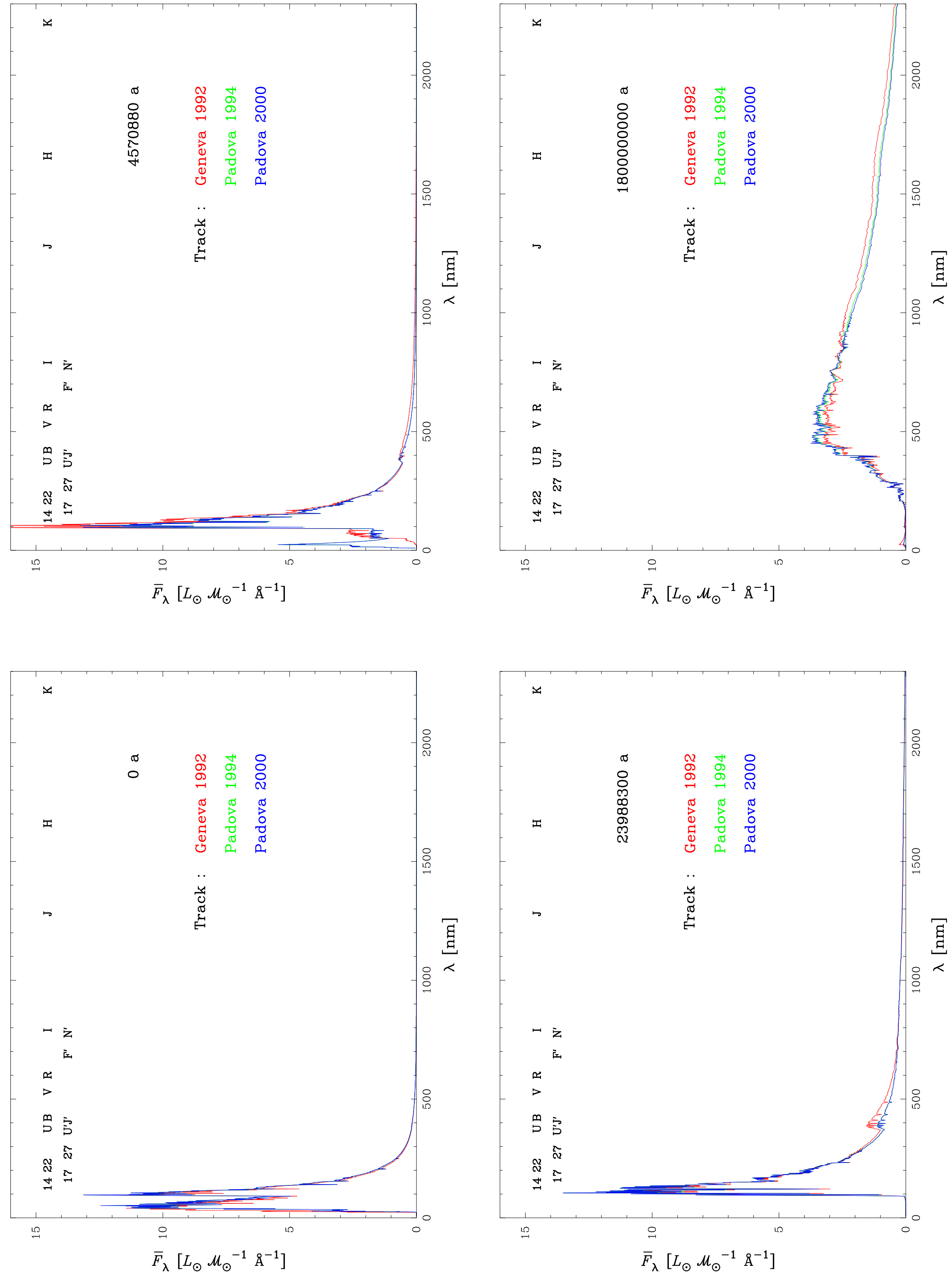

Figure 3.12: Temporal evolution of normalized integrated spectra calculated for different evolutionary tracks at $Z = 0.02$ (BaSeL 3.1 stellar library, Salpeter IMF). Corresponding colours in Figure 3.13.

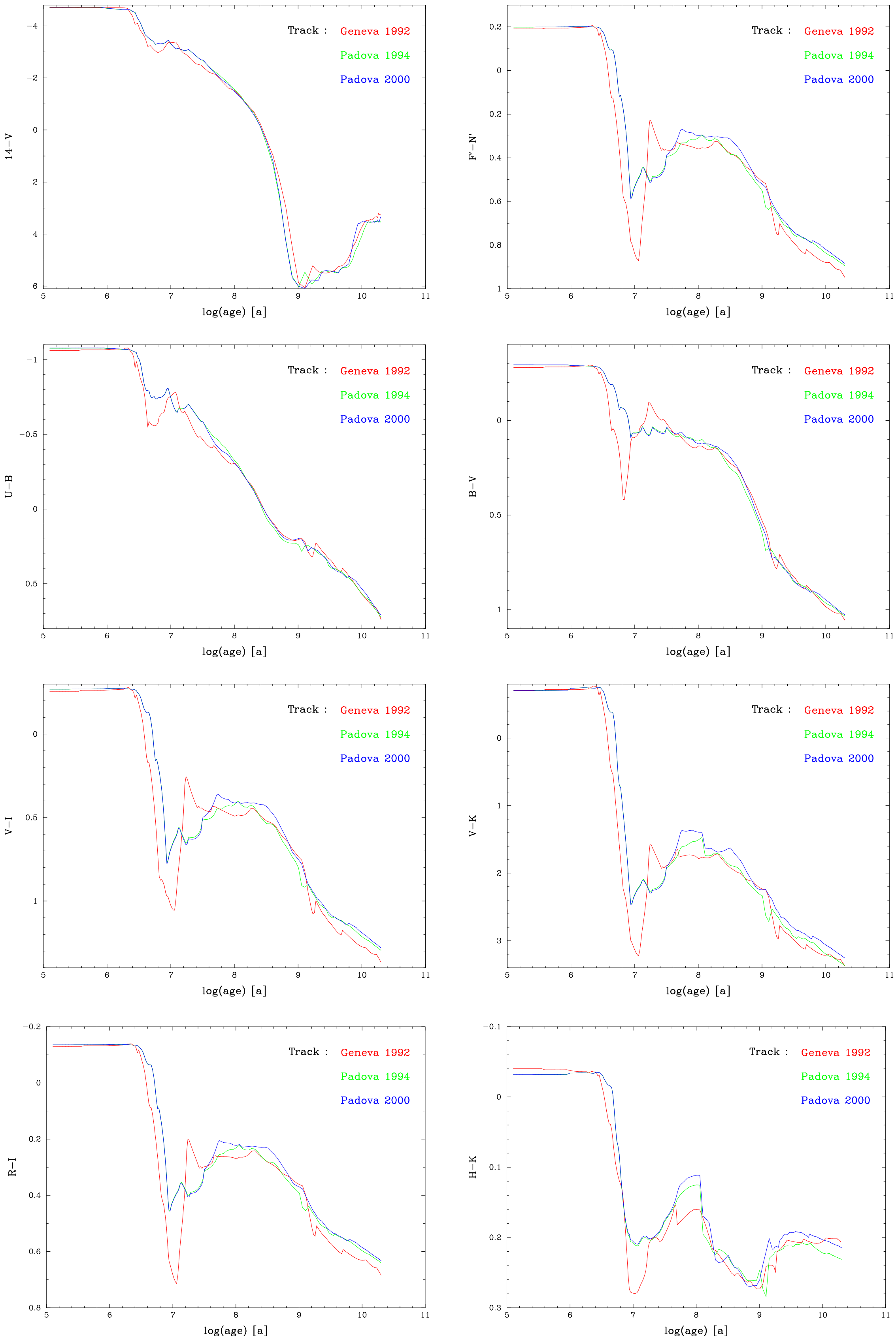

Figure 3.13: Temporal evolution of integrated colours calculated for different evolutionary tracks at $Z = 0.02$ (BaSeL 3.1 stellar library, Salpeter IMF). Corresponding spectra in Figure 3.12.

the two versions of the Padova tracks. First for the integrated spectra in **Figure 3.14**. Comparing this figure with Figure 3.12 the spectra based on the two tracks are roughly of the same kind. The differences are not very dramatic apart from the area between 0 and 200 nm at 20 Ga.

So we have a look at the integrated colours in **Figure 3.15**. Between 25 and 250 Ma the colours can differ up to 0.05 mag, while the Padova 1994 tracks seem to be redder (in general) than the Padova 2000 tracks. Above 4 Ga there is a 1.5 mag difference in 14–V. As already mentioned, we can see the upturn of the spectrum at that ages and in the corresponding wavelength area in Figure 3.14.

For the effects of the different track types we conclude:

- Geneva 1992 tracks can result in colour differences between +0.4 and –0.3 mag for intermediate ages (2.5 to 100 Ma) compared to Padova tracks.
- Padova 1994 tracks differ moderately ($<$ 0.1 mag) to Padova 2000 tracks only at intermediate ages.
- No changes to these statements can be found at other metallicities.

3.1.3 Stellar Spectral Libraries

The last item to be investigated for the SSPs is the choice of the different stellar spectra. For this comparison we chose three theoretical and one empirical library (see Table 2.2): BaSeL 2.2 (o: original and c: corrected), BaSeL 3.1, and STELIB.

In **Figure 3.16** there are the integrated spectra for the corresponding libraries calculated at $Z = 0.02$. The other input parameters stayed the same as above. Note that the STELIB spectra come at a higher resolution than the BaSeL spectra (see Table 3.1). To be able to compare the spectra we didn't normalize them. This lead to different scales of the y-axis for different ages. In general, there are slight differences amongst the theoretical libraries and some differences to the empirical library. The most obvious difference is at 50 nm and at 2.9 Ma. Note that we don't have a filter at that wavelength area available. Afterwards the STELIB spectra appear to have larger fluxes compared to the theoretical libraries, but this is due to the higher resolution which lead to deeper absorption lines. This, by the way, shows the difficulty of comparing spectra with different resolutions.

The corresponding integrated colours are shown in **Figure 3.17**. Apart from some cases (e.g. H–K) the colours show very few differences between 0 and 10 Ma. Afterwards the colours can differ up to 0.1 mag until roughly 400 Ma. We have minor differences again on to 1.5 Ga. Then they start to grow up to 0.1 mag at 20 Ga for some colours.

Analogous to above we made the same investigation for a metallicity value of $Z = 0.0004$. In **Figure 3.18** there are the corresponding integrated spectra. Again the most obvious difference occurs at an early age. Then the flux values show more or less the same behaviour as for the low metallicities above.

The corresponding integrated colours are shown in **Figure 3.19**. There we can see that the differences are of the same order of magnitude as for the high metallicity case (Figure 3.17). Contrary to this case, we can not make any statements as far as uniform trends are concerned. But we can say that the largest difference is 0.1 mag.

For the effects of the different libraries we conclude:

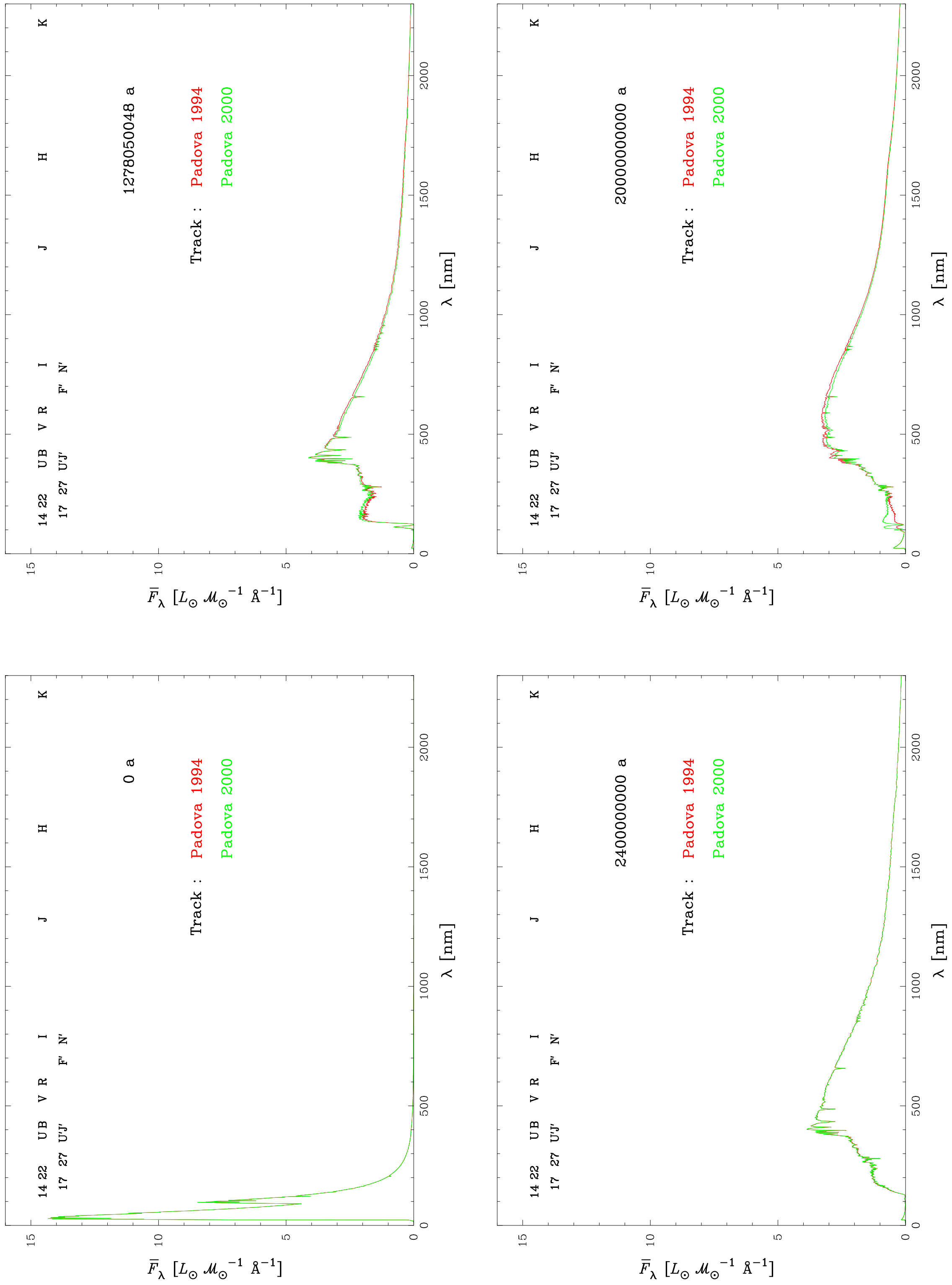

Figure 3.14: Temporal evolution of normalized integrated spectra calculated for different evolutionary tracks at $Z = 0.0004$ (BaSeL 3.1 stellar library, Salpeter IMF). Corresponding colours in Figure 3.15.

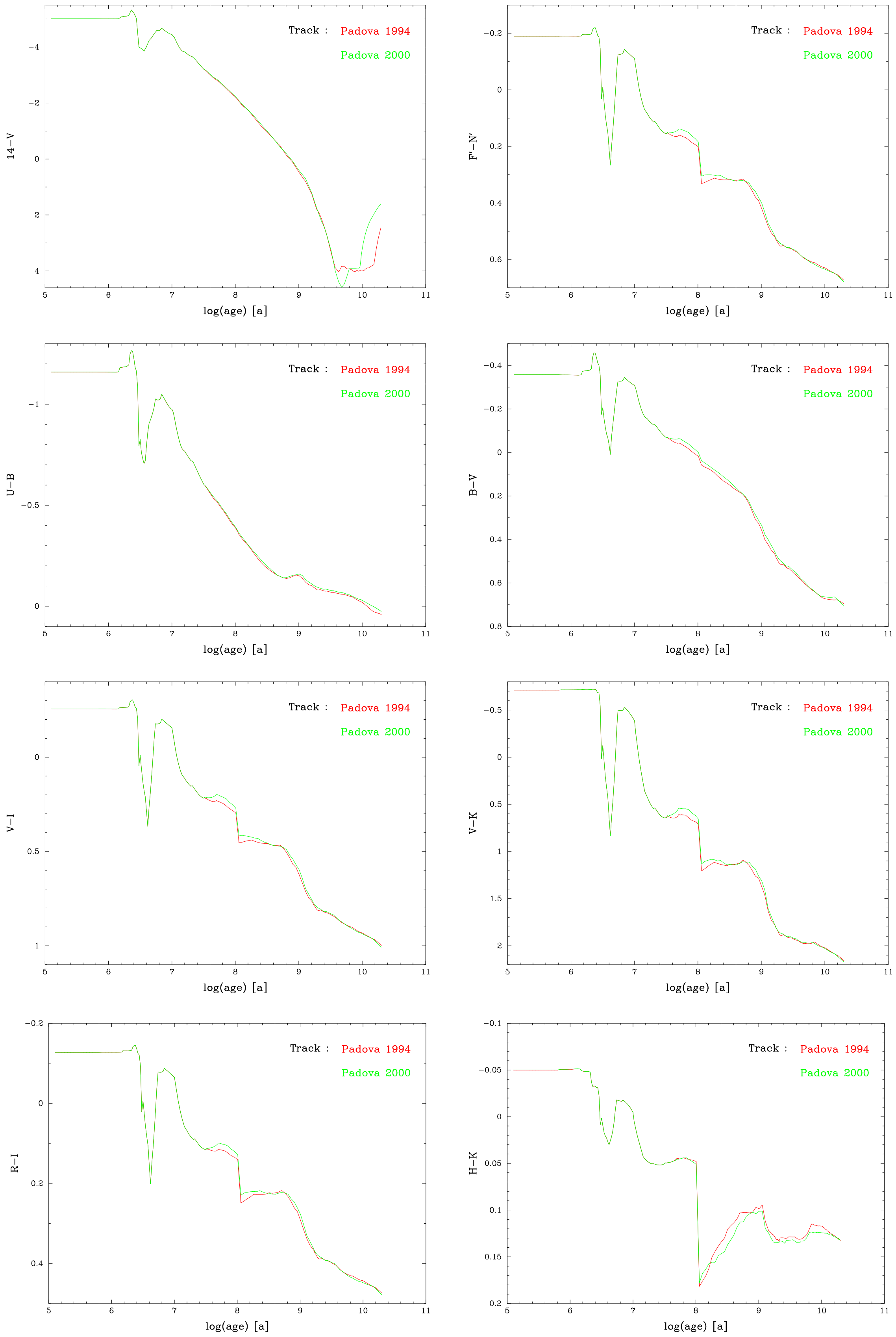

Figure 3.15: Temporal evolution of integrated colours calculated for different evolutionary tracks at $Z = 0.0004$ (BaSeL 3.1 stellar library, Salpeter IMF). Corresponding spectra in Figure 3.14.

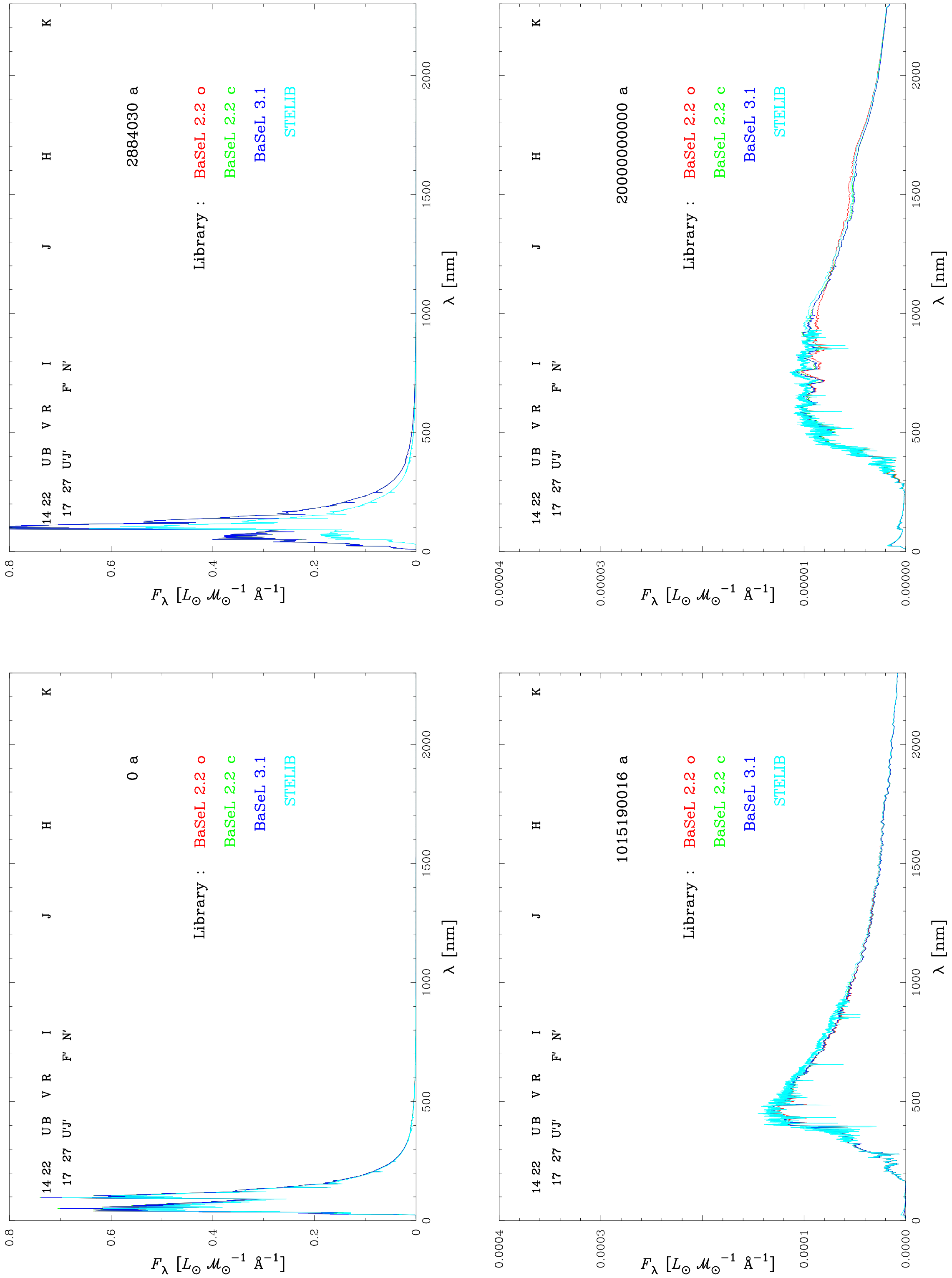

Figure 3.16: Temporal evolution of integrated spectra calculated for different stellar spectral libraries at $Z = 0.02$ (Padova 2000 tracks, Salpeter IMF). Corresponding colours in Figure 3.17.

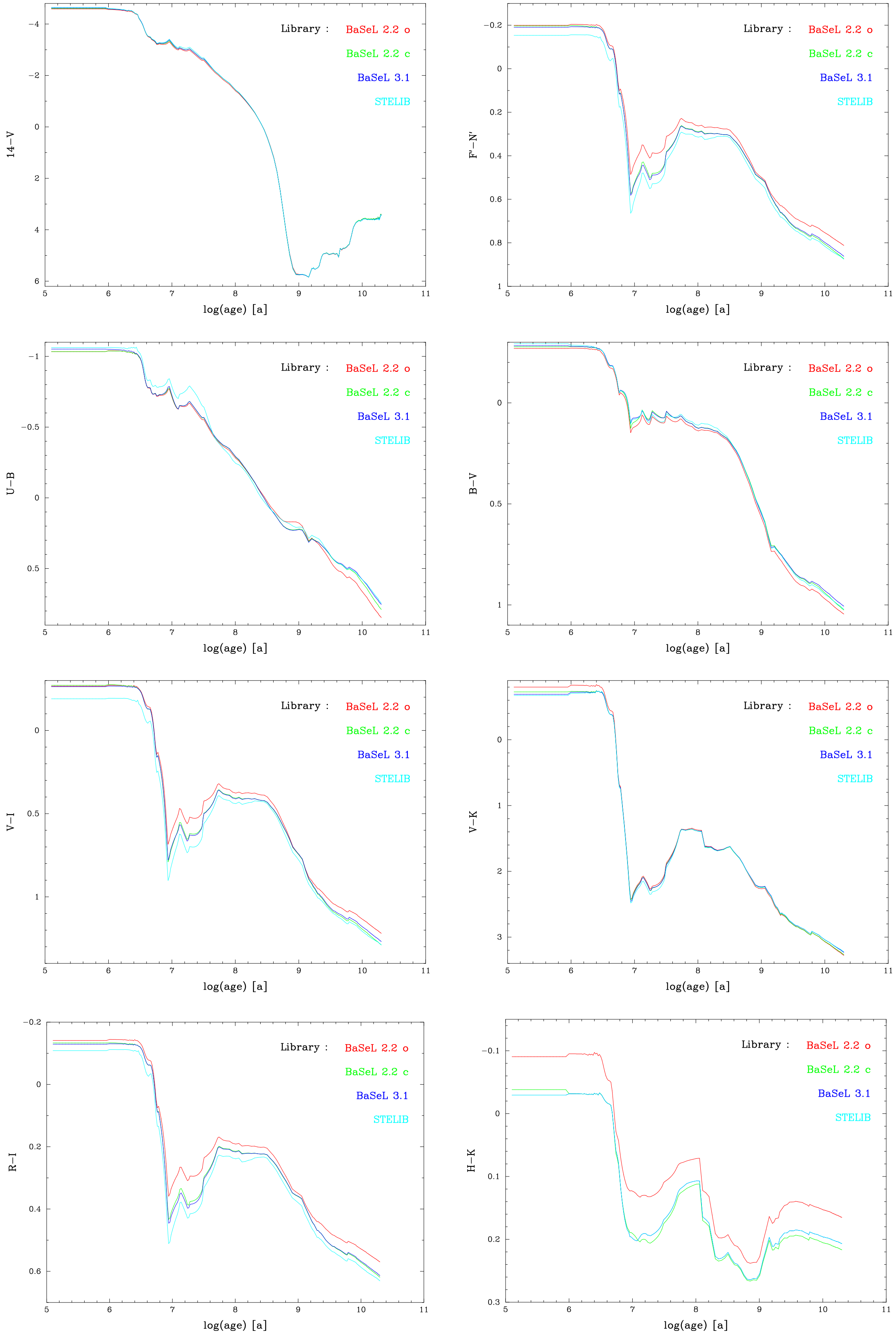

Figure 3.17: Temporal evolution of integrated colours calculated for different stellar spectral libraries at $Z = 0.02$ (Padova 2000 tracks, Salpeter IMF). Corresponding spectra in Figure 3.16.

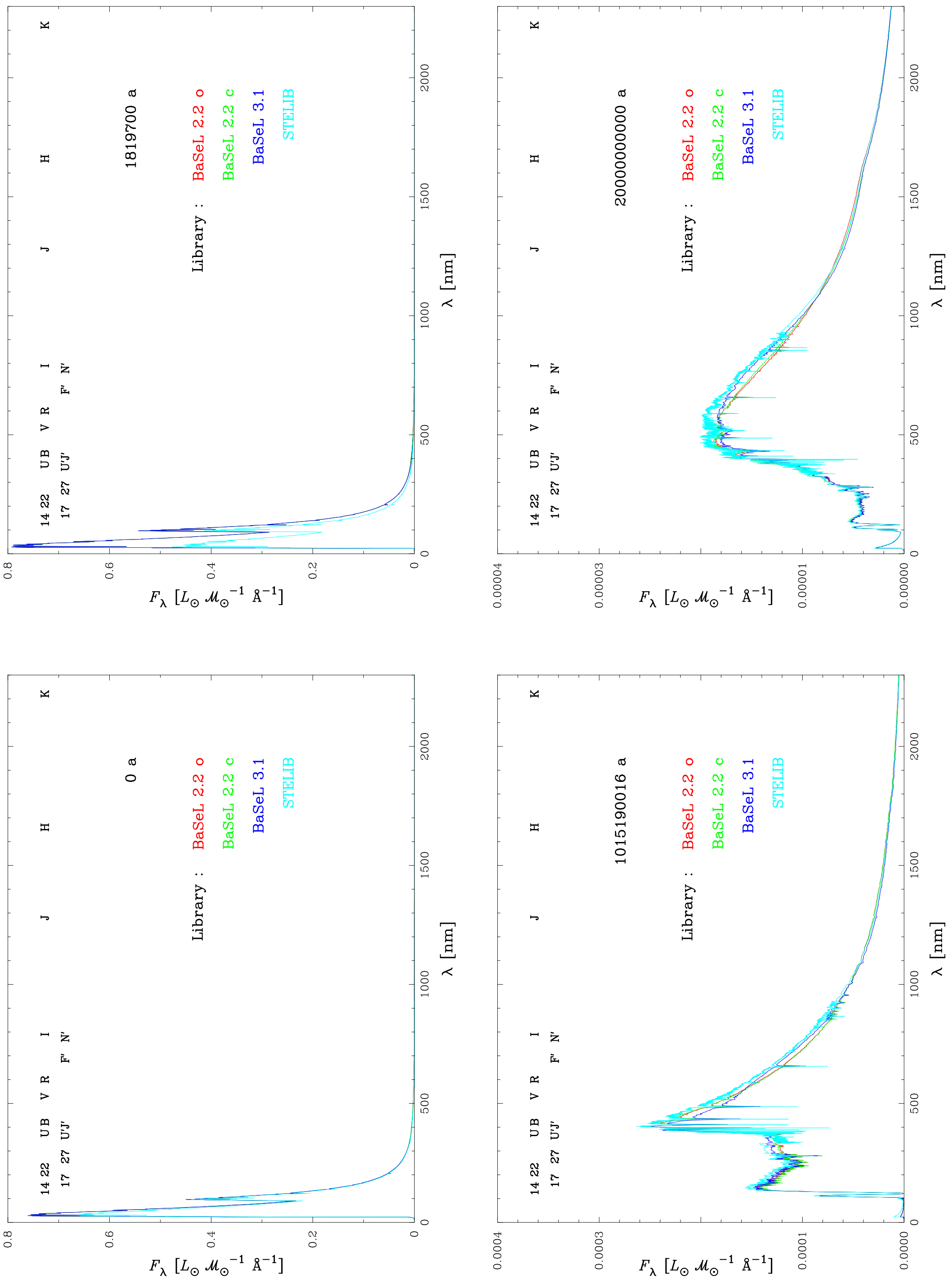

Figure 3.18: Temporal evolution of integrated spectra calculated for different stellar spectral libraries at $Z = 0.0004$ (Padova 2000 tracks, Salpeter IMF). Corresponding colours in Figure 3.19.

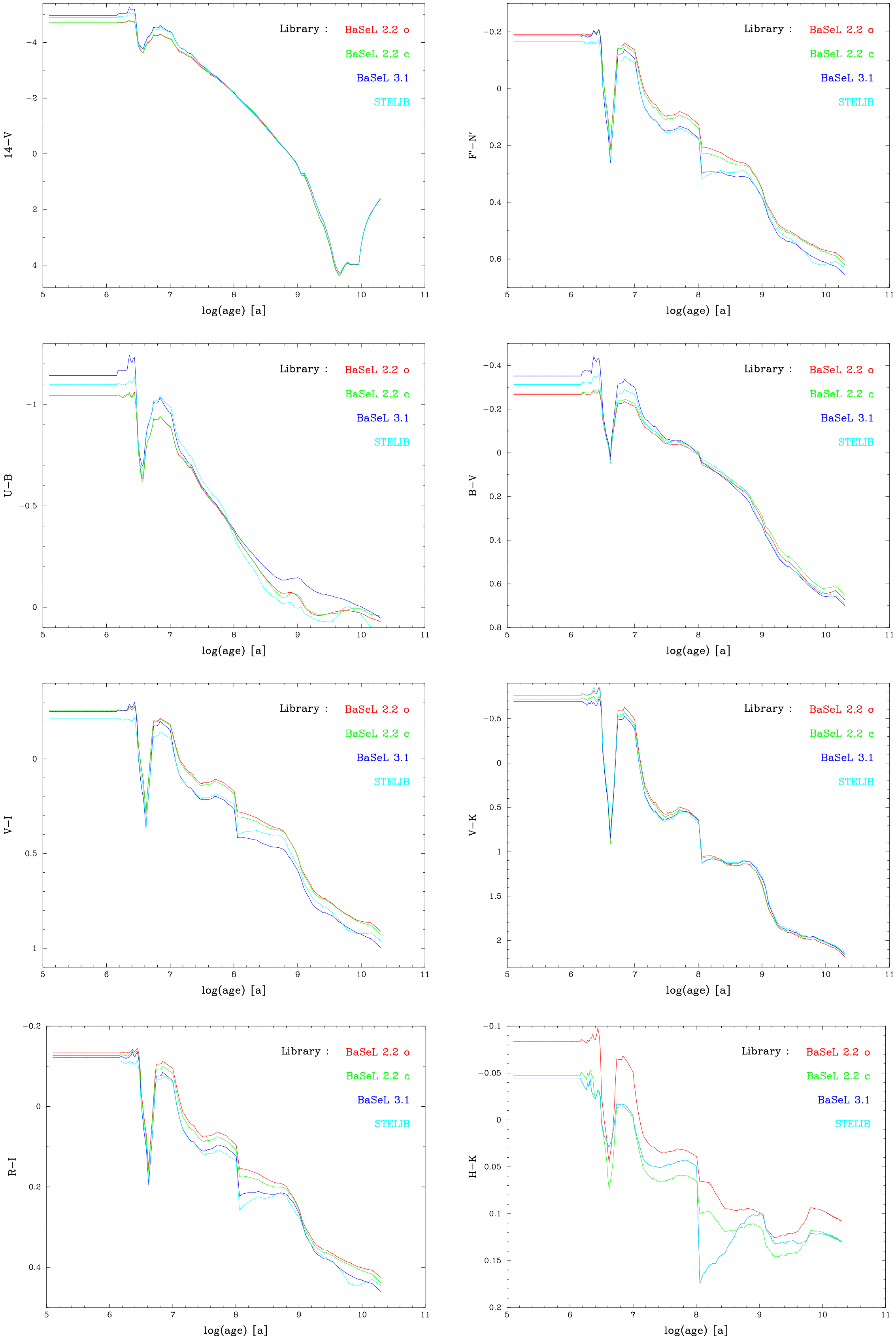

Figure 3.19: Temporal evolution of integrated colours calculated for different spectral stellar libraries at $Z = 0.0004$ (Padova 2000 tracks, Salpeter IMF). Corresponding spectra in Figure 3.18.

Property	**Choice**
IMF slope	1.35 (Salpeter), 2.0, 3.0
$\mathcal{M}_{\rm u}$	100, 50, 10, 2 $\mathcal{M}_\odot$
$\mathcal{M}_{\rm l}$	0.1, 1.0, 2.0 $\mathcal{M}_\odot$
track type	Padova 1994
metallicity Z:	0.0001, 0.0004, 0.004, 0.008, 0.02, 0.05, 0.1
stellar libraries	BaSeL 3.1, STELIB

Table 3.2: Properties of SSPs in BLoIS 1.1

- In general the differences in spectra and colours are small.
- For high metallicity the biggest differences (0.1 mag) are at intermediate and oldest ages.
- For low metallicity the differences are of the same order of magnitude but do not follow any specific trend.

3.1.4 Consequences for BLoIS 1.1

For the slope of the IMF we select the Salpeter IMF because there are only mild differences between slope 0.0 and slope 1.35. But as steeper slopes do lead to major differences we select slopes 2.0 and 3.0, too.

The different upper mass limits of the IMF are chosen at values that lead to distinctively different results, i.e., at 2, 10, 50, and 100 $\mathcal{M}_\odot$. The lower mass limits for their part are selected at 0.1, 1.0, and 2.0 $\mathcal{M}_\odot$. This results in 11 different combinations for the IMF mass ranges.

Since a two segmented IMF population can be derived by combining a full range IMF with a truncated IMF population, and a bimodal IMF population can be built by putting together IMFs with different mass limits, we skip those IMF types.

As the differences between the theoretical stellar libraries are not huge, we'll select only the BaSeL 3.1 library. For the empirical library we choose the STELIB due to its higher resolution.

Because the Padova 1994 tracks provide the largest parameter range and the differences to other tracks are not very pronounced we select this one.

As far as the SSPs are concerned we'll end up with 231 low resolution (theoretical stellar library) and 231 high resolution (empirical stellar library) populations corresponding to the parameter combinations listed in **Table 3.2**.

3.2 Composite Stellar Populations (CSPs)

In Section 2.6 we explained that a Composite Stellar Population can be derived by convolving a Simple Stellar Population with a given Star Formation Rate (see Figure 2.10 and Equation 2.6). Throughout this section we'll only investigate populations with respect to the BaSeL 3.1 stellar spectral library and the Padova 1994 evolutionary tracks along with a Salpeter IMF between 0.1 and 100 $\mathcal{M}_\odot$. The metallicity is set to $Z = 0.0001$ in any case because comparison with other values didn't show any qualitative differences.

There are several possibilities for the kind of SFRs that are implemented in the GISSEL code (see Figure 2.6 and Appendix D in chapter "GISSEL User Manual"). We start with the simplest case; the constant SFR.

3.2.1 Constant SFR

Two CSPs have been calculated, according to the values of 1 and 5 $\mathcal{M}_\odot$ /a. The integrated spectra of these CSPs are the same, except that all the flux values of one CSP are five times larger compared to the other. We have to mention that the GISSEL code provides the spectra for a population with increasing total mass for the case of a constant SFR. This is an exception because normally, the total mass of a synthetic population is scaled to 1 $\mathcal{M}_\odot$. After all, we only keep the spectra and colours for the 1 $\mathcal{M}_\odot$ /a population.

Let's compare the spectra of the SSP with the one of the CSP calculated for a constant SFR in **Figure 3.20**. While the SSP's spectrum shows its typical changes along its temporal evolution, the spectrum of the CSP doesn't change a lot. After 20 Ga we can clearly see that the spectrum is still dominated by O- and B-stars while the contribution of F-stars is quite weak (compare spectral types in Figure 2.3).

If we compare the corresponding colours in **Figure 3.21** we can see that the temporal evolution of the two populations is more or less similar up to an age of about 2.5 Ma. Then the SSP gets redder first just to turn bluer than the CSP between 5 and about 50 Ma. The reason for this is the behaviour of the double peaked spectrum (one peak at 50 and another at 100 nm) of hot stars. At 3 Ma the peak at 50 nm of the CSP is higher than the one of the SSP, thus the CSP is bluer. At 10 Ma the peak at 100 nm of the SSP is higher than the one of the CSP, thus the SSP is bluer. But as time goes by the SSP will evolve to redder colours again due to the constant feeding of the CSP with hot blue stars.

3.2.2 Short Burst SFR

Here, the SFR is considered as a short burst of finite length at birth of the population. The parameter to be chosen is the duration of the burst t_b in Ga. We took the following values:

$$t_\mathrm{b} \in \{0.1, 0.5, 1.0, 2.0, 5.0\}$$

All the other parameters are the same as for the constant SFR. The resulting integrated spectra are presented in **Figure 3.20** for the 0.5 and the 5.0 Ga burst along with the corresponding SSP and the population with a constant SFR (see previous subsection). One can recognize that, shortly after the 0.5 Ga burst has ended, the corresponding spectrum starts to differ from the spectrum of the CSP with a constant SFR. The same behaviour can be seen for the 5.0 Ga burst spectrum. Once the burst has ended, the spectra become similar to the one of an SSP. Generally we can conclude, that the spectra of a short burst population show a temporal evolution, which is delayed by the duration of the burst (e.g., the spectrum of a 0.1 Ga burst population after 1 Ga looks the same as the spectrum of an SSP after 0.9 Ga).

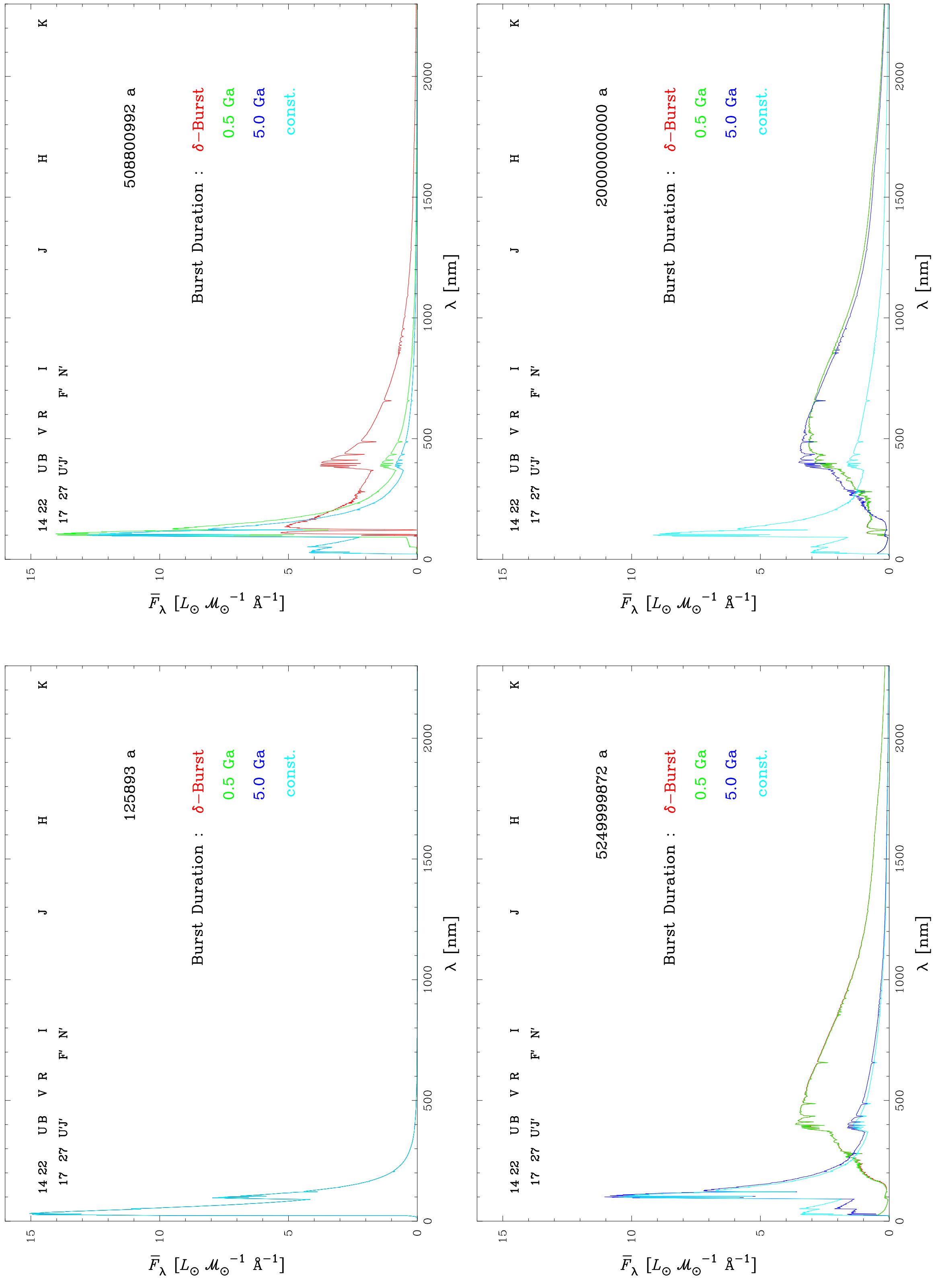

Figure 3.20: Temporal evolution of normalized integrated spectra calculated for a δ-burst, a constant, and two short burst of 0.5 and 5.0 Ga duration SFRs (Padova 1994 tracks, $Z = 0.0001$, BaSeL3.1 library, Salpeter IMF). Corresponding colours in Figure 3.21.

We now have a look at the colours in **Figure 3.21** where their temporal evolution is shown for all the five short burst populations along with the SSP and the CSP of the former subsection. Not very surprising, the colours for the short bursts show the same evolution as the constant SFR until the bursts end. Then the colours pass quite rapidly (~0.5 Ga) into the SSP colours. Qualitatively, these statements hold true for all the colours presented here, leaving us with some minor quantitative variations from one colour to another. Generally, the evolution for the constant SFR case is smoother than for the SSP or the short burst SFR populations.

For the constant and the short bursts of finite length SFRs we conclude that:

- Apart from ages around 10 Ma the constant SFR results in redder colours (up to 5 mag) than the SSP.
- Short burst SFR populations show a temporal evolution, which is delayed by the duration of the burst compared to an SSP.
- The colours of short burst SFR populations follow the same evolution as a constant SFR population until the bursts end. Then they pass into the evolution of an SSP within roughly 0.5 Ga.

3.2.3 Linearly decreasing SFR

Now we treat the case when the SFR decreases linearly. The parameter to provide is the time (in Ga) in which the SFR decreased to zero; let's call it the decrease time t_{d}. To make things comparable we chose the same values as for the short burst SFRs:

$$t_{\mathrm{d}} \in \{0.1, 0.5, 1.0, 2.0, 5.0\}$$

The integrated spectra are shown in **Figure 3.22** for the 0.5 and 5.0 Ga case along with the corresponding two short burst SFR populations from Figure 3.20. If we compare the 0.5 Ga short burst SFR spectrum with the 0.5 Ga linearly decreasing SFR spectrum, we can see that the latter has evolved a bit further than the former after 0.5 Ga. Around 1.0 Ga of age, the two spectra get nearly identical. The same holds true for the spectra belonging to SFRs of 5.0 Ga burst duration and decrease time, respectively. However, it takes about 10.0 Ga for the decreasing SFR spectrum to look similar to the short burst SFR spectrum. As a rule of thumb, we can say that the linearly decreasing SFR spectrum starts to evolve rapidly after half the decrease time and resembles more or less to a spectrum of a short burst SFR spectrum (ant thus to an SSP spectrum) after twice the decrease time.

We turn to the integrated colours of linearly decreasing SFR populations in **Figure 3.23**. In principle the statements about the integrated spectra can be verified by the integrated colours. If we compare Figure 3.23 and 3.21 we can see two things: First, there is no qualitative change from linearly decreasing SFR populations to short burst SFR populations. Second, the colours for the linearly decreasing population don't change as abruptly as for the short burst population once the bursts have ended, but they sort of move away smoothly from the colour evolution of an SSP.

Thus, we conclude for the linearly decreasing SFR populations:

- The spectra evolve after half of the decrease time and look similar to SSP spectra after twice the decrease time.

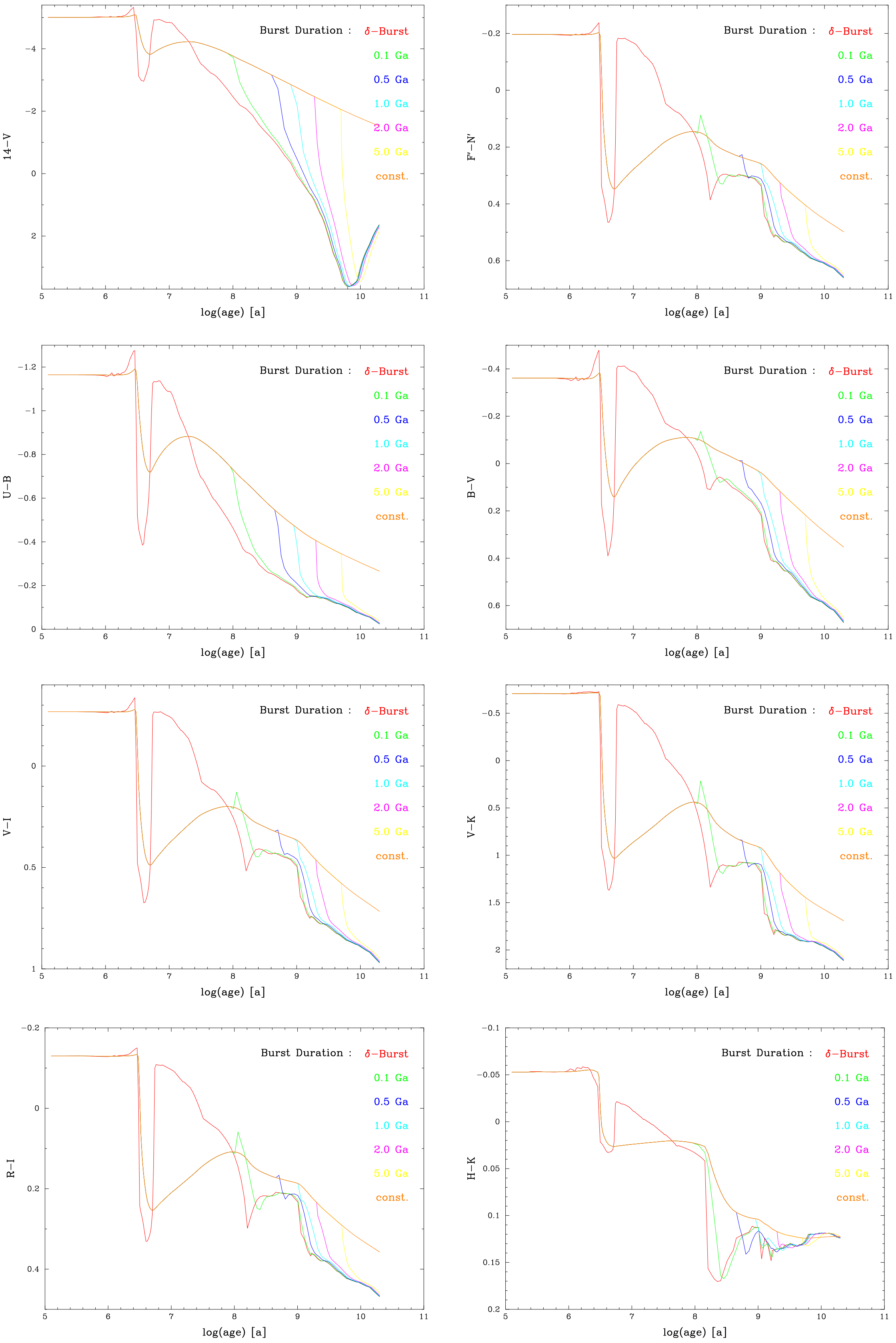

Figure 3.21: Temporal evolution of integrated colours calculated for a δ-burst, a constant, and two short burst of 0.5 and 5.0 Ga duration SFRs (Padova 1994 tracks, Z = 0.0001, BaSeL3.1 library, Salpeter IMF). Corresponding spectra in Figure 3.20.

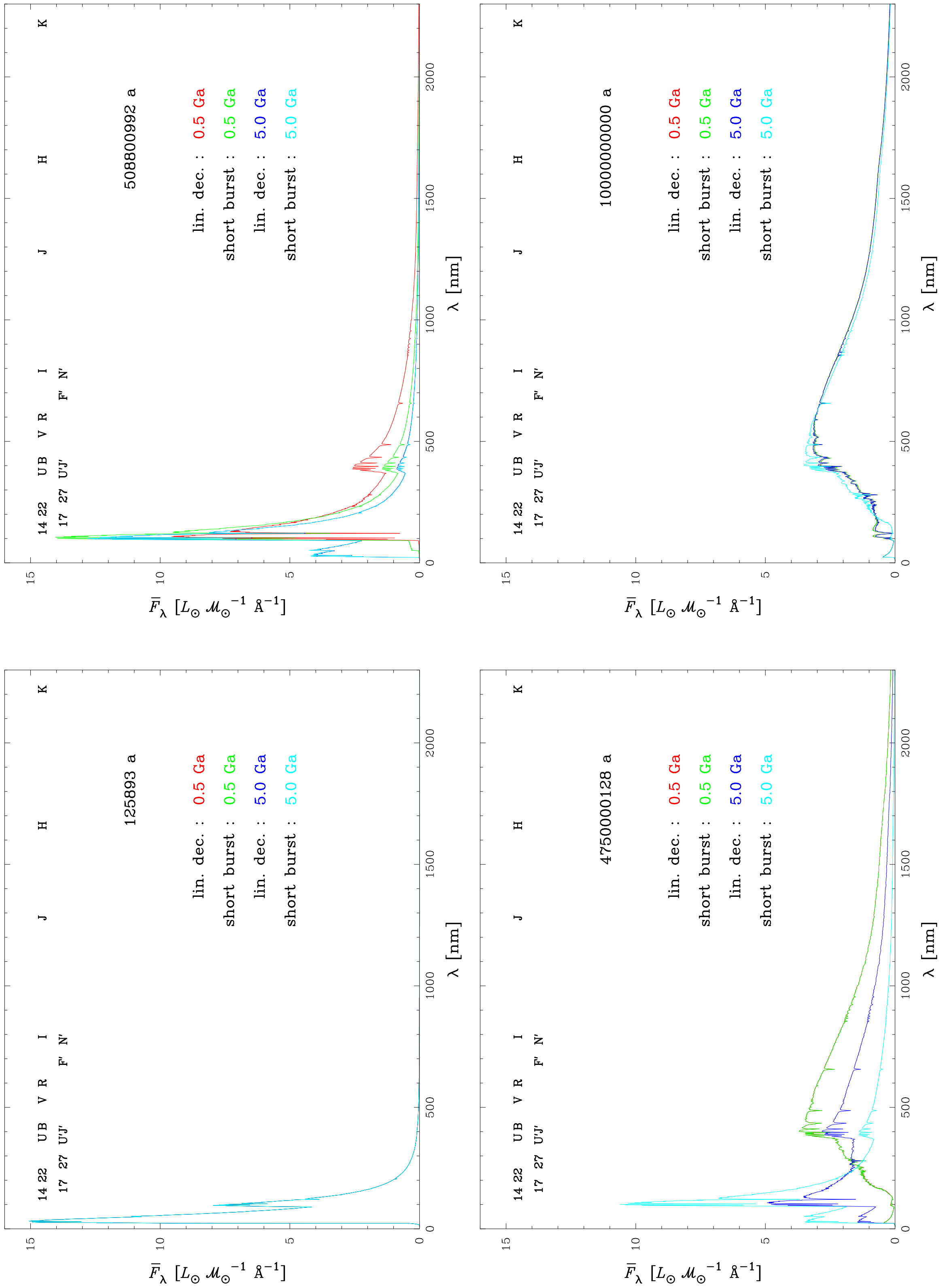

Figure 3.22: Temporal evolution of normalized integrated spectra calculated for two short burst of 0.5 and 5.0 Ga duration SFRs and two linearly decreasing SFRs of 0.5 and 5.0 Ga decrease time (Padova 1994 tracks, $Z = 0.0001$, BaSeL3.1 library, Salpeter IMF). Corresponding colours in Figure 3.23.

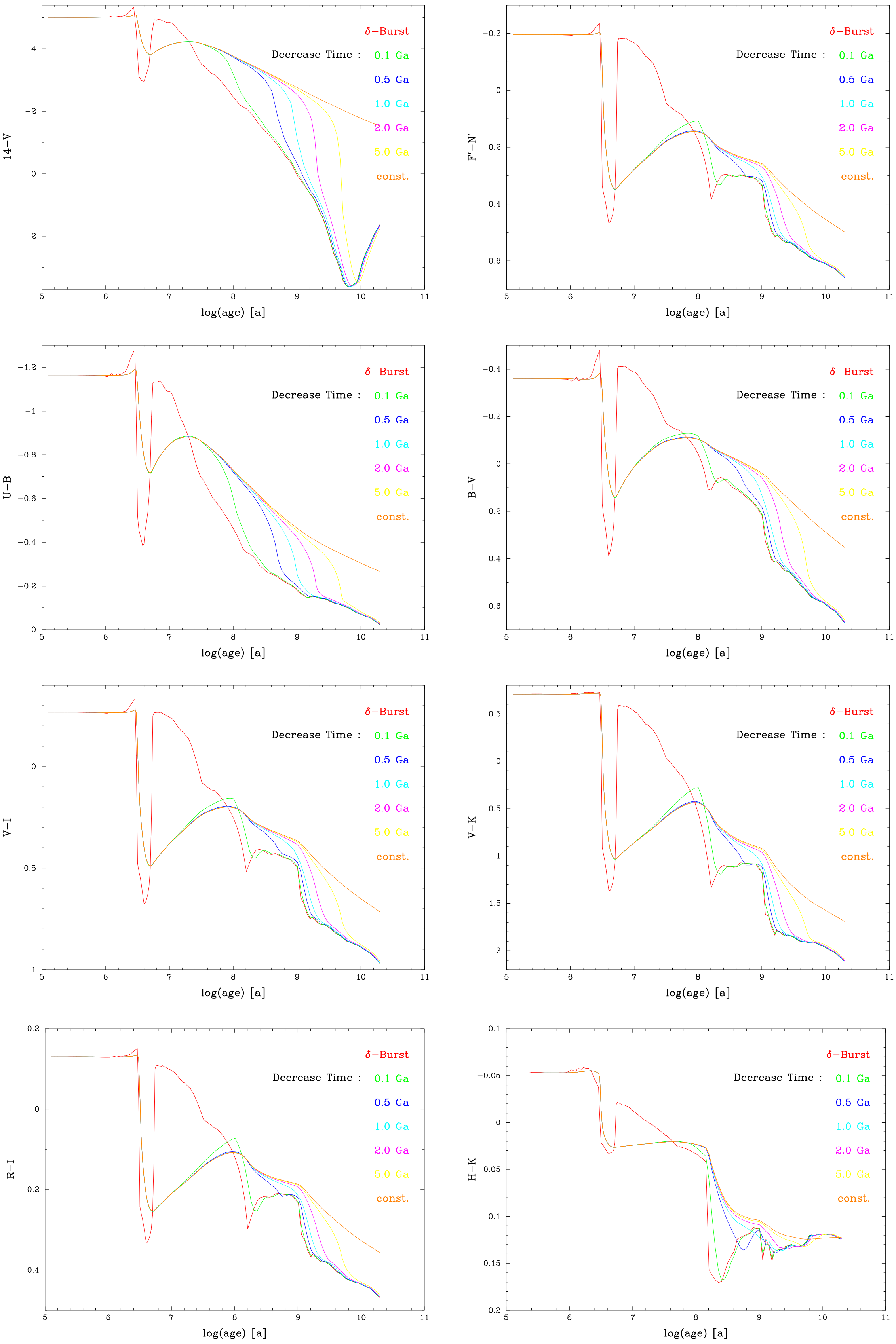

Figure 3.23: Temporal evolution of integrated colours calculated for a δ-burst, a constant, and 5 linearly decreasing SFRs (Padova 1994 tracks, $Z = 0.0001$, BaSeL3.1 library, Salpeter IMF). Corresponding spectra in Figure 3.22.

- The evolution of integrated colours is smoother than the one of short burst SFR populations.

- The spectral and the colour evolution is similar to the populations generated by short burst SFRs.

3.2.4 Exponentially decreasing SFR

The next shape of the SFR to be investigated is the exponentially decreasing SFR. Here, we have to choose the e-folding time t_{e} in Ga according to the following parametrisation:

$$\mathrm{SFR}\ (t, t_{\mathrm{e}})\ \propto\ \frac{1}{t_{\mathrm{e}}}\ \exp(\frac{-t}{t_{\mathrm{e}}})$$

For the third time we took the same values for t_{e} as before:

$$t_{\mathrm{e}} \in \{0.1,\ 0.5,\ 1.0,\ 2.0,\ 5.0\}$$

In **Figure 3.24** we show the temporal evolution of the spectra for a linearly decreasing, an exponentially decreasing, and a short burst SFR population. The decrease time, the e-folding time, and the burst duration is 1.0 Ga. We can see that between 0.5 and 1.0 Ga the exponentially decreasing SFR population evolves like the linearly decreasing with a short delay, though. As already mentioned in the section above, the short burst model looks similar to the linearly decreasing one at 2.0 Ga. The exponential model, however, stays blue, because there are still stars to be born. But after about ten times the e-folding time, the spectrum of the exponential model is similar to the two other spectra. So as a rule of thumb we can state that the spectrum of an exponentially decreasing SFR population starts to evolve after half of the e-folding time and looks similar to the spectrum of an SSP after ten times the e-folding time.

Now we have a look at the integrated colours of exponentially decreasing SFR populations in **Figure 3.25**. Again the statements about the integrated spectra can be confirmed by the integrated colours. The change in colours due to the decrease in the SFR is as smooth as in the case with linearly decreasing SFRs. Because the exponentially decreasing SFR doesn't decrease to zero after one e-folding time, the further evolution of the colours is delayed compared to the linearly decreasing SFR models. But in general, one can say that there isn't a dramatic difference in both spectra and colours if we compare short burst, linearly decreasing, and exponentially decreasing SFR populations.

For the exponentially decreasing SFR populations we conclude:

- The spectra evolve after half of the e-folding time and look similar to SSP spectra after ten times the e-folding time.

- The evolution of integrated colours is smoother than the one of short burst SFR populations.

- The spectral and the colour evolution is quite similar to the populations generated by linearly decreasing and short burst SFRs.

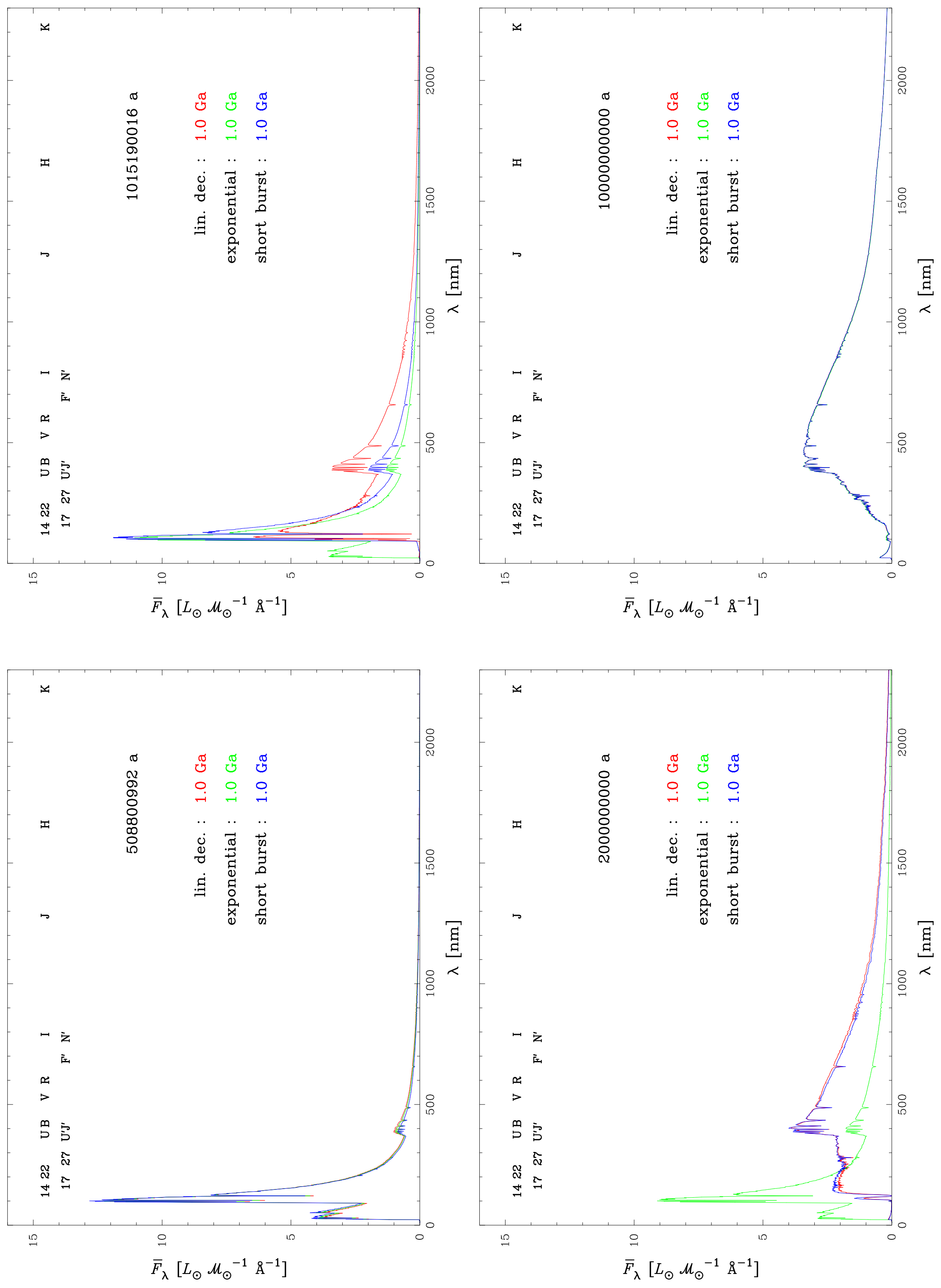

Figure 3.24: Temporal evolution of normalized integrated spectra calculated for a linearly decreasing, an exponentially decreasing, and a short burst SFR. Decrease time, e-folding time, and burst duration is set to 1.0 Ga (Padova 1994 tracks, Z = 0.0001, BaSeL3.1 library, Salpeter IMF). Corresponding colours in Figure 3.25.

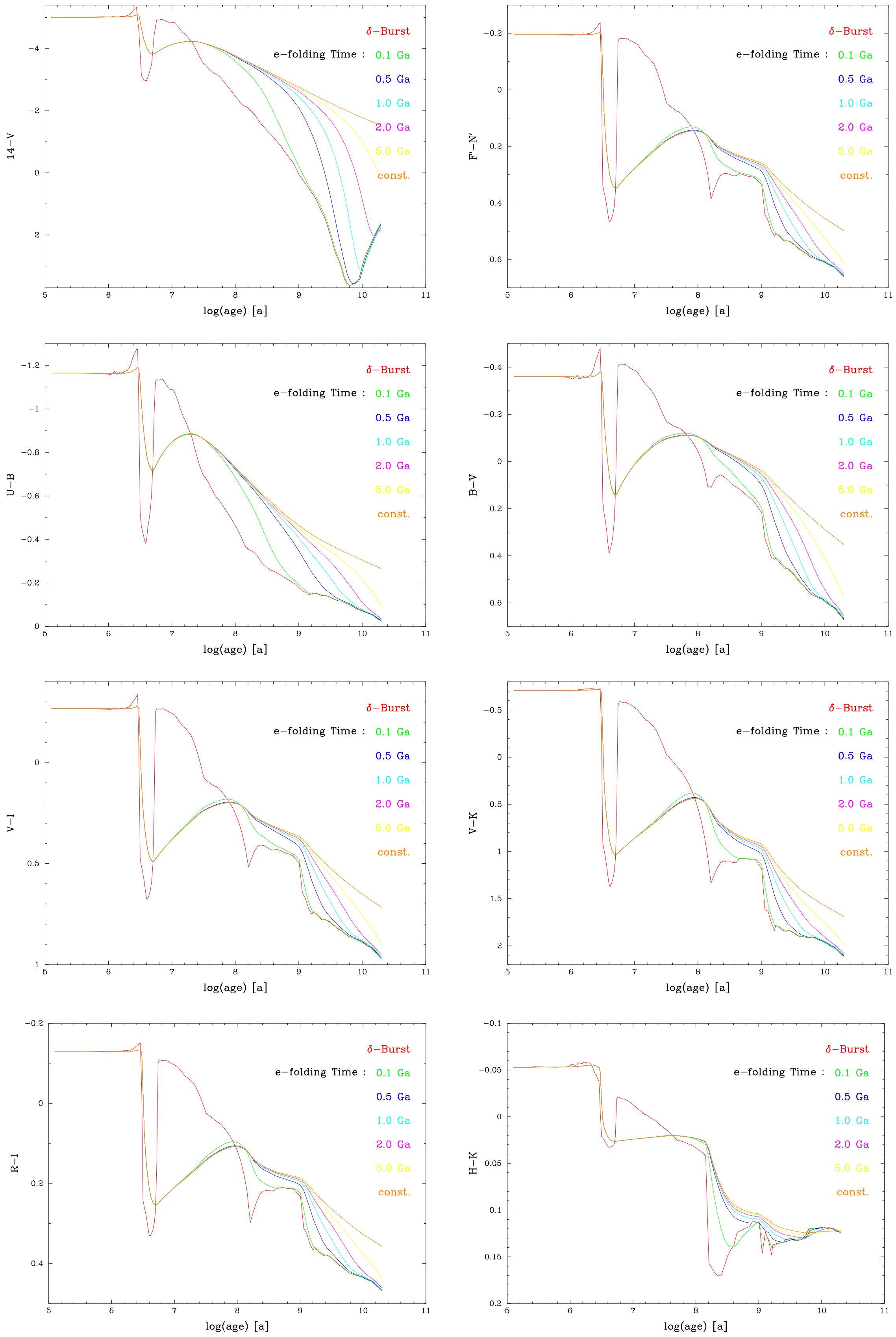

Figure 3.25: Temporal evolution of integrated colours calculated for a δ-burst, a constant, and 5 exponentially decreasing SFRs (Padova 1994 tracks, $Z = 0.0001$, BaSeL3.1 library, Salpeter IMF). Corresponding spectra in Figure 3.24.

3.2.5 Delayed SFR

The last SFR we'd like to consider is the delayed one. According to Bruzual & Kron 1980 this SFR is parameterized as follows where τ is the time of maximum star formation:

$$\text{SFR}\ (t, \tau)\ \propto\ \frac{1}{\tau}\,\frac{t}{\tau}\ \exp(\frac{-t}{\tau})$$

Again we chose τ in Ga as before:

$$\tau \in \{0.1,\, 0.5,\, 1.0,\, 2.0,\, 5.0\}$$

The corresponding temporal evolution of the spectra is presented in **Figure 3.26** along with the spectra for a linearly decreasing, a short burst, and an exponentially decreasing SFR population. The decrease time, the e-folding time, the burst duration, and the delay time is set to 0.5 Ga. We can see that after 0.25 Ga the spectra start to evolve. At 0.5 Ga the linearly decreasing SFR population shows the fastest evolution, followed by the short burst, the exponentially decreasing, and the delayed SFR population. After 1.0 Ga the spectrum for the linearly decreasing case looks similar to the short burst case, as stated above. At that time the exponentially decreasing SFR population starts to evolve before the delayed SFR population. After 10 Ga all the four spectra look similar again. So in general we can state, that the delayed SFR case is quite analogous to the exponential one: the spectra start to evolve after twice the delay time and look similar to the exponential case (and thus to the SSP case) after ten times the delay time.

If we look at the colours in **Figure 3.27** we can see that their temporal evolution is very similar to the case of the exponentially decreasing SFR in Figure 3.25. Thus the statements about the spectra we've just given hold true for the integrated colours as well.

So we conclude for the delayed SFR populations:

- The spectra evolve after twice the delay time and look similar to SSP spectra after ten times the delay time.
- The evolution of integrated colours is analogous to that of the exponentially decreasing SFR populations.
- In general, the spectral and colour evolutions are quite similar to those of the linearly decreasing, the short burst, and the exponentially decreasing SFR cases.

3.2.6 Consequences for BLoIS 1.1

Surely, we'll select the constant SFR population for BLoIS. It is worth mentioning that the other four SFR types all lie between this SFR type and the δ-burst case.

Because the short burst SFR population shows a temporal evolution, which is delayed by the duration of the burst compared to an SSP, we can in principle derive the latter from the former. So there's no need to incorporate this SFR type into BLoIS.

Since there are no dramatic differences between the linearly decreasing, the delayed, and the exponentially decreasing case, we chose the delayed SFR. The reason for this is that the delayed SFR is the most versatile of all the presented analytic functions.

As far as the CSPs are concerned, we'll end up with the SFRs and the parameters listed in **Table 3.3**. Together with the SSPs of Section 3.1 this leads to a total of 1 155 low resolution and 1 155 high resolution populations.

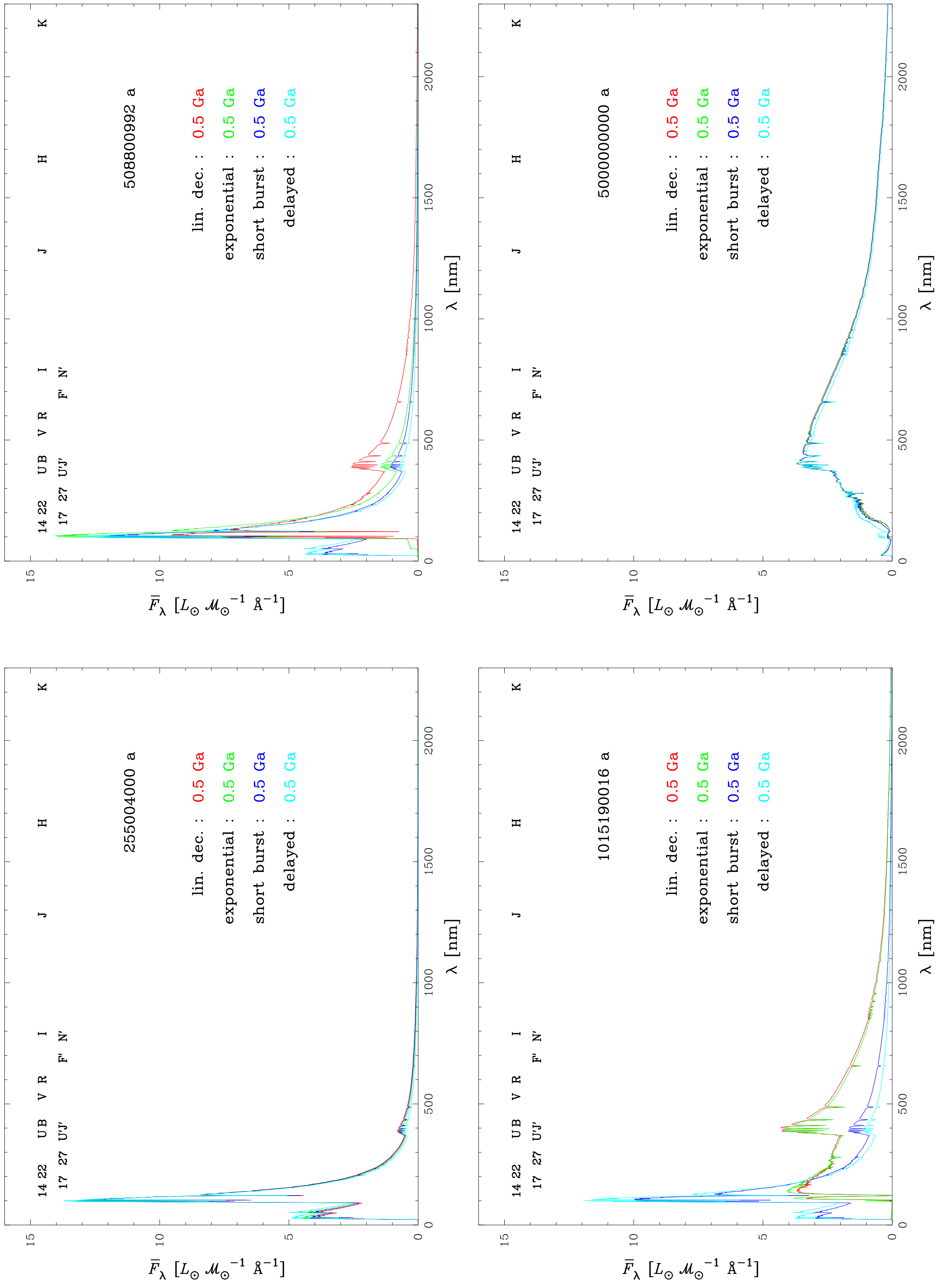

Figure 3.26: Temporal evolution of normalized integrated spectra calculated for a linearly decreasing, a short burst, an exponentially decreasing, and a delayed SFR. Decrease time, burst duration, e-folding time, and delay time is set to 0.5 Ga (Padova 1994 tracks, Z = 0.0001, BaSeL3.1 library, Salpeter IMF). Corresponding colours in Figure 3.27.

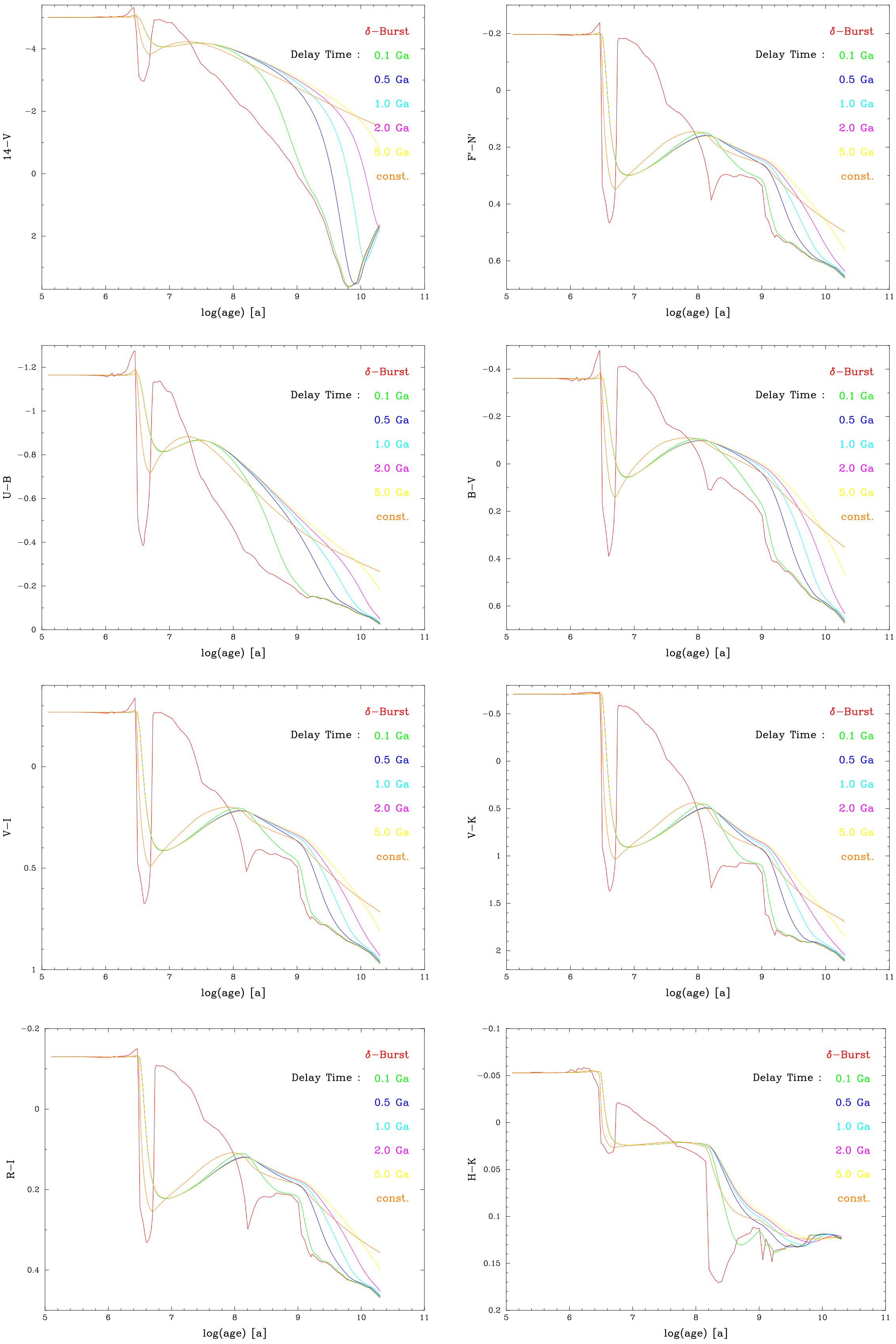

Figure 3.27: Temporal evolution of integrated colours calculated for a δ-burst, a constant, and 5 delayed SFRs (Padova 1994 tracks, $Z = 0.0001$, BaSeL3.1 library, Salpeter IMF). Corresponding spectra in Figure 3.26.

SFR
constant with 1 $\mathcal{M}_\odot$ /a
delayed with maximum at τ = 0.1 Ga
delayed with maximum at τ = 1.0 Ga
delayed with maximum at τ = 5.0 Ga

Table 3.3: Properties of CSPs in BLoIS 1.1

3.3 Samland-models

In **Figure 3.28** we show an example of a galaxy model calculated by SAMLAND. Respecting all the processes presented in Figure 2.8 and including dynamics, the evolution of 650 000 stellar particles is computed in a self consistent way. In the top left panel of Figure 3.28 the view of this model at the age of 13.5 Ga is shown face-on and edge-on in the panel to the right of it.

Because we are able to easily follow any stellar particle of interest we can decompose the model galaxy in subpopulations, e.g. according to their metallicity. This has been done for the 7 Padova 1994 metallicities (see Table 2.1) resulting in 7 subpopulations which are presented in the first two columns. Note that "z" stands for $Z_\odot$ and correspond to the 7 values of the Padova 1994 metallicities which mark the centers of metallicity ranges indicated in the panels.

The SFRs of the whole galaxy and of all the 7 subpopulations are shown in the third column. These 7 SFRs together with a set of 7 SSPs from BLoIS (in this case we took the Padova 1994 tracks, SALPETER IMF between 0.1 and 50 $\mathcal{M}_\odot$, and BaSeL 3.1 stellar spectral library), we are able to calculate the corresponding 7 CSPs using the programme "csp" (see Section 2.6 and chapter "GISSEL User Manual"). The integrated spectra of those CSPs, also at age 13.5 Ga, are presented in the fourth column. Besides the corresponding metallicity Z the proportionality factor p for each subpopulation (calculated from the masses of the subpopulations) is also indicated. Those factors help us to derive the total spectrum of the model galaxy presented in the top right panel.

The properties of this particular model are currently located in
`/neptun/usr4/stellarpop/Samland/Scd`.

3.4 File structure of BLoIS 1.1

The folder `BLoIS` is currently located in `/pluto/usr3/westera/stellarpop`. The files containing the integrated spectra and the integrated colours are all on the same level of a hierarchically structured directory tree. The hierarchy is shown in **Figure 3.29**.

The folder names are coded with numbers (bold in Figure 3.29), e.g., the spectra of a stellar population calculated with the STELIB library, with Padova 1994 tracks, at a constant SFR, with a 3.00 IMF slope, and an IMF mass range between 1 and 2 $\mathcal{M}_\odot$ are located in the folder named `BLoIS/02/01/02/03/05`.

The metallicity is coded in the filenames, e.g., file named
`bc2003_lr_m22_salp_ssp_ML010_MU002.ised` corresponds to $Z = 0.0001$. For the different

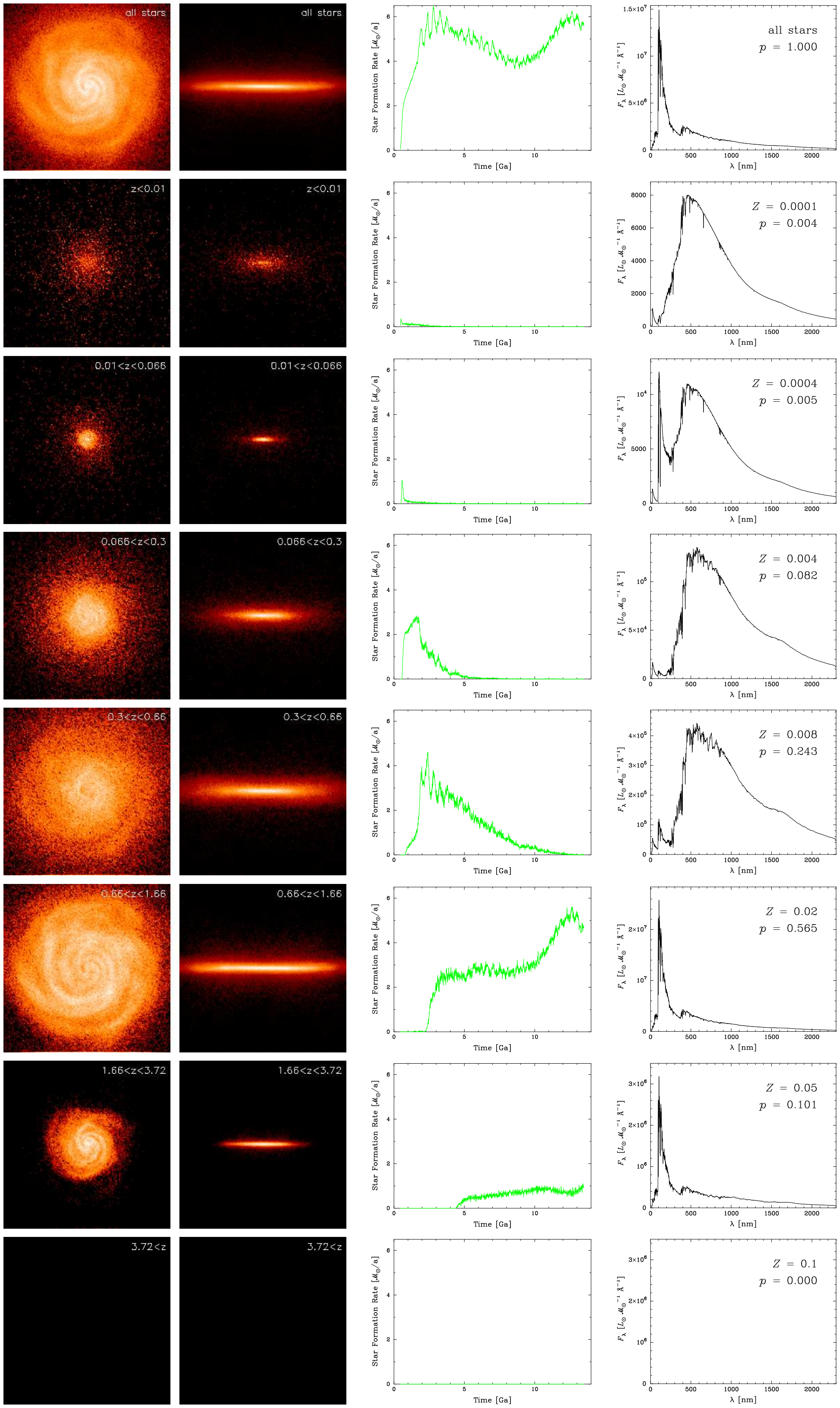

Figure 3.28: Scd-galaxy model at 13.5 Ga by Samland (Samland 2003). The first row shows the properties of all stars, whereas in row 2 to 8 the properties of 7 subpopulations corresponding to the metallicity ranges indicated in the panels. The SFRs in the third column were also calculated by Samland and were used to derive the spectra of the subpopulations in the last column. See text for details.

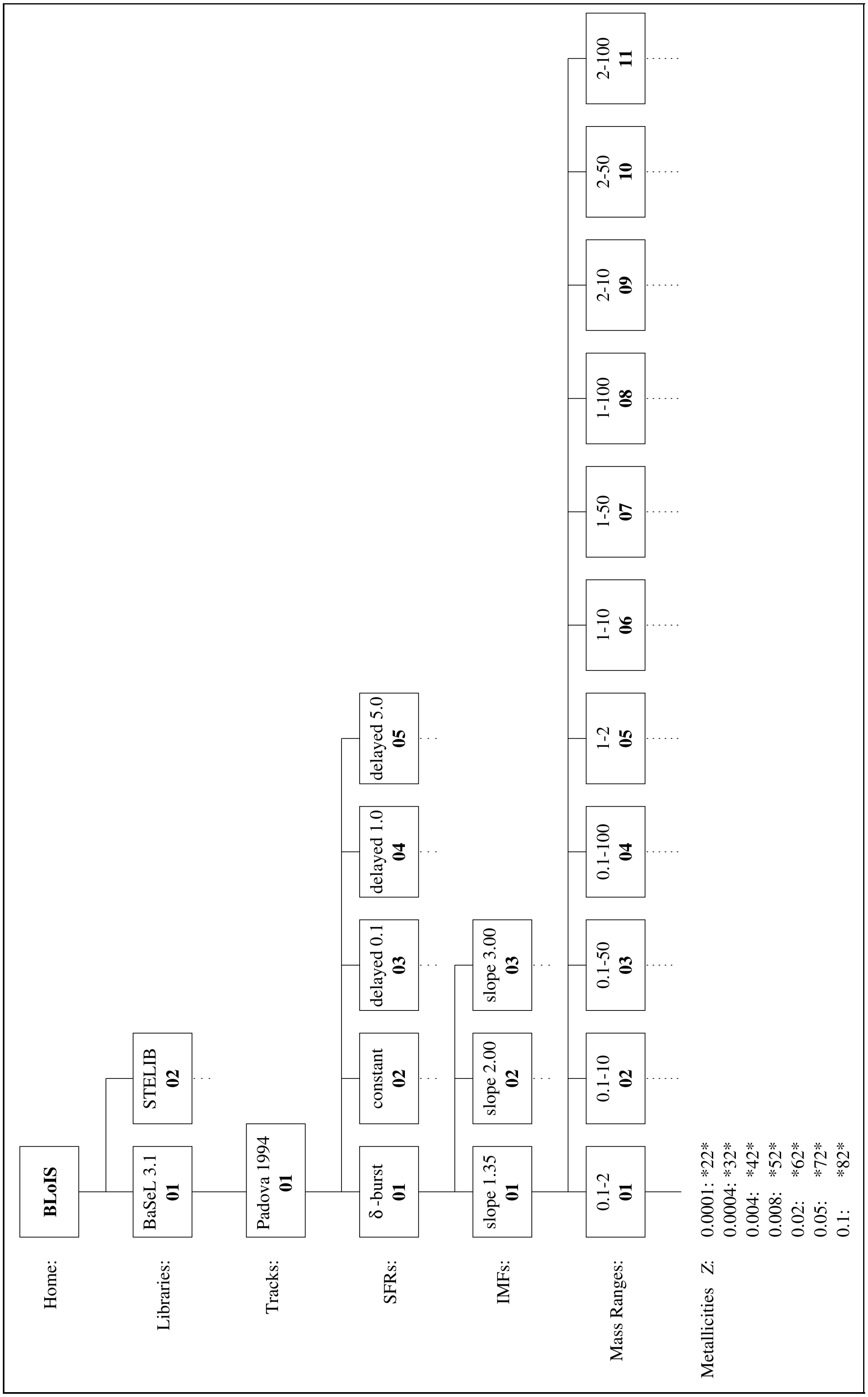
Home:
BLoIS
Libraries:
BaSeL 3.1
01
STELIB
02
Tracks:
Padova 1994
01
SFRs:
δ -burst
01
constant
02
delayed 0.1
03
delayed 1.0
04
delayed 5.0
05
IMFs:
slope 1.35
01
slope 2.00
02
slope 3.00
03
Mass Ranges:
0.1-2
01
0.1-10
02
0.1-50
03
0.1-100
04
1-2
05
1-10
06
1-50
07
1-100
08
2-10
09
2-50
10
2-100
11
Metallicities Z:
0.0001: *22*
0.0004: *32*
0.004: *42*
0.008: *52*
0.02: *62*
0.05: *72*
0.1: *82*

Figure 3.29: Directory structure of BLoIS 1.1. The different metallicities (see Table 2.1) are coded with numbers in the filenames. Bold numbers correspond to the coded folder names.

metallicities see Table 2.1.

The integrated spectra can be found in the `*.ised` files. To economise on disc space they are in binary format. One file contains 221 spectra corresponding to the 221 different ages of the population (see chapter "GISSEL User Manual"). The filenames for the low resolution spectra contain the string `_lr_` and the high resolution spectra files come with `_hr_`.

The 6 files with the integrated colours (`*.ABmag`, `*.*color`) are in ASCII-format. For the high resolution spectra there are 6 additional line strength index files (`*.*lsindx*`).

4 Fitting Methods

Data fitting and parameter estimation is one of the most widely spread tasks in natural sciences. A straightforward method to fit theory to observations is the so-called chi-square fit. It will be presented in the first section. One method of parameter estimation is the so-called least-squares adjustment technique which we shall recapitulate in the second section. There, an adapted version of this approach will be proposed. In the third section we shall present the software that will be used for the analysis of the spectral library BLoIS. Although we shall not fit models to real data within the framework of this thesis the software for this purpose is similar to the one developed for the analysis of BLoIS.

4.1 Chi-Square Fitting

One of the easiest fitting procedures is the so-called χ^2 fit. The goal of this method is to minimize the sum of squared and weighted residuals, which can be calculated as the differences between observed data and an assumed model function.

The vectorial model function $\boldsymbol{G}$ describes the mathematical relations between the observations and the parameters:

$$\boldsymbol{L} = \boldsymbol{G}(\boldsymbol{X}) \tag{4.1}$$

where $\boldsymbol{L}$: observations
$\boldsymbol{G}$: model function
$\boldsymbol{X}$: parameters

From theory we choose a set of parameters and define the parameter vector $\boldsymbol{X}$:

$$\boldsymbol{X} = \begin{pmatrix} X_1 \\ \vdots \\ X_j \\ \vdots \\ X_m \end{pmatrix} \tag{4.2}$$

where m : number of parameters

From actual measurements we obtain a set of observations along with their errors. So we can denote the observation vector $\boldsymbol{l}$ and the error vector $\boldsymbol{\varepsilon}$:

$$\boldsymbol{l} = \begin{pmatrix} l_1 \\ \vdots \\ l_i \\ \vdots \\ l_n \end{pmatrix} \qquad \boldsymbol{\varepsilon} = \begin{pmatrix} \varepsilon_1 \\ \vdots \\ \varepsilon_i \\ \vdots \\ \varepsilon_n \end{pmatrix} \tag{4.3}$$

where n : number of observations

We assume that the errors of the measurements are normally distributed:

$$\begin{aligned} \langle \varepsilon_i \rangle &= 0 \\ \langle \varepsilon_i^2 \rangle &= \sigma_i^2 \end{aligned} \tag{4.4}$$

where σ_i^2 : a priori variance of the i-th observation

Thus, we can denote χ^2 – the sum of the squared and weighted residuals – as:

$$\chi^2(\boldsymbol{X}) = \sum_{i=1}^{n} \left\{ \frac{[\,l_i - \boldsymbol{G}(\boldsymbol{X})\,]^2}{{\sigma_i}^2} \right\} \tag{4.5}$$

The goal of χ^2 fitting is to minimize this expression by assuming not only different model functions but also different sets of parameters.

Usually, our observations come as data points measured with respect to another quantity (e.g. time). This argument quantity is considered as error free. So the observation vector $\boldsymbol{l}$ in Equation 4.3 becomes:

$$\boldsymbol{l} = \begin{pmatrix} (t_1, l_1) \\ \vdots \\ (t_i, l_i) \\ \vdots \\ (t_n, l_n) \end{pmatrix} \tag{4.6}$$

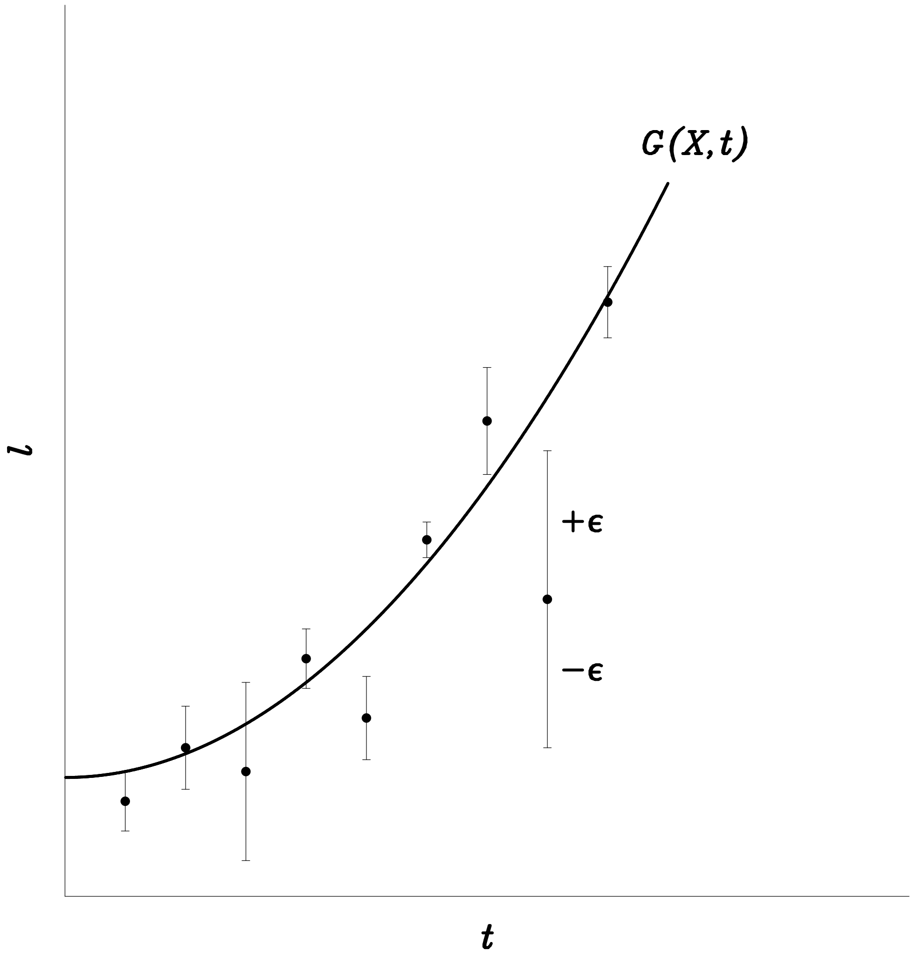

Figure 4.1: Schematic drawing of the observational situation where l_i, t_i, and ε_i are the observations, the arguments, and the errors, respectively. $\boldsymbol{G}(\boldsymbol{X}, t)$ is the model function.

where t_i : i-th argument

In **Figure 4.1** we explain this situation with a schematic drawing. With this notation, the expression for χ^2 in Equation 4.5 becomes:

$$\chi^2(\boldsymbol{X}) = \sum_{i=1}^{n} \left\{ \frac{[(t_i, l_i) - \boldsymbol{G}(\boldsymbol{X}, t_i)]^2}{{\sigma_i}^2} \right\} \tag{4.7}$$

Note that $\boldsymbol{G}$ is an analytic function and that the expression $\boldsymbol{G}(\boldsymbol{X}, t_i)$ provides the value of this function at the position t_i.

As we have seen in Section 2.6 evolutionary synthesis uses a set of input parameters to calculate a particular model. In this sense *the model represents the input parameters.* But there is no model function $\boldsymbol{G}$ that would describe the relations between the input parameters and the models. In the context of χ^2 fitting this is not a problem because we can simply replace the value of the model function at a certain position by the value of the model at this position.

Analog to the observation vector we define the model vector $\boldsymbol{M}$ as:

$$\boldsymbol{M} = \begin{pmatrix} (t_1, M_1) \\ \vdots \\ (t_i, M_i) \\ \vdots \\ (t_n, M_n) \end{pmatrix} \tag{4.8}$$

With these definitions the formula for χ^2 looks like this:

$$\chi^2(\boldsymbol{M}) = \sum_{i=1}^{n} \left\{ \frac{[(t_i, l_i) - (t_i, M_i)]^2}{{\sigma_i}^2} \right\} \tag{4.9}$$

Now there is not just one model. Instead, we have different sets of input parameters that lead to different models. So we replace the model vector by the model matrix $\boldsymbol{M}_j$:

$$\boldsymbol{M}_j = \begin{pmatrix} (t_1, M_{11}) & \dots & (t_1, M_{1j}) & \dots & (t_1, M_{1m}) \\ \vdots & & \vdots & & \vdots \\ (t_i, M_{i1}) & \dots & (t_i, M_{ij}) & \dots & (t_i, M_{im}) \\ \vdots & & \vdots & & \vdots \\ (t_n, M_{n1}) & \dots & (t_n, M_{nj}) & \dots & (t_n, M_{nm}) \end{pmatrix} \tag{4.10}$$

where m : number of models (or sets of input parameters)

Note that m no longer represents the number of parameters. The number of input parameters for the evolutionary synthesis algorithm has no importance to the χ^2 fit.

In the context of evolutionary synthesis we end up with the final expression for the χ^2 of the j-th model:

$$\chi^2(\boldsymbol{M}_j) = \sum_{i=1}^{n} \left\{ \frac{[(t_i, l_i) - (t_i, M_{ij})]^2}{{\sigma_i}^2} \right\} \tag{4.11}$$

The goal of minimizing this expression can be achived by assuming different models, i.e., different sets of input parameters for the evolutionary synthesis algorithm.

4.2 Least-Squares Adjustment (LSA)

As explained in the former section , we can assume a model function $\boldsymbol{G}$ that describes the functional relations between the observations and the parameters (see Equation 4.1):

$$\boldsymbol{L} \; = \; \boldsymbol{G}(\boldsymbol{X}) \tag{4.12}$$

where $\boldsymbol{L}$: observations
$\boldsymbol{G}$: model function
$\boldsymbol{X}$: parameters

For the most simple case, i.e., where there is a linear relation between the observations and the parameters, we can formulate the observation equation system as follows:

$$\boldsymbol{A}\,\boldsymbol{x} \; = \; \boldsymbol{l} + \boldsymbol{v} \tag{4.13}$$

where $\boldsymbol{A} = \left(\frac{\partial \boldsymbol{G}}{\partial \boldsymbol{x}} \right)$: first design (or Jacobi) matrix

$$\boldsymbol{x} = \begin{pmatrix} \boldsymbol{x}_1 \\ \vdots \\ \boldsymbol{x}_j \\ \vdots \\ \boldsymbol{x}_m \end{pmatrix}$$: solution vector

m : number of parameters

$$\boldsymbol{l} = \begin{pmatrix} \boldsymbol{l}_1 \\ \vdots \\ \boldsymbol{l}_i \\ \vdots \\ \boldsymbol{l}_n \end{pmatrix}$$: observation vector

$$\boldsymbol{v} = \begin{pmatrix} \boldsymbol{v}_1 \\ \vdots \\ \boldsymbol{v}_i \\ \vdots \\ \boldsymbol{v}_n \end{pmatrix}$$: residual vector

n : number of observations

The solution vector $\boldsymbol{x}$ can be written as:

$$\boldsymbol{x} = (\boldsymbol{A}^T \boldsymbol{A})^{-1} \boldsymbol{A}^T \boldsymbol{l} \tag{4.14}$$

As for the χ^2 fit we assume that the errors ε_i of the observations are normally distributed:

$$\begin{aligned} \langle \varepsilon_i \rangle &= 0 \\ \langle \varepsilon_i^2 \rangle &= \sigma_i^2 \end{aligned} \tag{4.15}$$

where σ_i^2 : a priori variance of the i-th observation

If the errors are not correlated the stochastic model for the observations can be described by a diagonal weight matrix $\boldsymbol{P}$:

$$\boldsymbol{P} = \sigma_0^2 \begin{pmatrix} \frac{1}{\sigma_1^2} & & & & 0 \\ & \ddots & & & \\ & & \frac{1}{\sigma_i^2} & & \\ & & & \ddots & \\ 0 & & & & \frac{1}{\sigma_n^2} \end{pmatrix} \tag{4.16}$$

where σ_0^2 : a priori variance of unit weight
σ_i^2 : a priori variance of the i-th observation

Thus, the solution vector $\boldsymbol{x}$ in Equation 4.14 becomes:

$$\boldsymbol{x} = (\boldsymbol{A}^T \boldsymbol{P}\, \boldsymbol{A})^{-1} \boldsymbol{A}^T \boldsymbol{P}\, \boldsymbol{l} \tag{4.17}$$

The estimated standard deviation of unit weight m_0 (or root mean square error "RMS") is computed as:

$$m_0 = \sqrt{\frac{\boldsymbol{v}^T \boldsymbol{P}\, \boldsymbol{v}}{f}} \tag{4.18}$$

where $\boldsymbol{v}^T \boldsymbol{P} \boldsymbol{v} = \boldsymbol{l}^T \boldsymbol{P} \boldsymbol{l} - \boldsymbol{x} \boldsymbol{A}^T \boldsymbol{P} \boldsymbol{l}$
$f = n - m > 0$: degree of freedom

The estimated standard deviations of the individual model parameters m_x are:

$$m_x = m_0 \sqrt{q_{jj}} \tag{4.19}$$

where q_{jj} : j-th diagonal element of the matrix $\boldsymbol{Q}$
$\boldsymbol{Q} = (\boldsymbol{A}^T \boldsymbol{P} \boldsymbol{A})^{-1}$: cofactor matrix of the model parameters (or inverse normal equation matrix)

The goal of the least-squares adjustment is to minimize the expression $\boldsymbol{v}^T \boldsymbol{P} \boldsymbol{v}$ by assuming different model functions. Unlike to the χ^2 fitting technique, we don't have to assume parameters because they are estimated in the adjustment process.

As we have mentioned in the former section, evolutionary synthesis uses input parameters to calculate models. But there is no model function that would describe the relations between the input parameters and the models. As the least-squares adjustment technique calculates the unknown parameters of an assumed model function, this approach seems useless in the context of evolutionary synthesis.

But still there's a way of fitting models to observations taking advantage of the parameter estimation technique just presented; let's call it "least-squares fitting".

We denote the observation equation system like in Equation 4.13, but replace the first design matrix by the model matrix (see Equation 4.10):

$$\boldsymbol{M}\, \boldsymbol{x} = \boldsymbol{l} + \boldsymbol{v} \tag{4.20}$$

In explicit form the new observation equation system looks like this:

$$\begin{pmatrix} (t_1, M_{11}) & \dots & (t_1, M_{1j}) & \dots & (t_1, M_{1m}) \\ \vdots & & \vdots & & \vdots \\ (t_i, M_{i1}) & \dots & (t_i, M_{ij}) & \dots & (t_i, M_{im}) \\ \vdots & & \vdots & & \vdots \\ (t_n, M_{n1}) & \dots & (t_n, M_{nj}) & \dots & (t_n, M_{nm}) \end{pmatrix} \begin{pmatrix} x_1 \\ \vdots \\ x_j \\ \vdots \\ x_m \end{pmatrix} = \begin{pmatrix} l_1 \\ \vdots \\ l_i \\ \vdots \\ l_n \end{pmatrix} + \begin{pmatrix} v_1 \\ \vdots \\ v_i \\ \vdots \\ v_n \end{pmatrix} \tag{4.21}$$

where m : number of models (or sets of input parameters)

Instead of the partial derivatives of the function model with respect to the unknown parameters, we directly assign the models that were calculated using different sets of input parameters. Thus, the solution vector $\boldsymbol{x}$ in Equation 4.20 does no longer represent the unknown parameters of an assumed model function. Instead, we can treat the model spectra as model vectors (see Equation 4.8) and state:

On condition that all the model vectors are linearly independent, the j-th element in the solution vector $\boldsymbol{x}$ is equal to one, if the j-th model is identical to the observation.

Here's a simple example:

$$\begin{pmatrix} 1 & 5 & 9 \\ 2 & 6 & 10 \\ 3 & 7 & 11 \\ 4 & 8 & 12 \end{pmatrix} \begin{pmatrix} 0 \\ 1 \\ 0 \end{pmatrix} = \begin{pmatrix} 5 \\ 6 \\ 7 \\ 8 \end{pmatrix} \tag{4.22}$$

In practice no model will fit the observation exactly. So we will have to search for the one element in the solution vector that is closest to one.

Like for the χ^2 fit we achieve the goal of minimizing the expression $\boldsymbol{v}^T \boldsymbol{P}\ \boldsymbol{v}$ by assuming different models, i.e., different sets of input parameters for the evolutionary synthesis algorithm.

4.3 Software

Both methods of the former sections have been applied to analyse BLoIS, treat the age-metallicity degeneracy, and to put constraints on observations. The first subsection deals with chi-square fitting and the second with least-squares techniques. All programmes are written in FORTRAN.

4.3.1 SPECFIT, SPECFITSIM, COLFIT, COLFITSIM

SPECFIT

In Chapter 2 we saw that one important output quantity of the evolutionary synthesis algorithm GISSEL is the integrated spectrum of a stellar population; the so-called integrated spectral energy distribution ISED. Each model population consists of 221 ISEDs corresponding to 221 ages from 0 to 20 Ga. Each ISED consists of 1 221 or 6 900 flux values, depending on the chosen stellar spectral library. For an example of a low resolution spectrum see Figure 4.4.

The purpose of the programme "SPECFIT" is to fit model spectra to observations. Following the χ^2 fitting scheme of Section 4.1 we set the observation vector $\boldsymbol{f}$ from Equation 4.6 as follows:

$$\boldsymbol{f} = \begin{pmatrix} (\lambda_1, f_1) \\ \vdots \\ (\lambda_i, f_i) \\ \vdots \\ (\lambda_n, f_n) \end{pmatrix} \tag{4.23}$$

where λ_i : i-th wavelength value of the observation
f_i : i-th flux value of the observation
n : number of observed flux values

Then we denote the model matrix $\boldsymbol{F}_j$ according to Equation 4.10 as:

$$\boldsymbol{F}_j = \begin{pmatrix} (\lambda_1, F_{11}) & \dots & (\lambda_1, F_{1j}) & \dots & (\lambda_1, F_{1m}) \\ \vdots & & \vdots & & \vdots \\ (\lambda_i, F_{i1}) & \dots & (\lambda_i, F_{ij}) & \dots & (\lambda_i, F_{im}) \\ \vdots & & \vdots & & \vdots \\ (\lambda_n, F_{n1}) & \dots & (\lambda_n, F_{nj}) & \dots & (\lambda_n, F_{nm}) \end{pmatrix} \tag{4.24}$$

where F_{ij} : i-th flux value of the j-th model
m : number of models (or sets of input parameters)

From Equation 4.11 we get the expression for χ^2 of the j-th model:

$$\chi^2(\boldsymbol{F}_j) = \sum_{i=1}^{n} \left\{ \frac{[(\lambda_i, f_i) - (\lambda_i, F_{ij})]^2}{{\sigma_i}^2} \right\} \tag{4.25}$$

It is worth noting that the observed flux values correspond to the same wavelength values as the models. In practice this won't be the case; so there will be the need for choosing a homogeneous wavelength sequence.

Next we'd like to explain the programme "SPECFIT" by the flow chart in **Figure 4.2**. We start with reading the observed spectrum and the corresponding errors. Then we can normalize the observed spectrum if necessary. The normalized spectrum $\bar{\boldsymbol{f}}$ is produced by scaling all flux values by the mean of all flux values as follows:

$$\bar{\boldsymbol{f}} = \frac{\boldsymbol{f}}{\frac{1}{n} \sum_{i=1}^{n} f_i} \tag{4.26}$$

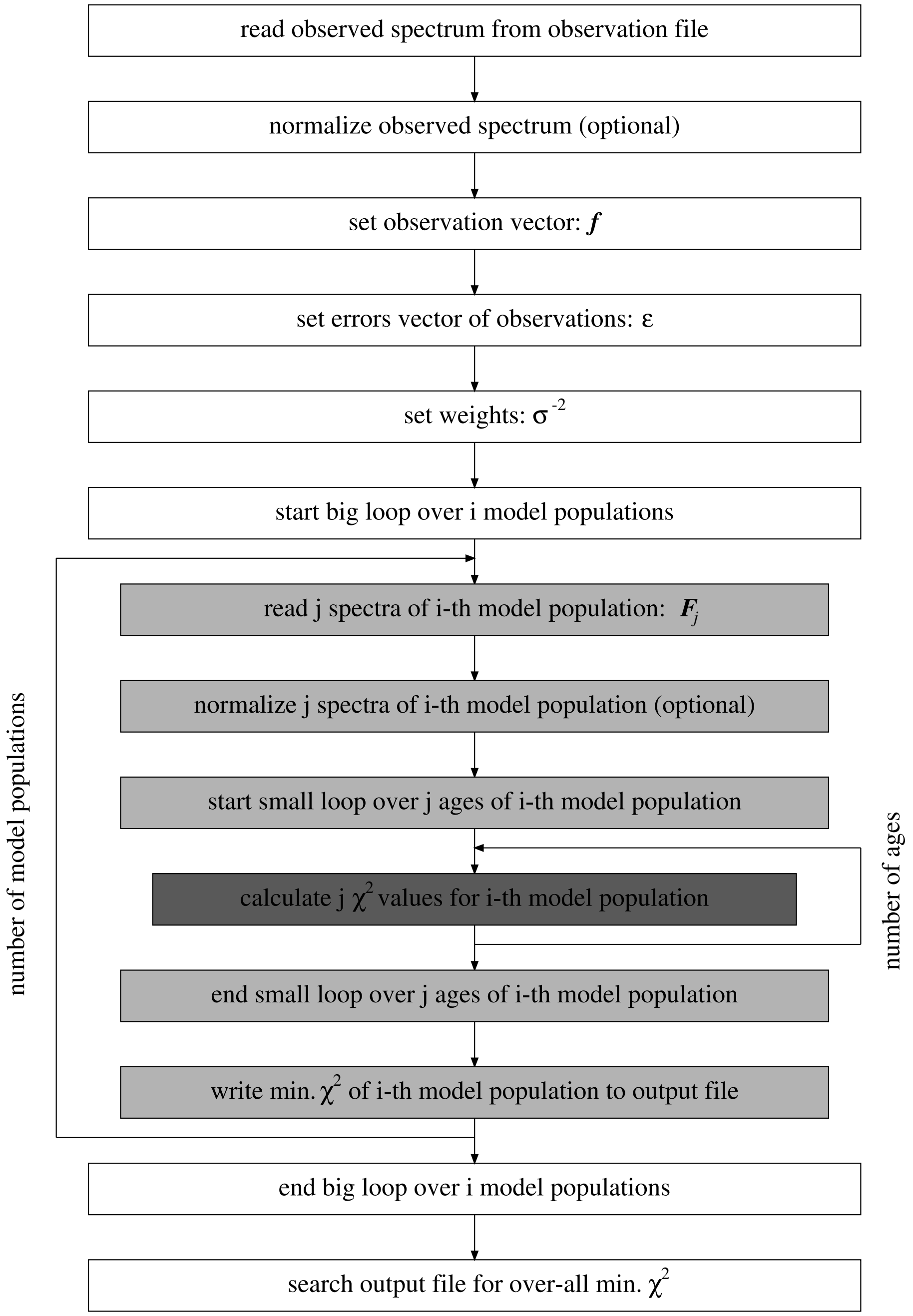
read observed spectrum from observation file
normalize observed spectrum (optional)
set observation vector: $\boldsymbol{f}$
set errors vector of observations: ε
set weights: σ^{-2}
start big loop over i model populations
read j spectra of i-th model population: $\boldsymbol{F}_j$
normalize j spectra of i-th model population (optional)
start small loop over j ages of i-th model population
calculate j χ^2 values for i-th model population
end small loop over j ages of i-th model population
write min. χ^2 of i-th model population to output file
end big loop over i model populations
search output file for over-all min. χ^2
number of model populations
number of ages

Figure 4.2: Flow chart of SPECFIT

Whether we have to normalize the spectra depends on the kind of question we'd like to answer. Apart from the model populations calculated with a constant SFR the unit of the ISEDs is $L_{\odot}/\mathcal{M}_{\odot}$ /Å. If one likes to fit the integral spectrum of an observed population one would have to know the exact mass of this population in order to scale the model spectrum correctly. Most of the time this is not the case, so we'll end up with normalizing both observed and model flux first and then perform the fit.

The next two steps of the programme consist in setting the observation vector $\boldsymbol{f}$ as in Equation 4.23 and the error vector ε as in Equation 4.3.

Then we define the proper weights to be used for the residuals. According to Equations 4.15 and 4.16 the weights $1/\sigma_i^2$ are set as:

$$\frac{1}{\sigma_i^2} = \frac{1}{\varepsilon_i^2} \tag{4.27}$$

Measurements with larger errors will result in smaller weights to the corresponding residua and vice versa.

Now we are ready to start the big loop over all i model populations. It begins with reading (and optionally normalizing) all j spectra of the i-th model population in order to set the model matrix $\boldsymbol{F}_j$ as in Equation 4.24. So i is the number of model populations (up to 1 155) and j is the number of ages (here 221) of one model population.

Afterwards we can start the small loop over all j ages to calculate the corresponding j χ^2 values of the i-th population according to Equation 4.25.

Having left the small loop, the minimum χ^2 value of the i-th population is written to the output file. The reason for keeping only the smallest χ^2 value of one model population is that we'd like to compare model populations and not spectra within one model population. Here's an example of such an output list showing the χ^2 values, the age number, and the name of the model file:

```
0.040890973   221   /BLoIS/01/01/01/01/01/bc2003_lr_m22_salp_ssp_ML010_MU002.ised
0.097598152   221   /BLoIS/01/01/01/01/01/bc2003_lr_m32_salp_ssp_ML010_MU002.ised
0.110467956   138   /BLoIS/01/01/01/01/01/bc2003_lr_m42_salp_ssp_ML010_MU002.ised
0.150373758   139   /BLoIS/01/01/01/01/01/bc2003_lr_m52_salp_ssp_ML010_MU002.ised
0.195036394   139   /BLoIS/01/01/01/01/01/bc2003_lr_m62_salp_ssp_ML010_MU002.ised
0.283086573   139   /BLoIS/01/01/01/01/01/bc2003_lr_m72_salp_ssp_ML010_MU002.ised
0.154152581   131   /BLoIS/01/01/01/01/01/bc2003_lr_m82_salp_ssp_ML010_MU002.ised
0.040890800   221   /BLoIS/01/01/01/01/02/bc2003_lr_m22_salp_ssp_ML010_MU010.ised
0.097598138   221   /BLoIS/01/01/01/01/02/bc2003_lr_m32_salp_ssp_ML010_MU010.ised
0.110259606   138   /BLoIS/01/01/01/01/02/bc2003_lr_m42_salp_ssp_ML010_MU010.ised
```

The output file will then be searched for the over-all minimum χ^2 after leaving the big loop. The best fitting model spectrum along with it's properties is written on the screen in the end.

The calculation of a maximum of 1 155 model populations (i.e. 255 255 model spectra) χ^2 fit to a low resolution spectrum (1 221 flux values) takes about 10 minutes on an Alpha 500 MHz workstation.

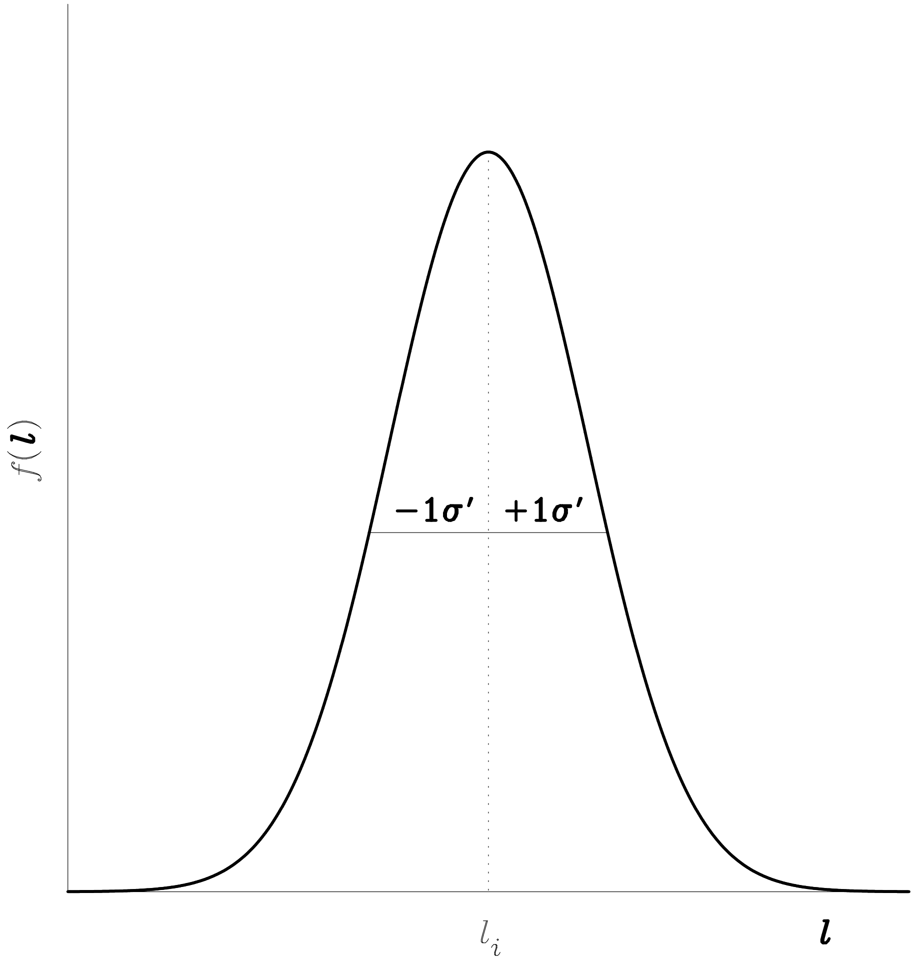

Figure 4.3: Probability density function $f(\boldsymbol{l})$ for the normal distribution.

SPECFITSIM

There is a version of "SPECFIT" for Monte Carlo simulation called "SPECFITSIM". The purpose of this programme is to add artificial noise to a model spectrum which will be treated as an observed spectrum in order to study the effects on the behaviour of the χ^2 fit. After setting the observation vector $\boldsymbol{f}$ like in "SPECFIT" normally distributed noise can be applied to $\boldsymbol{f}$. One can enter the percentage p that leads to individual *relative* 1 σ' noise values for each *absolute* flux value: 1 $\sigma_i' = p\, f_i$ (please don't confuse σ_i' with σ_i in Equation 4.27). As shown in **Figure 4.3** 69 % of the simulated flux values will lie between the positive and the negative 1 σ_i' boundary. Note that we have chosen the general notation for the observation vector $\boldsymbol{l}$ in order to avoid confusion between the observed flux values $\boldsymbol{f}$ and the probability density function f. The percentage p can be used to calculate the more common term "signal to noise" by S/N = $100/p$. In **Figure 4.4** we show an illustrative example of a low resolution spectrum from BLoIS without and with noise at a level of $p = 0.1$ or S/N = 10.

It is questionable, though, whether choosing *absolute* noise would be better than relative noise. But as the flux values cover a large range (up to orders of magnitudes) within one population, relative noise is considered as adequate enough. Besides one always has to be

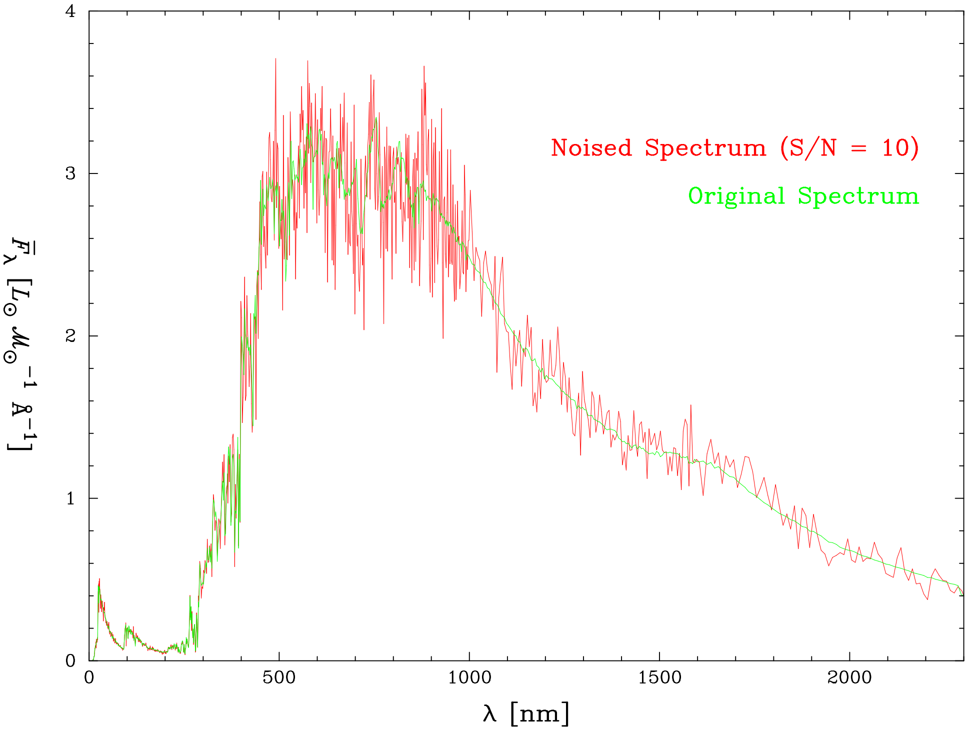

Figure 4.4: Example of a model spectrum from BLoIS without and with noise at a level of S/N = 10.

aware of negative flux values.

The simulation then is done by performing a chosen number of very big loops (here 1 000) over the whole χ^2 fit procedure writing only one over-all minimum χ^2 value per loop to an output file. Then the statistics in interest can be done by analysing this file.

A 1 000 runs simulation including 7 model populations (1 547 spectra) takes about 5 minutes on a 500 MHz Alpha workstation.

COLFIT

Analogously to "SPECFIT" we have written "COLFIT", which performs a χ^2 fit on the basis of integrated colours. In principle colour magnitudes can be regarded as *reduced integrated spectra*. Instead of having e.g. 1 221 flux values at certain wavelength points we only have a handful of colour magnitudes to characterize the energy distribution of a population in a certain wavelength area. The actual colours are then calculated as magnitude differences. For an illustrative example see Figure 4.6.

With this in mind we can denote the observation vector $\boldsymbol{c}$ in Equation 4.6 as:

$$\boldsymbol{c} = \begin{pmatrix} (\Delta m_1, c_1) \\ \vdots \\ (\Delta m_i, c_i) \\ \vdots \\ (\Delta m_n, c_n) \end{pmatrix} \tag{4.28}$$

where Δm_i : i-th magnitude difference of the observation
c_i : i-th colour value of the observation
n : number of observed colour values

According to Equation 4.10 we can set the model matrix $\boldsymbol{C}_j$ as follows:

$$\boldsymbol{C}_j = \begin{pmatrix} (\Delta m_1, C_{11}) & \dots & (\Delta m_1, C_{1j}) & \dots & (\Delta m_1, C_{1m}) \\ \vdots & & \vdots & & \vdots \\ (\Delta m_i, C_{i1}) & \dots & (\Delta m_i, C_{ij}) & \dots & (\Delta m_i, C_{im}) \\ \vdots & & \vdots & & \vdots \\ (\Delta m_n, C_{n1}) & \dots & (\Delta m_n, C_{nj}) & \dots & (\Delta m_n, C_{nm}) \end{pmatrix} \tag{4.29}$$

where C_{ij} : i-th colour value of the j-th model
m : number of models (or sets of input parameters)

Equation 4.11 then provides the expression for χ^2 of the j-th model:

$$\chi^2(\boldsymbol{C}_j) = \sum_{i=1}^{n} \left\{ \frac{[\,(\Delta m_i, c_i) - (\Delta m_i, C_{ij})\,]^2}{\sigma_i{}^2} \right\} \tag{4.30}$$

Note that both the observed and the model colours have to be defined in the same photometric system. If this isn't the case one will first have to derive the model colours by synthetic photometry of the model spectra, using the same passbands as the observed colours.

Then we are set for the programme "COLFIT" which is explained in the flow chart in **Figure 4.5**. The structure of this programme is quite identical to "SPECFIT". One difference though is that we do not have to normalize the colours because they are independent of the mass (and the distance) of an observed population. The second difference is, that we don't have a model spectrum with a certain amount of flux values but a set of colours (here 24) per model population and per age.

A full χ^2 fit over 1 155 model populations (255 255 sets of colours, 24 colours per set) takes about 1 minute on a 500 MHz Alpha workstation.

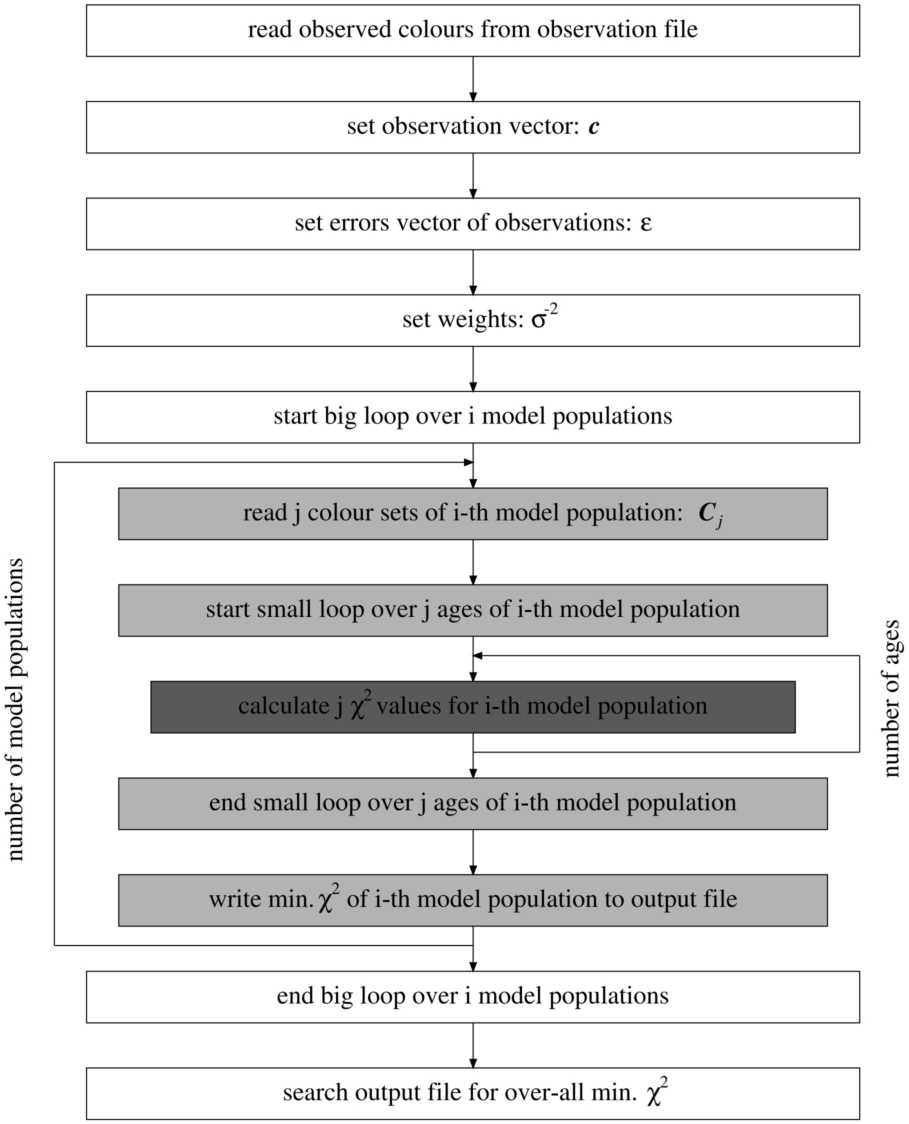
read observed colours from observation file
set observation vector: c
set errors vector of observations: ε
set weights: σ-2
start big loop over i model populations
read j colour sets of i-th model population: Cj
start small loop over j ages of i-th model population
calculate j χ2 values for i-th model population
end small loop over j ages of i-th model population
write min. χ2 of i-th model population to output file
end big loop over i model populations
search output file for over-all min. χ2
number of model populations
number of ages

Figure 4.5: Flow chart of COLFIT

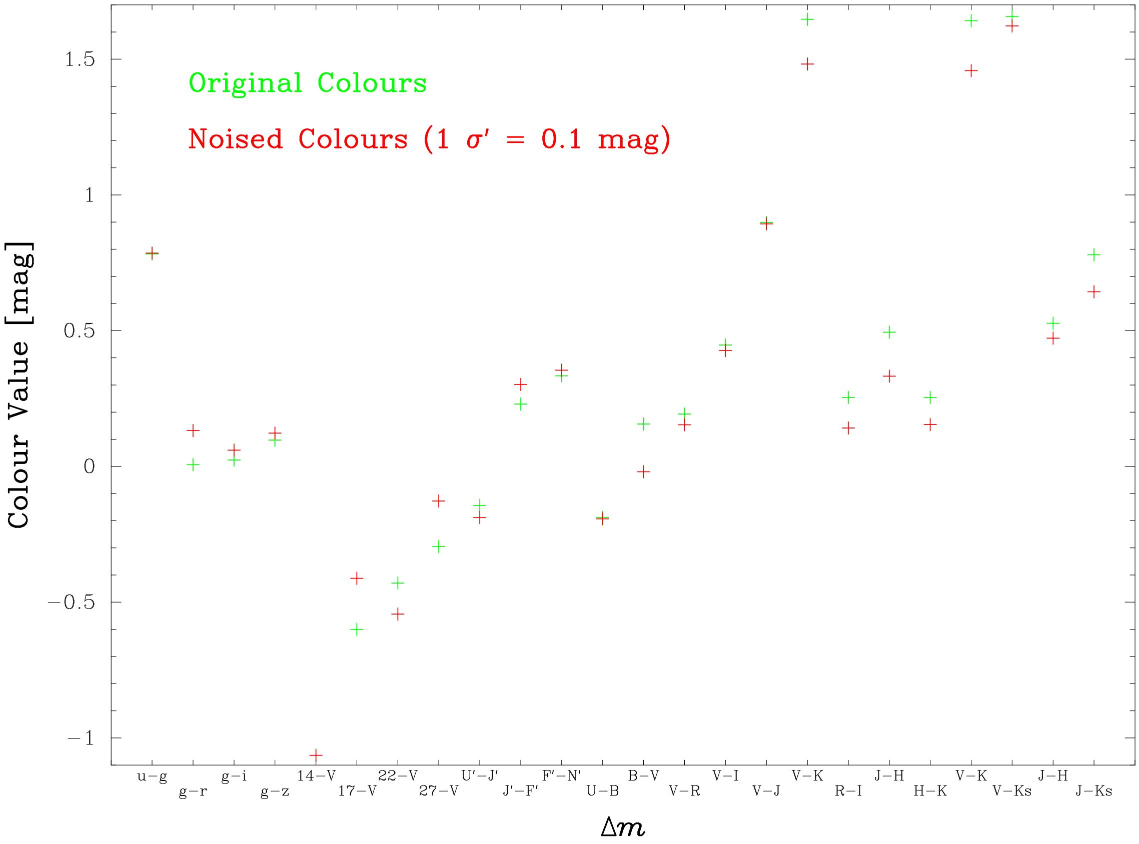

Figure 4.6: Example of a set of model colours from BLoIS without and with noise at a level 1 $\sigma' = 0.1$ mag.

COLFITSIM

Analogously to "SPECFITSIM" we generated "COLFITSIM". This Monte Carlo simulation code follows the same pattern as the first, i.e. it adds artificial noise to a set of model colours which will be used as observed colours. Here we neither have the problem of large differences in colour values nor the problem of negative values. So we can add one single *absolute* noise value to all observations: $1\ \sigma' = p\ \boldsymbol{c}$. In **Figure 4.6** we show an illustrative example of a set of 24 integrated colours once with the original values and once with a noise of $1\ \sigma' = 0.1$ mag (see Table 3.1 and chapter "GISSEL User Manual" for the definition of the colours). Apart from a different file reading subroutine "COLFITSIM" performs the same 1 000 runs simulation as "SPECFITSIM".

A 1 000 runs simulation including 7 model populations (1 547 colour sets, 24 colours per set) takes less than 1 minute on a 500 MHz Alpha workstation.

The four programmes that perform χ^2 fits are listed in **Table 4.1**.

Purpose	**Spectra**	**Colours**
simple search	SPECFIT	COLFIT
Monte Carlo simulation	SPECFITSIM	COLFITSIM

Table 4.1: Programmes performing χ^2 fitting

4.3.2 SPECLSA, COLLSA, SPECSUBPOP, COLSUBPOP

SPECLSA

In Section 4.2 we proposed a method to fit models to observations by least-squares adjustment techniques. The programme that applies this method to spectra fitting is called "SPECLSA" which we'd like to present now.

In analogy to the χ^2 fit we set the observation vector $\boldsymbol{f}$ as in Equation 4.23. The same is done with the model matrix $\boldsymbol{F}$ (see Equation 4.24). The observation equation system in Equation 4.20 is then set to:

$$\boldsymbol{F}\,\boldsymbol{x} = \boldsymbol{f} + \boldsymbol{v} \tag{4.31}$$

Or explicitly:

$$\begin{pmatrix} (\lambda_1, F_{11}) & \dots & (\lambda_1, F_{1j}) & \dots & (\lambda_1, F_{1m}) \\ \vdots & & \vdots & & \vdots \\ (\lambda_i, F_{i1}) & \dots & (\lambda_i, F_{ij}) & \dots & (\lambda_i, F_{im}) \\ \vdots & & \vdots & & \vdots \\ (\lambda_n, F_{n1}) & \dots & (\lambda_n, F_{nj}) & \dots & (\lambda_n, F_{nm}) \end{pmatrix} \begin{pmatrix} x_1 \\ \vdots \\ x_j \\ \vdots \\ x_m \end{pmatrix} = \begin{pmatrix} f_1 \\ \vdots \\ f_i \\ \vdots \\ f_n \end{pmatrix} + \begin{pmatrix} v_1 \\ \vdots \\ v_i \\ \vdots \\ v_n \end{pmatrix} \tag{4.32}$$

where
m : number of models (or sets of input parameters)
n : number of observed flux values

One could now have the idea of solving the corresponding normal equation system regarding all possible model populations. For fitting a low resolution spectrum (1 221 flux values) this would lead to a $1\,221 \times 255\,255$ model matrix. Apart from the ridiculously large normal equation matrix to be inverted (see Equation 4.14 and 4.19) the method would fail for theoretical reasons:

- The number of parameters to determine is larger than the number of observations.
- There are identical spectra within one model population (neighbouring ages) which contradicts the condition, that the model vectors have to be linearly independent.

To overcome these problems one could now think of the opposite idea, i.e., just taking one model spectrum and conduct the adjustment 255 255 times solving for just one scalar x instead of a solution vector $\boldsymbol{x}$. This on the other hand is too sophisticated a method to fit a spectrum because this problem is more efficiently solved by a χ^2 fit.

The solution to the problem is to adequately choose the set of models to be fed into the normal equation system. First there's the absolute upper limit of 1 221 low resolution or 6 900 high resolution models mentioned above. Then one has to avoid identical models because of their linear dependence as vectors. Two or more spectra of one model population can be identical if they are time neighbours. This, however, is not much of a problem, because we don't really want to compare the spectra within one model population but rather compare the spectrum of a model population to spectra of other model populations. So we shall only compare spectra of the same ages which would lead to 221 model matrices each $1\,221 \times 1\,155$ of dimension. Thus we'd have to invert a $1\,155 \times 1\,155$ normal equation matrix 221 times. This is theoretically possible but computationally too expensive. So we have to go even further.

The search strategy that has finally been chosen is the following: Because one particular set of input parameters for the evolutionary synthesis algorithm (i.e. library type, track type, SFR, IMF, IMF mass range) leads to a certain subset of model populations (e.g. choosing Padova 1994 tracks leads to 7 model populations corresponding to 7 different metallicities), we select this subset for the adjustment. Following the example just mentioned, we would choose only 7 model populations and compare the corresponding model spectra with the observed spectrum time step after time step. This means that we'd have to invert a 7×7 normal equation matrix 221 times for this model subset; and this 165 times because that's the number of model subsets of this kind in BLoIS 1.1. So we end up with 36 465 inversions of a 7×7 matrix which is computationally feasible. A search for a low resolution spectrum with this least-squares adjustment method takes about 15 minutes on a 500 MHz Alpha workstation.

So we'd like to explain the flow chart of "SPECLSA" in **Figure 4.7**. We start with the reading (and optionally normalizing) of the observed spectra along with their errors. Then we can set the vectors of the observation, the errors and the weights as above. Now we are ready to read (and optionally normalize) the model spectra. After this the small loop over all the ages is started. It begins with setting the model matrix. After that all the necessary steps for solving the normal equation system are made, i.e., the calculations of $\boldsymbol{B}$, $\boldsymbol{N}$, $\boldsymbol{Q}$, $\boldsymbol{x}$, and $\boldsymbol{v}$. The normal equation matrix $\boldsymbol{N}$ is normalized before its inversion in order to avoid computation problems with small and large numbers. After the inversion, the cofactor matrix $\boldsymbol{Q}$ is then renormalized, of course. Having left the small loop the minimal estimated standard deviation of unit weight m_0 along with the corresponding solution vector $\boldsymbol{x}$ are written to the output file. When the big loop over all model subsets is terminated the output file is searched for the over-all minimal m_0.

COLLSA

As in the subsection above, we compiled a version of the least-squares adjustment algorithm for integrated colours called "COLLSA". Apart from the file reading routines it follows the same pattern as "SPECLSA". The observation vector $\boldsymbol{c}$ is filled with 24 colour values per model, and the model matrix $\boldsymbol{M}_j$ is of dimension 24×7 corresponding to the 7 metallicities. A simple search for the best fitting model takes less than one minute on a 500 MHz Alpha workstation.

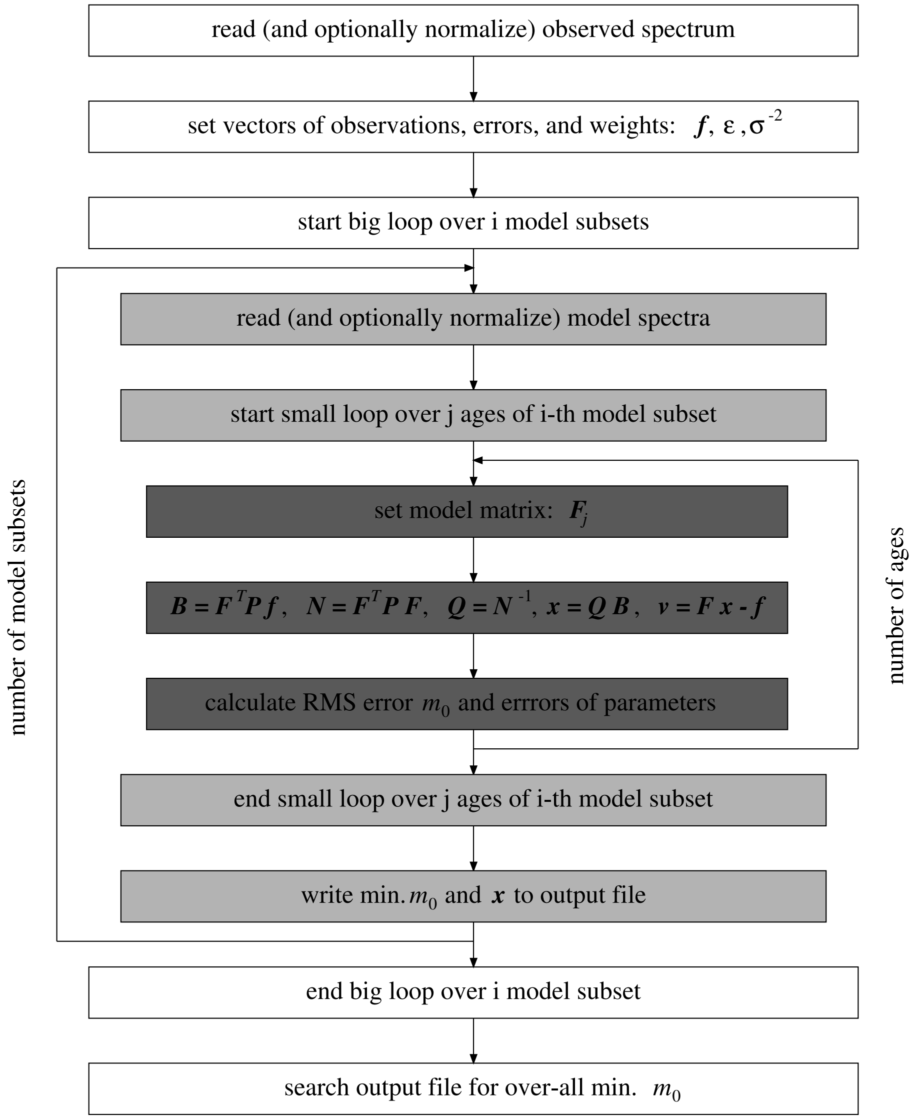
read (and optionally normalize) observed spectrum
set vectors of observations, errors, and weights: $\boldsymbol{f}$, ε, σ^{-2}
start big loop over i model subsets
read (and optionally normalize) model spectra
start small loop over j ages of i-th model subset
set model matrix: $\boldsymbol{F}_j$
$\boldsymbol{B} = \boldsymbol{F}^T \boldsymbol{P} \boldsymbol{f}$, $\boldsymbol{N} = \boldsymbol{F}^T \boldsymbol{P} \boldsymbol{F}$, $\boldsymbol{Q} = \boldsymbol{N}^{-1}$, $\boldsymbol{x} = \boldsymbol{Q} \boldsymbol{B}$, $\boldsymbol{v} = \boldsymbol{F} \boldsymbol{x} - \boldsymbol{f}$
calculate RMS error m_0 and errrors of parameters
end small loop over j ages of i-th model subset
write min. m_0 and $\boldsymbol{x}$ to output file
end big loop over i model subset
search output file for over-all min. m_0
number of model subsets
number of ages

Figure 4.7: Flow chart of SPECLSA

But finding the best fitting model spectrum or colour set is not the actual purpose of the adjustment technique, for χ^2 fitting is perfectly enough for this task. Besides the χ^2 fit provides a goodness of fit parameter for each single spectrum whereas the least-squares adjustment algorithm calculates only an "RMS" error for an ensemble of several (here 7) spectra. However, the advantage of the proposed method is that we can *derive subpopulations* because the solution vector $\boldsymbol{x}$ includes information about how much one particular model spectrum (belonging to a certain metallicity, thus stellar population) contributes to a total spectrum of an observed population consisting of different subpopulations. E.g. if two elements of the solution vector are 0.5 and all the other elements are 0 we can state that the observed spectrum is composed of those two subpopulation spectra which the solution vector indicates. Here's a simple example:

$$\begin{pmatrix} 1 & 5 & 9 \\ 2 & 6 & 10 \\ 3 & 7 & 11 \\ 4 & 8 & 12 \end{pmatrix} \begin{pmatrix} 0.5 \\ 0.5 \\ 0 \end{pmatrix} = \begin{pmatrix} 3 \\ 4 \\ 5 \\ 6 \end{pmatrix} \tag{4.33}$$

So we have written "SPECSUBPOP" for the purpose of deriving subpopulations on the basis of spectra. To test this method we generated an observed spectrum by summing up different (here 7) model spectra each of a different age and with an own proportionality factor $\boldsymbol{p}$ as:

$$\boldsymbol{p} = p_j \quad , \qquad \sum_{j=1}^{m} p_j = 1 \tag{4.34}$$

where m : number of model subpopulations (or metallicities)

An example of the spectrum of such a composed population is shown in Figure 5.8. Then we applied the least-squares adjustment method as described above to see, whether we are able to recover all the proportionality factors correctly. The details of the successful test is written in Section 5.3. The reason for this success is that metallicity makes each spectrum unique, thus linearly independent from others. It can well be that for one single wavelength point different combinations of the (7) model flux values lead to the same observed flux value. But this does not hold for all the other flux values, i.e. the whole spectrum. We can state that the metallicity characteristics of the spectra of model populations are so unique that putting them in one single normal equation system leads to an unambiguous solution which describes the extent of the contribution of the different subpopulations to the composed spectrum of an observation.

Now CSPs can't be characterized by one single age. In this context we define the age of a subpopulation as the time span since the first appearance of stars of the corresponding metallicity. CSPs are therefore composed of subpopulations of different ages. So comparing only subpopulations of the same age (as "SPECLSA") is not adequate. The picture to have in mind is sketched in **Figure 4.8**, where $SP(Z_j)$ is the subpopulation of the j-th

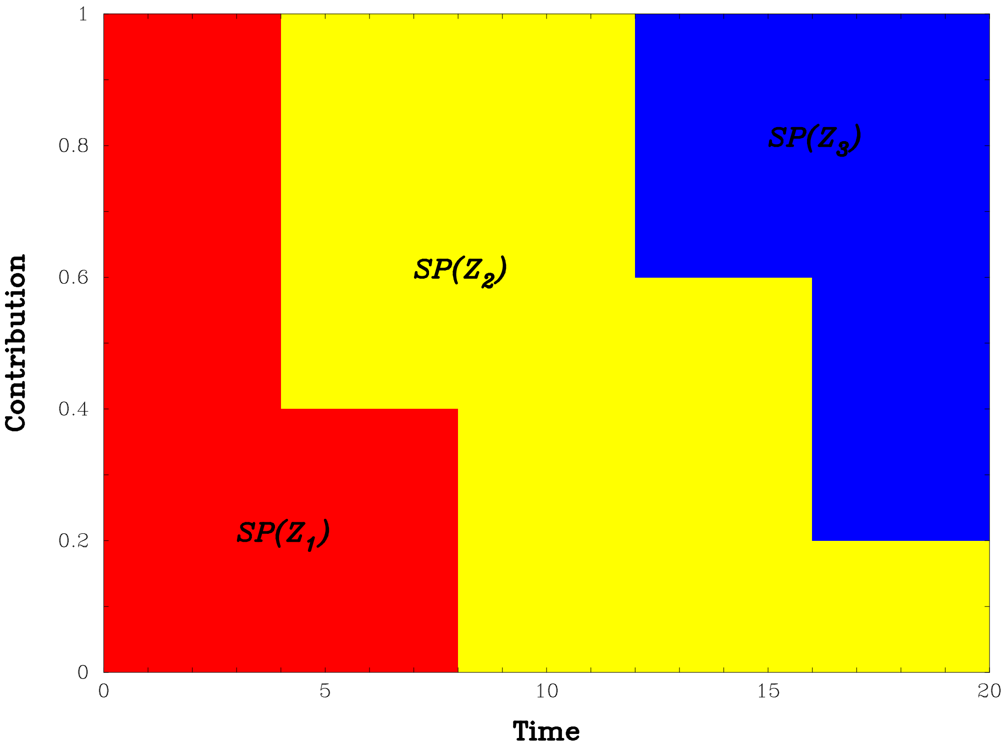

Figure 4.8: Contributions of different subpopulations to the total light

metallicity. The scetch shows the different contributions of the different subpopulations to the total light of a CSP at different ages.

Schematically this CSP consists of one single subpopulation (thus one single metallicity Z_1) at the beginning. Then this first generation produced a second population of a higher metallicity Z_2. After the total disappearance of the first generation this second generation was the only one to contribute to the total light of the CSP for a while. Then it produced a third generation of even higher metallicity Z_3 with which it shared its contribution in the end. Of course, real CSPs would show smooth changes of the different contributions. But as the GISSEL code provides spectra at discrete age steps the chosen approach is adequate.

If we'd like to derive subpopulations without any assumptions we'd have to consider all possible combinations of ages, metallicities, tracks, stellar spectral libraries, etc. So let's focus on just one set of subpopulations that varies only in age and metallicity. For m subpopulations (or metallicities) and t ages we can write the total number of possible age and metallicity combinations: $nc = t^m$. In spite of the least-squares algorithm calculating m subpopulations at once, it is clear that we have to limit the number of combinations to a reasonable size.

One possibility of reduction is to think of a stellar population as a closed box model (no infall, no merging etc.). So we can assume that higher metallicity stars evolved from lower metallicity stars and we can thus exclude all combinations where higher metallicity subpopulations are older than lower metallicity subpopulations. In this case the total number of possible combinations nc is reduced to:

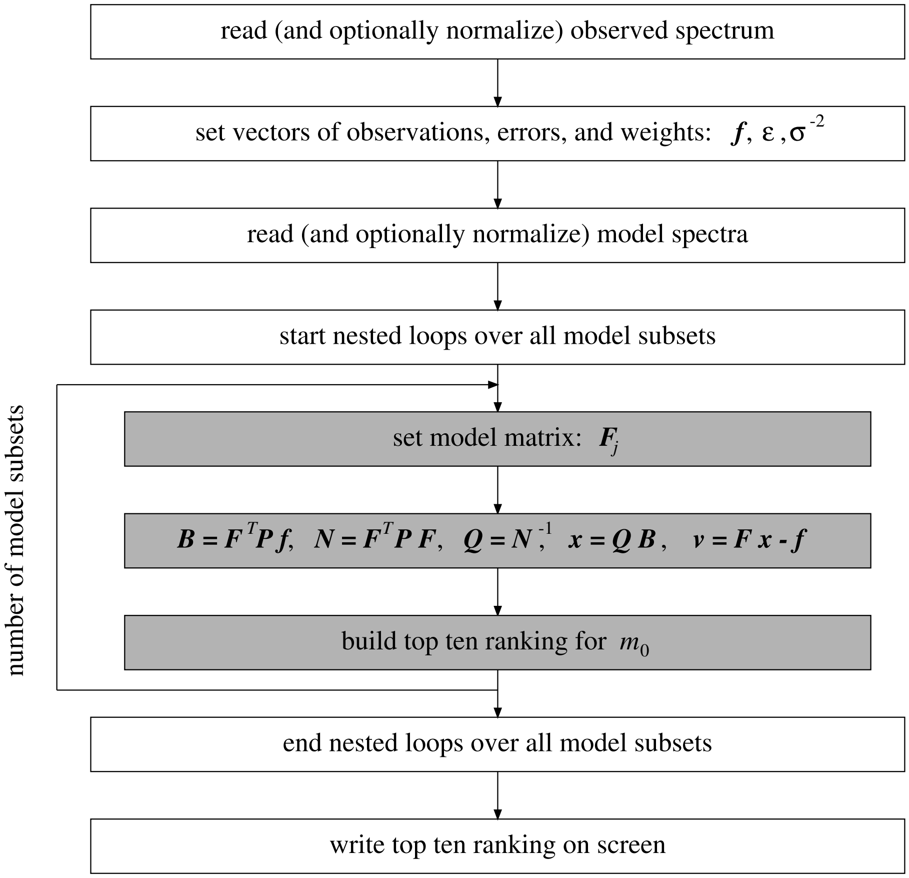
read (and optionally normalize) observed spectrum
set vectors of observations, errors, and weights: f, ε, σ^{-2}
read (and optionally normalize) model spectra
start nested loops over all model subsets
number of model subsets
set model matrix: F_j
$B = F^T P f$, $N = F^T P F$, $Q = N_j^{-1}$, $x = Q B$, $v = F x - f$
build top ten ranking for m_0
end nested loops over all model subsets
write top ten ranking on screen

Figure 4.9: Flow chart of SPECSUBPOP

$$nc = \prod_{i=1}^{t-1} (1 + \frac{m}{i}) \tag{4.35}$$

where m : number of model subpopulations (or metallicities)
t : number of age steps

This does not mean that a lower metallicity subpopulation is not allowed to rise its contribution again after falling. It simply means that a higher metallicity subpopulation can't appear for the first time *before* a lower metallicity subpopulation.

Now we are ready to explain the flow chart of "SPECSUBPOP" in **Figure 4.9**. As for "SPECLSA" it begins with reading the observations and setting of the vectors $\boldsymbol{f}$, $\boldsymbol{\varepsilon}$, and $\boldsymbol{\sigma}^{-2}$. Then we read all the spectra of the model subpopulations. In principle any model subset can be chosen. But in the context of deriving subpopulations we select 7 models (according to the 7 different Padova 1994 metallicities) with a constant SFR because subpopulations can produce stars at every age after first appearance. Now we have to start m nested loops where m is the total number of model subpopulations. There, one

Purpose	**Spectra**	**Colours**
simple search	SPECLSA	COLLSA
deriving subpopulations	SPECSUBPOP	COLSUBPOP

Table 4.2: Programmes performing least-squares adjustment

can choose whether to allow every possible age-metallicity combination or just the ones as explained above (see Equation 4.35). During the inner most loop the model matrix $\boldsymbol{F}_j$ is set, the parameter estimation is done, and a top ten list according to the "RMS" error m_0 is built up. After leaving all the loops we are ready to write the top ten list (containing the 10 most probable solutions) on the screen.

Taking into account 10 age steps and assuming a closed box model population a search for an observed spectrum consisting of 7 subpopulations lasts about one minute on a 500 MHz Alpha workstation.

COLSUBPOP

Analogously to the subsection above we have written a version of "SPECSUBPOP" for deriving subpopulations on the basis of integrated colours named "COLSUBPOP". Again they both follow the same patterns except for the reading routines.

If we are dealing with 24 integrated colours per subpopulation we can perform a search for 20 ages and 7 metallicities in about one minute on a 500 MHz Alpha workstation.

Attention: Contrary to Equation 4.28 the observation vector $\boldsymbol{c}$ should be:

$$\boldsymbol{c} = \begin{pmatrix} m_1 \\ \vdots \\ m_i \\ \vdots \\ m_n \end{pmatrix} \tag{4.36}$$

where m_i : i-th colour magnitude of the observation
n : number of observed colour magnitudes

And, as a consequence, the model matrix $\boldsymbol{C}_j$ in Equation 4.29 should also be filled with colour magnitudes of the models instead of the colours. So "COLSUBPOP" has only been written to test, whether the least-squares adjustment routine still works with 24 values. It has to be adapted for colour magnitudes first if one wants to use it for real data.

The four programmes that perform least-squares adjustments are listed in **Table 4.2**.

5 Results

In this chapter we'd like to present some theoretical applications of the integrated library established in Chapter 3 with the help of the software developed in Chapter 4. In the first section we investigate the characteristics of BLoIS. The second section is dedicated to the famous age-metallicity degeneracy, the third to the task of deriving subpopulations from a composed stellar population, and the fourth to Monte Carlo simulations, giving us an idea of the constraints to observations.

5.1 Characteristics of BLoIS 1.1

Two major topics concerning libraries in general are the uniqueness and the similarities of their contents. So we'd like to know, whether there are identical spectra and colour sets in BLoIS 1.1. Furthermore, we want to investigate to which extent the populations differ from each other. Each model population in BLoIS 1.1 can be characterized by a parameter vector with the following elements:

$$\begin{pmatrix} a \\ b \\ c \\ d \end{pmatrix} : \begin{pmatrix} \text{Star Formation Rate} \\ \text{IMF Slope} \\ \text{IMF Mass Range} \\ \text{Metallicity } Z \end{pmatrix} \tag{5.1}$$

Along with a stellar library parameters a through d define a population. Each population consists of 221 spectra corresponding to 221 ages between 0 and 20 Ga (see "GISSEL User Manual"). For each spectrum a set of 24 default colours are available (see Table 3.1).

Because it would be computationally too expensive to compare e.g. all 255 255 low-resolution spectra to each other, we had to focus on a representative test sample. This has been done by choosing 9 populations as follows:

$$
\begin{array}{cccccc}
1 : & \begin{pmatrix} \text{delayed } 1.0 \\ 2.00 \\ 1-10 \\ 0.008 \end{pmatrix} & 2 : & \begin{pmatrix} \delta-\text{burst} \\ 2.00 \\ 1-10 \\ 0.008 \end{pmatrix} & 3 : & \begin{pmatrix} \text{constant} \\ 2.00 \\ 1-10 \\ 0.008 \end{pmatrix} \\[2ex]
4 : & \begin{pmatrix} \text{delayed } 1.0 \\ 1.35 \\ 1-10 \\ 0.008 \end{pmatrix} & 5 : & \begin{pmatrix} \text{delayed } 1.0 \\ 3.00 \\ 1-10 \\ 0.008 \end{pmatrix} & 6 : & \begin{pmatrix} \text{delayed } 1.0 \\ 2.00 \\ 0.1-2 \\ 0.008 \end{pmatrix} \\[2ex]
7 : & \begin{pmatrix} \text{delayed } 1.0 \\ 2.00 \\ 2-100 \\ 0.008 \end{pmatrix} & 8 : & \begin{pmatrix} \text{delayed } 1.0 \\ 2.00 \\ 1-10 \\ 0.0001 \end{pmatrix} & 9 : & \begin{pmatrix} \text{delayed } 1.0 \\ 2.00 \\ 1-10 \\ 0.1 \end{pmatrix}
\end{array}
\tag{5.2}
$$

Population 1 corresponds to parameters which lie somewhere in the middle of the parameter space, whereas the other 8 populations each have one parameter that is at the edge of the parameter space.

5.1.1 Uniqueness

Although we tried to avoid identical spectra while creating BLoIS, we'd like to test the uniqueness of the populations in the library.

In a first step we took the low resolution spectra of the 9 populations corresponding to the parameters in (5.2) and compared them at the ages 0, 5, and 20 Ga to all the other 1 155 low resolution populations in BLoIS using the programme ”SPECFIT” (see Subsection 4.3.1). Thus 27 spectra were to be compared, resulting in 27 output lists each containing the 1 155 χ^2-values, the ages, and the names of the best fitting populations (see Subsection 4.3.1 for an example of such a list). The analysis of these lists showed that for no other than the test spectrum $\chi^2 = 0$, thus the 9 populations *all had different spectra*. This means that the parameters for building up BLoIS were chosen in a way that, as a first and general statement, the spectra do vary significantly from population to population. The fact that the χ^2-values in each of the 27 output lists were unique supports this statement. Furthermore, we can already state that there is no such thing as a 100 % degeneracy in age and metallicity as far as the model spectra in BLoIS are concerned (see Section 5.2 below).

The next step was to compare the 221 spectra of one population to see whether there are identical spectra at different ages within this population. To investigate this we took the same 9 populations as above. Here we could see that each of the 8 CSPs (population 1 and 3 to 9) had different spectra at any age, whereas the only SSP (population 2) had an identical spectrum for the first 50 ages i.e. for 4 Ma. This held true when we changed the slope of the IMF, i.e. $x \in \{1.35, 3.00\}$.

So we varied the IMF mass range while leaving all the other input parameters as in population 2. The results are shown in **Figure 5.1**. For a maximum mass range of 0.1 –

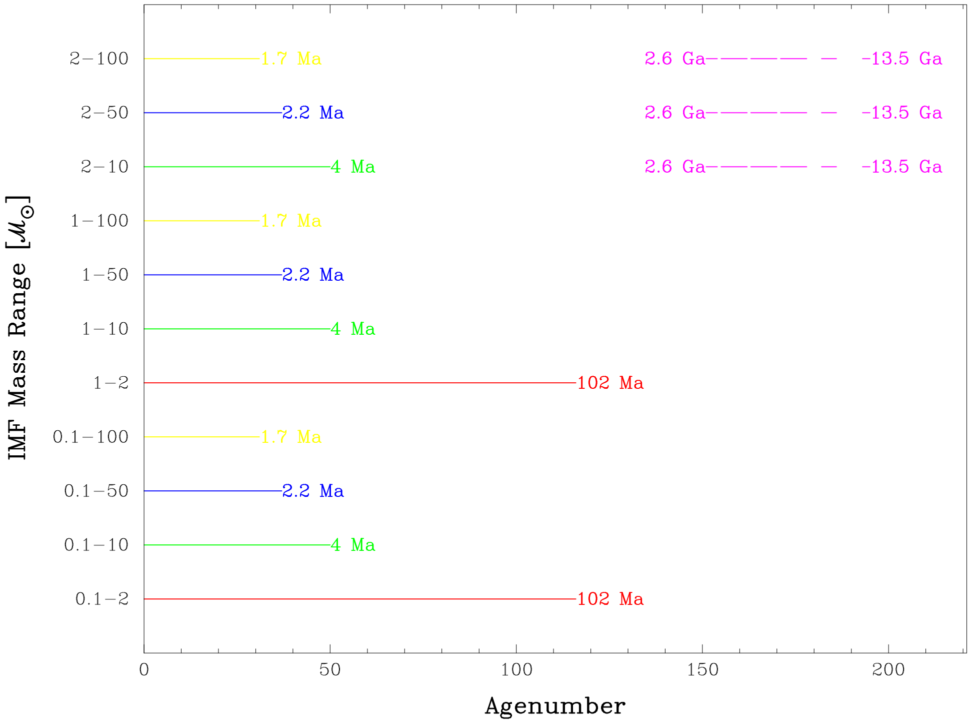

Figure 5.1: Identical spectra of an SSP with different IMF mass ranges. Lines connect ages with identical spectra. Note that the age-scale is not uniform.

100 $\mathcal{M}_\odot$ the first 31 ages (i.e. for 1.7 Ma) have identical spectra. This can be explained by the fact that even O- and B-stars need some time to develop. When we decrease the upper mass cut-off the identical spectra persist even longer (e.g. up to 102 Ma for a mass range of 0.1 – 2 $\mathcal{M}_\odot$).

For the mass ranges with lower cut-offs at 1 $\mathcal{M}_\odot$ and different upper cut-offs we find the same pattern just mentioned. And when we look at the spectra of a young SSP with an even higher lower cut-off (i.e. at 2 $\mathcal{M}_\odot$) we can state that it is the upper mass limit of the IMF which decides on the persistence of the spectra to be identical. In addition to this we state for old SSPs with a 2 $\mathcal{M}_\odot$ lower cut-off that their spectra don't change much, because there are only 6 different spectra between 2.6 and 13.5 Ga. Here we can recognize the White Dwarf cooling sequence (see the step-shaped behaviour of the colour evolution in Figure 3.7).

Since the same comparisons as above but done with high resolution spectra (STELIB) showed the very same results as with low resolution spectra (BaSeL 3.1), we now investigate the uniqueness of the integrated colours in BLoIS. Although we could calculate as many integrated colours as available filters, a set of colours in BLoIS consists of 24 values per spectrum. If we compare this to the number of flux-values per spectrum (1 221 or 6 900) it is plausible that we can't expect the same degree of uniqueness for the colours as for the spectra.

By using the programme COLFIT (see Subsection 4.3.1) the comparison of the 27 colour sets of the 9 populations to all the other 1 155 populations in BLoIS showed that, at age 0, none of the colour sets was unique. For all the 9 populations there were 5 identical colour sets corresponding to the 5 different SFRs available in BLoIS. This is not much of

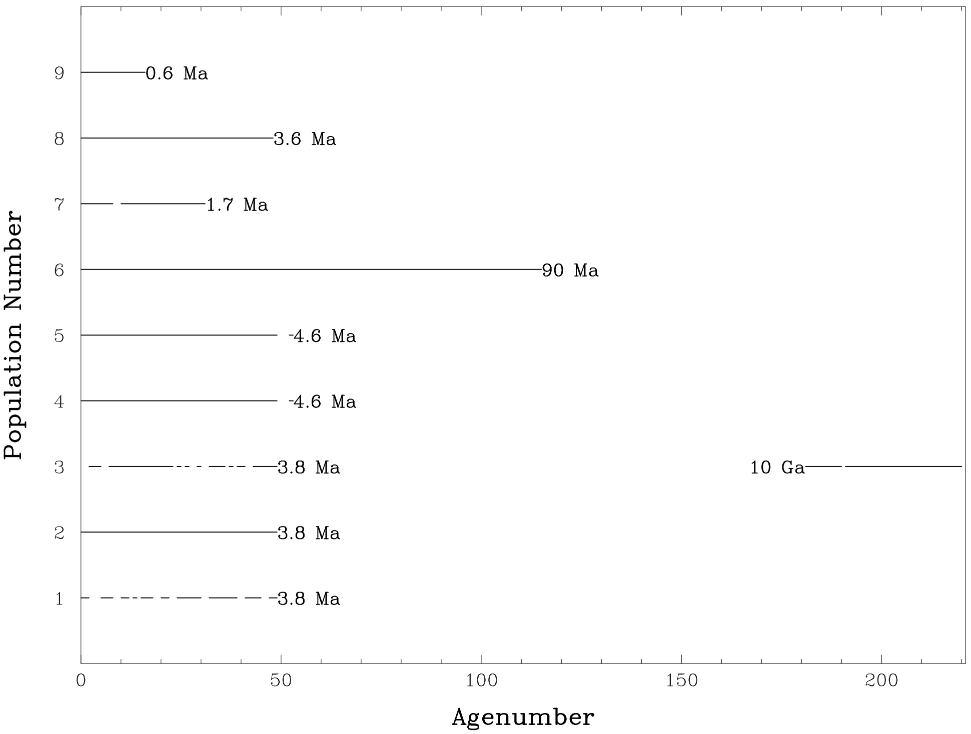

Figure 5.2: Identical colours for the populations as defined in (5.2). Lines connect ages with identical colours. Note that the age-scale is not uniform.

a surprise because at early ages all the CSPs look similar to an SSP and the important wavelengths in the spectrum of a young population are lying outside most implemented filters (see Figure 3.6).

Furthermore, the colour sets are not unique at high metallicity. Population 9 with $Z = 0.1$ has the same colours as the populations with an IMF mass range of 1 – 50 and 1 – 100 $\mathcal{M}_\odot$ at 5 and 20 Ga (the case of 0 age has already been treated above). The same behaviour can be detected for the SSP at those two ages. Although the IMF mass range parameter is sensitive to the integrated properties of stellar populations (see Subsection 5.1.2 below) the decrease from 100 to 50 $\mathcal{M}_\odot$ for the upper mass limit is too small to produce much of a difference in high-metallicity.

Besides these cases of identical colour sets, there are 231 other colour sets on the average that have exactly the same χ^2-values as others, which makes it likely that they are identical, too.

As for the spectra we'd like to know whether there are identical colours at different ages within one population. The results of this investigation is shown in **Figure 5.2**. The populations have either identical or very similar colours up to an age of roughly 4 Ma (see Figure 3.27). Here we can repeat the statement we made for the spectra, i.e., even very hot stars do need some time to develop. As we have seen in Figure 5.1 the population with an IMF mass range of 2 – 100 $\mathcal{M}_\odot$ (population 7) evolves faster than the one with 0.1 – 2 $\mathcal{M}_\odot$ (population 6). Interesting, however, is that the population with the highest metallicity (population 9) is the fastest to evolve. Another remarkable fact is that the colours of population 3 (constant SFR) don't change much at old ages.

At the end of this subsection we'd like to mention once more that the investigations above were made with a test sample. There is no guarantee that the identical spectra and colour sets found here are the only ones in BLoIS.

For the uniqueness of the spectra and the colours in BLoIS we can state:

- All the populations have different spectra.
- At young (< 100 Ma) and old (> 2 Ga) ages the spectra and the colours within one particular population can be identical.
- Colours of young (< 100 Ma) populations with different SFRs are identical at the same ages.
- At the same ages the colours of SSPs and high-metallicity populations may not be unique.

5.1.2 Sensitivity with respect to parameters

The goal of this subsection is to answer the question, which parameters have the largest impacts on the spectra and the colours. So we don't look for identical populations but at the differences from one population to another.

First we took the 3 low resolution spectra of population 1 (see 5.2) according to the ages 0.1, 2, and 15 Ga. This choice is based on the fact just mentioned, that ages around 0 and 20 Ga can lead to identical spectra. As in the subsection above we then compared these 3 spectra to all the other low resolution spectra in BLoIS using the programme "SPECFIT". This resulted in 3 lists each containing 1 155 χ^2-values and the corresponding ages and populations (see example in Subsection 4.3.1).

After sorting these 3 output lists according to the χ^2-values, we looked at the first 100 entries giving us the model populations with the 100 lowest χ^2-values. Then we made the statistics of how many times the correct and incorrect values for age, metallicity, IMF slope, SFR-type, and IMF mass range were found by the χ^2-fitting algorithm "SPECFIT".

In **Figure 5.3** we show the results for the low resolution models. From the top panel we can conclude, that for age 0.1 Ga of the test population the scatter around the correct value is quite large (± 0.1 Ga) and that the most findings are at 0.036 Ga. A similar situation is at the intermediate age (2 Ga): the scatter around the correct age is ± 2 Ga and peak-value is at 1.3 Ga. And at the oldest age (15 Ga) we have to realize, that a majority of the 100 found model populations were around 8.5 Ga with a scattering of ± 4 Ga.

In the middle left panel of Figure 5.3 we show the results for the 7 metallicities. Here we can see that only for age 0.1 Ga the correct metallicity ($Z = 0.008$) has the most hits. The intermediate age peaked at $Z = 0.004$ and the old age at $Z = 0.02$.

The middle right panel displays the results for the different IMF slopes. Here, too, the correct value of $x = 2$ was only in maximum for the youngest age. The intermediate age peaked at slope $x = 3$ and the oldest age at $x = 1.35$.

From the lower left panel we can learn, that the SFR-type is correctly recovered only at age 2 Ga. For 0.1 and 15 Ga the δ-burst are more often.

In the lower right panel we can see that for the IMF mass range the correct value of $1 -$

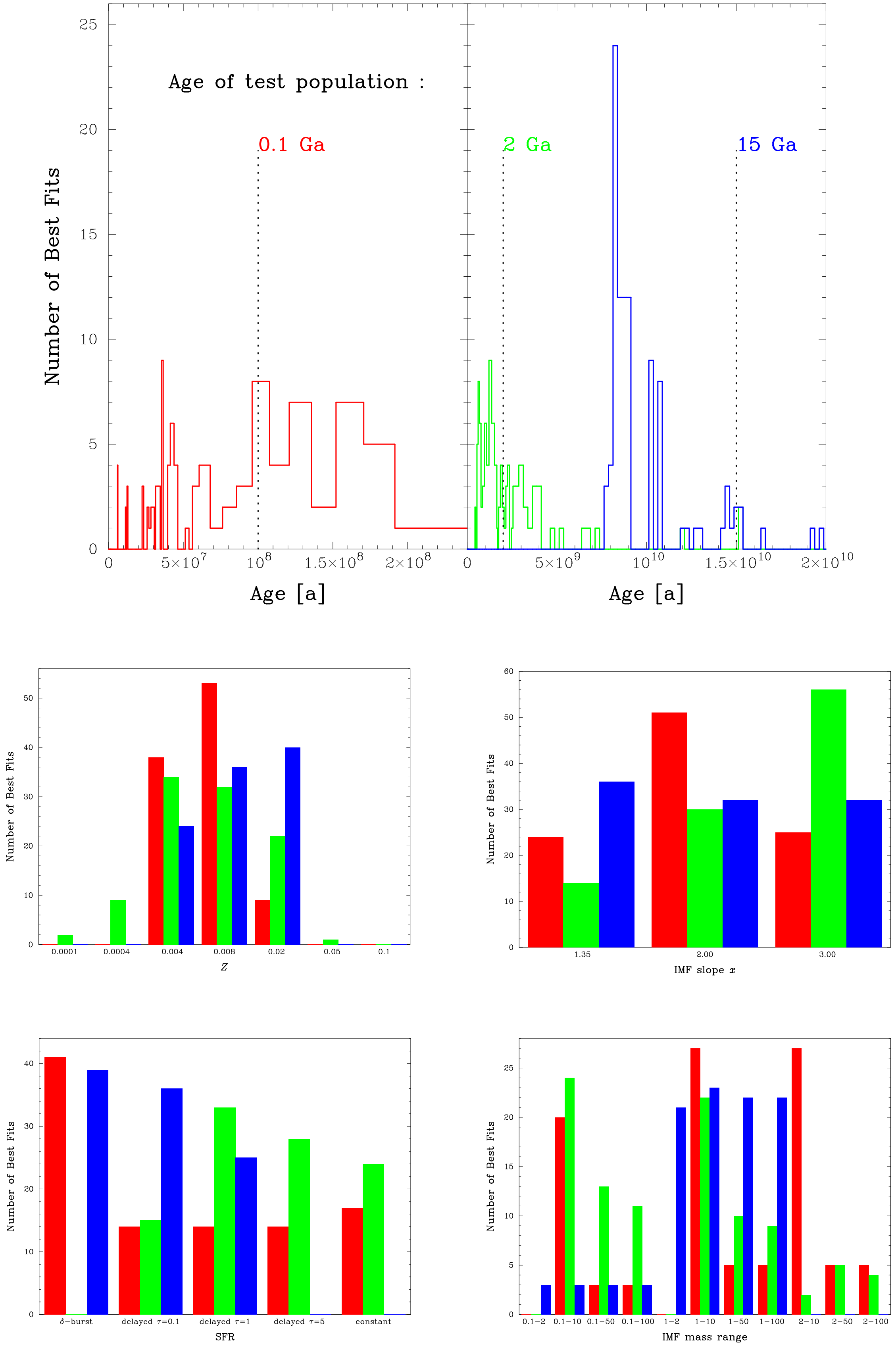

Figure 5.3: Important parameters for low resolution spectra

Population	2	3	4	5	6	7	8	9
$\bar{\chi}^2$	0.466	0.278	0.034	0.106	3.545	2.245	0.511	0.254

Table 5.1: χ^2-fit for spectra. The populations are coded as in (5.2). The $\bar{\chi}^2$-values represent the mean of 221 χ^2-fits to population 1.

10 $\mathcal{M}_\odot$ peaked for the youngest and the oldest age, whereas for 2 Ga 0.1 – 10 $\mathcal{M}_\odot$ has the most findings.

The same investigations as above we made with high resolution spectra. The results are shown in **Figure 5.4**. Comparing this figure with Figure 5.3 we can conclude that there are no substantial differences in general. In particular, the youngest age peaked at 0.145 Ga, the correct IMF slope was found at 15 Ga (instead of 0.1 Ga), and the correct IMF mass range peaked at the oldest age (instead of the youngest).

Finally, we show the same analysis as above for the integrated colours in **Figure 5.5**. In general, we can see that the only success is the better recovery of the age at 0.1 Ga. Nearly all the other panels show worse results compared to the case with spectra (e.g., the correct SFR never peaked).

So we can conclude for the spectra, that the metallicity is the most important parameter, because the scattering is the lowest. For both low and high resolution spectra two ages peaked at the correct value of the IMF mass range. Thus, we consider this parameter as important, too. Because the age, the IMF slope, and the SFR show quite a large scattering, we assume those parameters as less important. For the colours we can state that the SFR and the IMF mass range are a bit bitter defined compared to the spectra case.

Note that the conclusions made here only hold true for BLoIS 1.1, i.e., another parameter-spacing would lead to other results. E.g. if we had only 3 IMF mass ranges instead of 11, the probability of finding the correct range would increase.

Besides, a similar investigation as above will be presented in Section 5.4. There, we'll add artificial noise to model spectra and colours before trying to recover the parameters. This will give us an idea of the recovery probabilities rather than the similarities treated here.

Another (more global) way to analyse the degree of similarities between the model populations is the following: We took population 2 to 9 from (5.2) and calculated the differences to population 1 by comparing the 221 spectra all at the same 221 ages resulting in 221 χ^2-values from which a mean χ^2-value ($\bar{\chi}^2$) was calculated. In this way 8 $\bar{\chi}^2$-values corresponding to population 2 to 9 were derived. They are listed in **Table 5.1**. We can already spot the large $\bar{\chi}^2$-values of the two populations with different IMF mass ranges (population 6 and 7). From Table 5.1 we can then calculate the sum of the two $\bar{\chi}^2$-values corresponding to the same input parameter: ($\bar{\chi}^2_{2,4,6,8} + \bar{\chi}^2_{3,5,7,9}$). Those values together with the corresponding input parameters are listed in **Table 5.2** (values for high resolution spectra are in brackets). We can see that the IMF mass range is by far the most sensitive input parameter, both for low and high resolution spectra. On second rank lies the metallicity that is more important for high resolution spectra than for low resolution spectra. Third and fourth places are taken by the SFR and slope of the IMF, where the rank dependens on the resolution of the spectra.

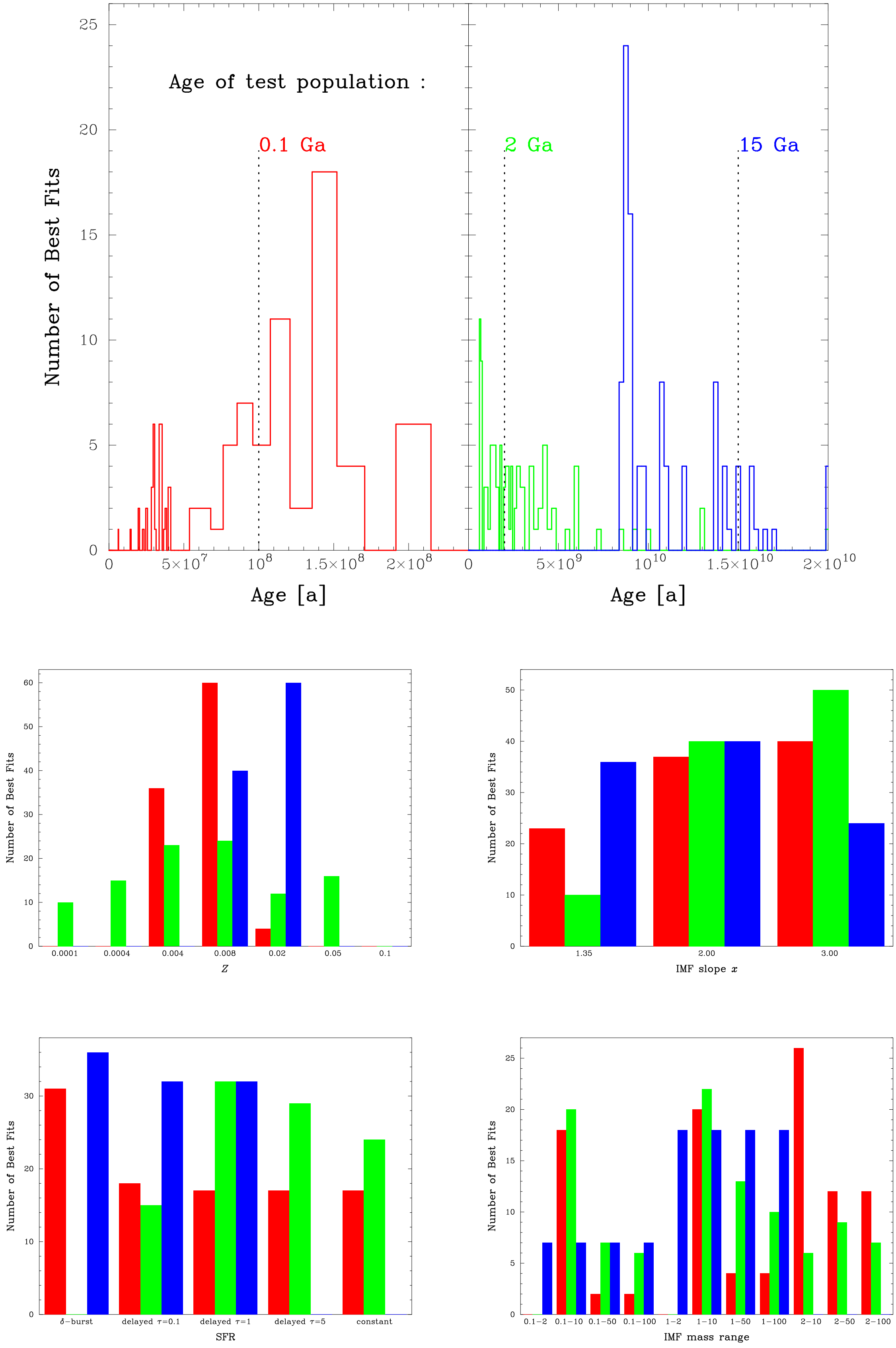

Figure 5.4: Important parameters for high resolution spectra

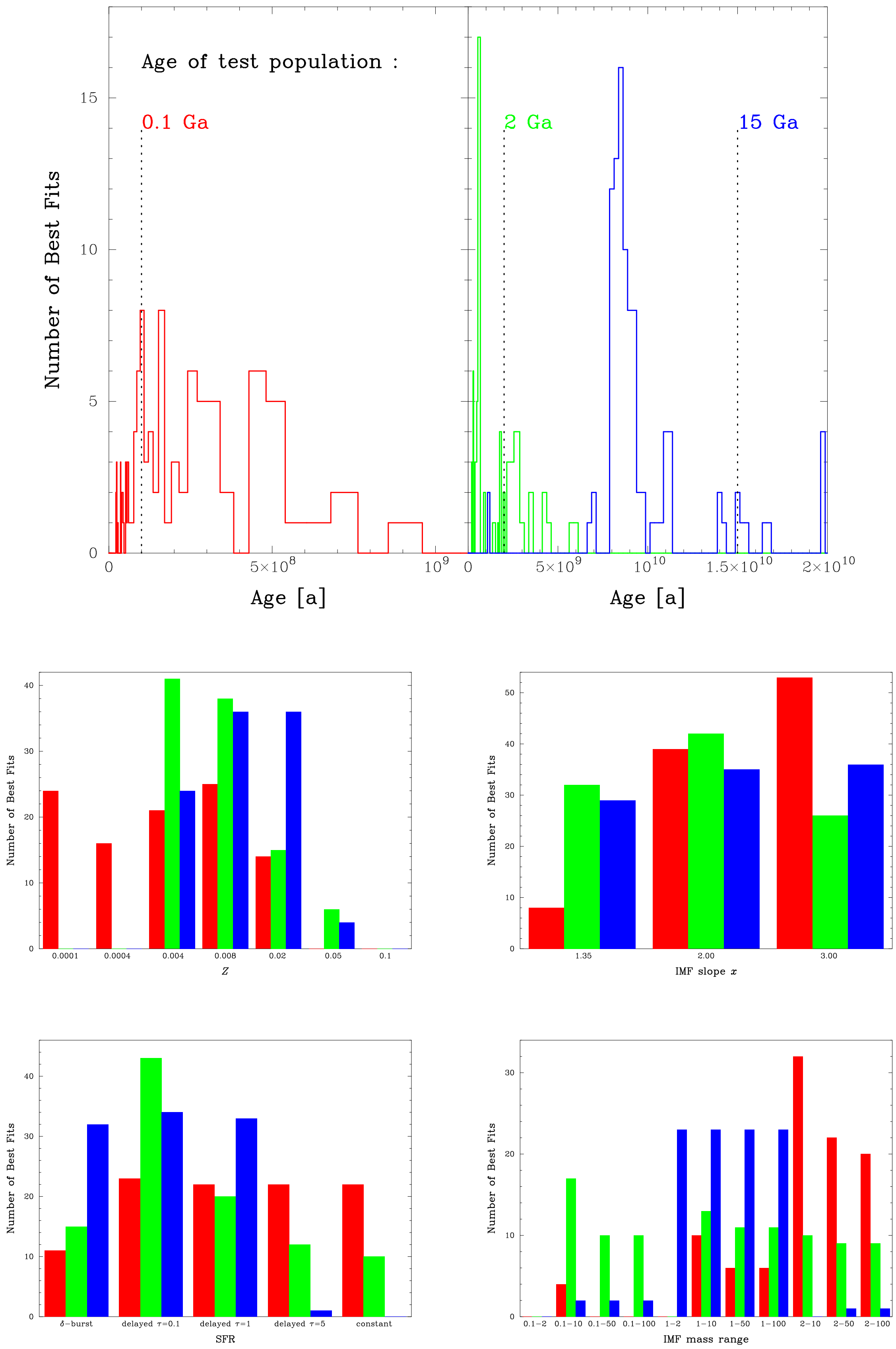

Figure 5.5: Important parameters for colours

Parameter	**Populations**	$(\bar{\chi}^2_{2,4,6,8} + \bar{\chi}^2_{3,5,7,9})$	**Percentage**
IMF Mass Range	6 + 7	5.790 (5.454)	77.8 (71.5)
Metallicity	8 + 9	0.765 (1.606)	10.3 (21.1)
SFR	2 + 3	0.744 (0.216)	10.0 (2.8)
IMF Slope	4 + 5	0.140 (0.348)	1.9 (4.6)
sum		*7.439 (7.624)*	*100.0 (100.0)*

Table 5.2: Sensitivity with respect to parameters for spectra. The $\bar{\chi}^2$-values of two populations corresponding to one input parameter have been taken from Table 5.1. Values in brackets were calculated with high resolution spectra.

Parameter	$(\bar{\chi}^2_{2,4,6,8} + \bar{\chi}^2_{3,5,7,9})$	**Percentage**
SFR	2.336	42.8
IMF Mass Range	2.186	40.1
Metallicity	0.868	15.9
IMF Slope	0.068	1.2
sum	*5.458*	*100.0*

Table 5.3: Sensitivity with respect to parameters for colours (compare Table 5.2).

We turn to colours and do the same investigation. In analogy to Table 5.2 the results are listed in **Table 5.3**. Here the SFR is the most sensitive parameter. Because we can see a set of colour magnitudes as a very low-resolution spectrum and as the low-resolution spectra are more sensitive to the SFR than high resolution spectra, the reason for this behaviour can be found in the number of available data points. Obviously, the chosen filters are at wavelengths where the changes in the SFR become most important.

As the two investigations showed similar results, we can state for the parameter sensitivity of the properties in BLoIS 1.1:

- High and low resolution spectra are most sensitive to the IMF mass range parameter, followed by the metallicity.
- For colours the SFR is the most important parameter closely followed by the IMF mass range.
- The impact of the parameters depends on the number of available data points (number of flux values, number of colours).

5.2 Age-Metallicity Degeneracy (AMD)

For integrated spectra and colours of an SSP an increase in age (resulting in redder colours due to the decreasing number of hot blue stars) can be compensated by a decrease in

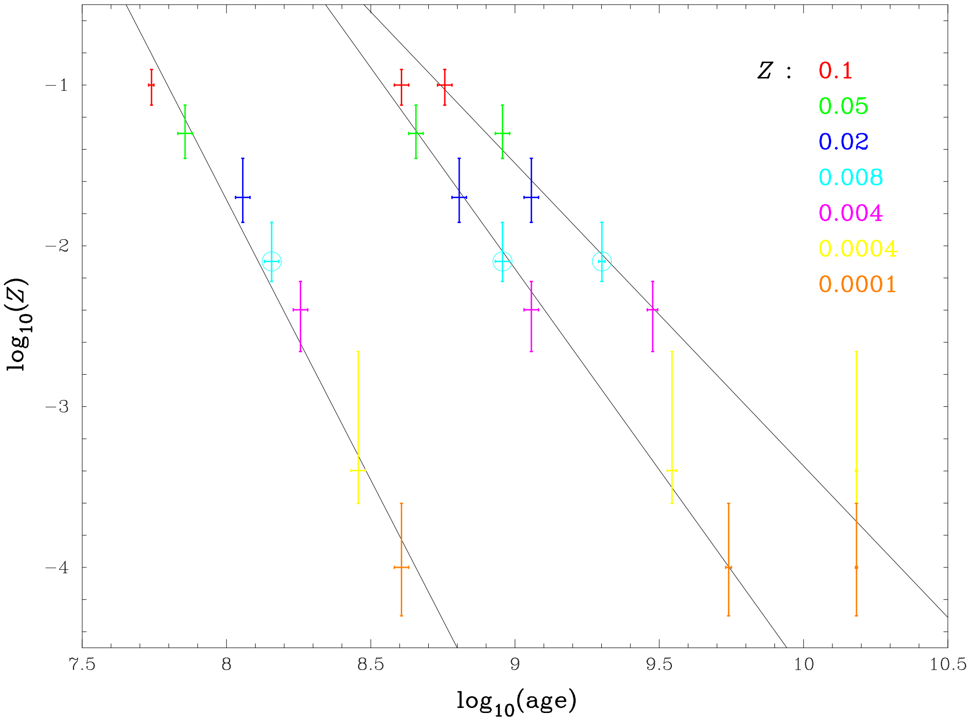

Figure 5.6: The age-metallicity degeneracy for spectra. The 3 ages of the test population ($Z = 0.008$; ages: 0.14, 0.9, 2.0 Ga) are marked with circles. The error bars indicate the age-metallicity grid.

metallicity (resulting in bluer colours because of the decreasing opacity). We have already stated in Subsection 5.1.1 that there is no such thing as a 100 % degeneracy in age and metallicity as far as BLoIS spectra are concerned, because all population spectra are unique. However, it is true that certain combinations of age and metallicity lead to very similar spectra (see Figure 5.8). So we focus on these cases.

First we looked at the AMD in the spectra by generating the following test population:

$$\begin{pmatrix} a \\ b \\ c \\ d \end{pmatrix} : \begin{pmatrix} \delta\text{-burst} \\ 1.35 \\ 0.1 - 100 \\ 0.008 \end{pmatrix} \tag{5.3}$$

Then we compared the low resolution spectra of this population at the ages 0.14, 0.9, and 2.0 Ga to all the other spectra of 6 populations with the same input parameters but different metallicities (i.e. Z = 0.0001, 0.0004, 0.004, 0.02, 0.05, 0.1). The ages and the metallicity of the test population were chosen around the center of the age-metallicity parameter space. For each of the 3 ages and each of the 6 metallicities we calculated a best fit spectrum by using the programme SPECFIT (see Subsection 4.3.1) resulting in 18 best-fit ages. These ages are shown in **Figure 5.6** where the 3 ages of the test population are marked with circles. Note that the error bars don't represent errors of measurements but indicate the extent of the grid in age and metallicity as present in parameter space in

age [Ga]	s	c
0.14	−3.49	26.18
0.90	−2.50	20.37
2.00	−1.88	15.46

Table 5.4: Estimated AMD parameters according to Equation 5.4 for spectra from Figure 5.6.

BLoIS 1.1. In Figure 5.6 we can see that there is a power law relationship between age and metallicity. In logarithmic scale we can write:

$$\log_{10}(Z) \;=\; s \cdot \log_{10}(t) + c \tag{5.4}$$

where Z : metallicity
s : slope
t : age
c : constant

The slope and the constant depending on the 3 ages can be calculated by standard curve fitting routines and are shown in **Table 5.4**. We can state: the younger the test population the steeper the slope.

For the quantitative view we show the χ^2-values of all the spectra of the comparison above in **Figure 5.7**. Note that the minima are better defined at younger ages. But the absolute χ^2-values are smaller at older ages, thus the AMD is more pronounced at these ages.

As an illustrative example the spectra of the test population at 2.0 Ga and of the best fit population ($Z = 0.004$) at 3.0 Ga are presented in **Figure 5.8**. At this position in the parameter space a 50 % decrease of the metallicity can be (roughly) compensated by a 50 % increase of the age.

Finally we made the same investigation as above for the integrated colours of the test population. In analogy to Figure 5.6, Table 5.4, and Figure 5.7 we present the best fitting ages in **Figure 5.9**, the corresponding slopes in **Table 5.5**, and the complete sets of χ^2-values in **Figure 5.10**. Generally, the slopes of the AMD are steeper, the minima are less well defined, and the χ^2-values are similar compared to the spectra case.

We conclude for the AMD:

- There is no 100 % degeneracy between age and metallicity in BLoIS spectra, but certain combinations of these parameters can lead to very similar spectra.
- In the age-metallicity plane populations characterized by similar spectra are located at positions that can be approximated by a power law.
- The slope of this power law depends on the place in the parameter space; it can vary from −5 for young to −1 for old populations.

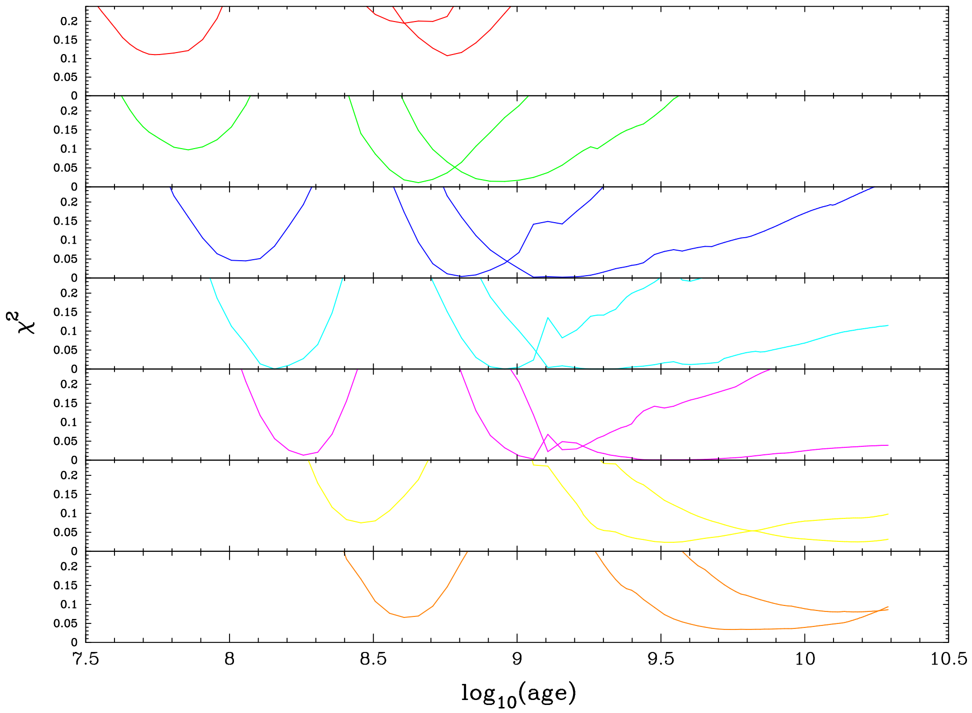

Figure 5.7: Complete sets of χ^2-values from Figure 5.6.

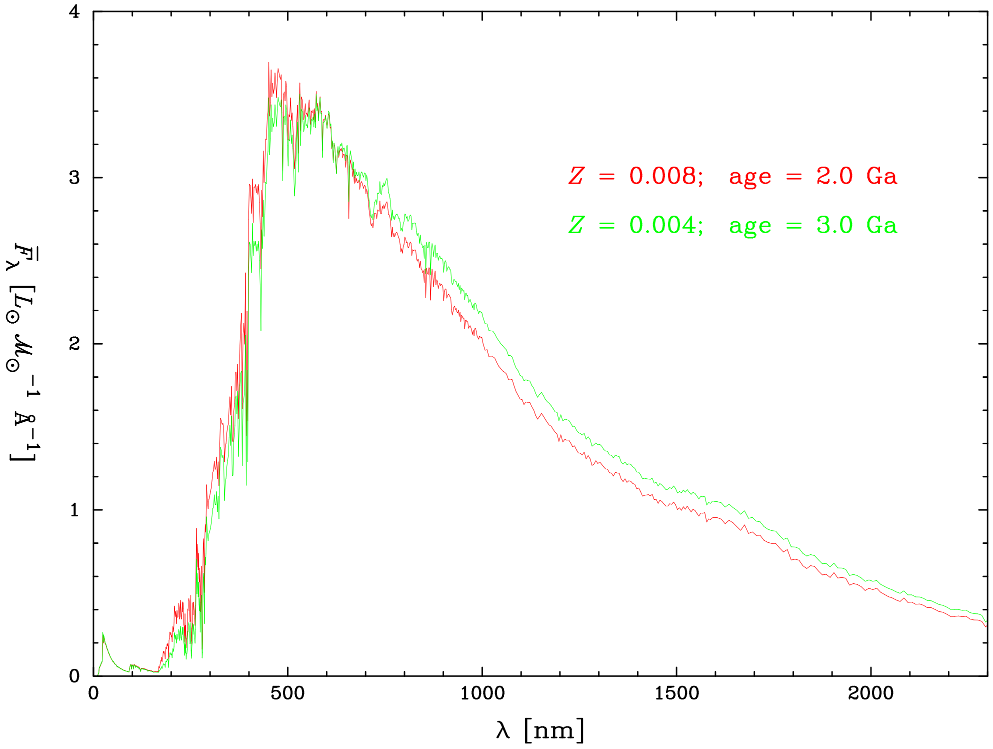

Figure 5.8: Example of the AMD in spectra.

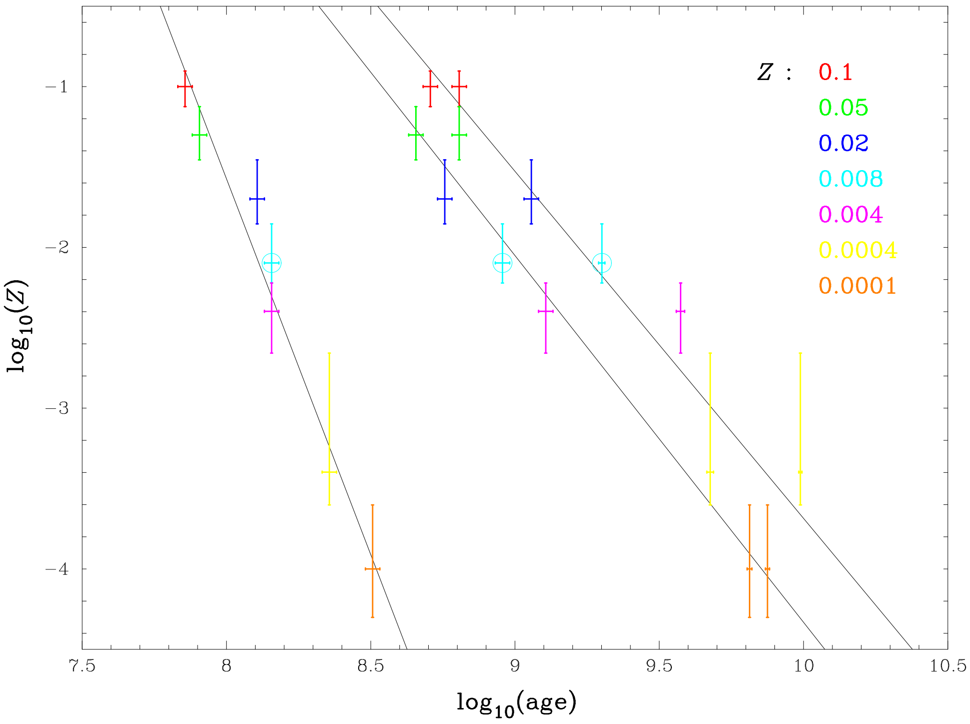

Figure 5.9: The age-metallicity degeneracy for colours (compare Figure 5.6). The 3 ages of the test population ($Z = 0.008$; ages: 0.14, 0.9, 2.0 Ga) are marked with circles. The error bars indicate the age-metallicity grid.

age [Ga]	***s***	***c***
0.14	−4.68	35.84
0.90	−2.28	18.48
2.00	−2.16	17.90

Table 5.5: Estimated AMD parameters according to Equation 5.4 for colours from Figure 5.9.

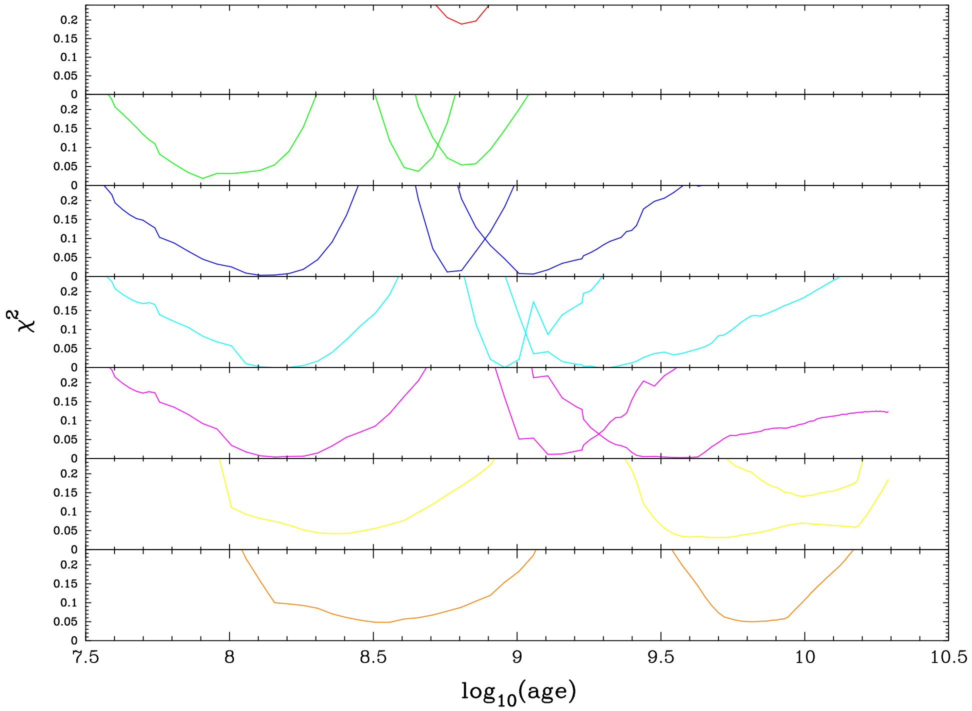

Figure 5.10: Same as Figure 5.7 but for colours.

- At younger ages the χ^2-minima are better defined but larger compared to older ages.
- The AMD looks similar for spectra and colours.

5.3 Deriving Subpopulations

Stellar subpopulations can be defined in different ways. One example is the concept of so-called stellar components of a galaxy such as the bulge or the thin disk. In our approach a subpopulation is defined as an ensemble of stars having all same metallicity (compare Subsection 4.3.2). The idea is that a first generation of stars is born from a molecular cloud with a certain (low) metallicity. From this first generation a second generation with a higher metallicity is born then. Under the assumption of a closed box model for galaxy formation (no infall of gas, no merging, etc.) a subpopulation with a higher metallicity can not appear before a subpopulation with a lower metallicity (see Figure 4.8).

In Subsection 4.3.2 we developed a programme called "SPECSUBPOP" that derives the contribution of subpopulations to the total spectrum by least-squares adjustment techniques. Here we'd like to show an example; we took the normalized low resolution spectra of 7 SSPs (IMF slope $x = 1.35$, IMF mass range $0.1 - 100\ \mathcal{M}_\odot$) at metallicities (Padova 1994) and ages as indicated in **Figure 5.11**. These 7 subpopulations were then summed up according to the following proportionality factors $\boldsymbol{p}$ (see Equations 4.32):

$$\boldsymbol{p} \;=\; (0.1, 0.2, 0.1, 0.2, 0.1, 0.2, 0.1)$$

To recover these input parameters we ran "SPECSUBPOP" with 10 possible ages (the 7 ages chosen for the composed spectrum were amongst those 10 ages). In **Table 5.6** we

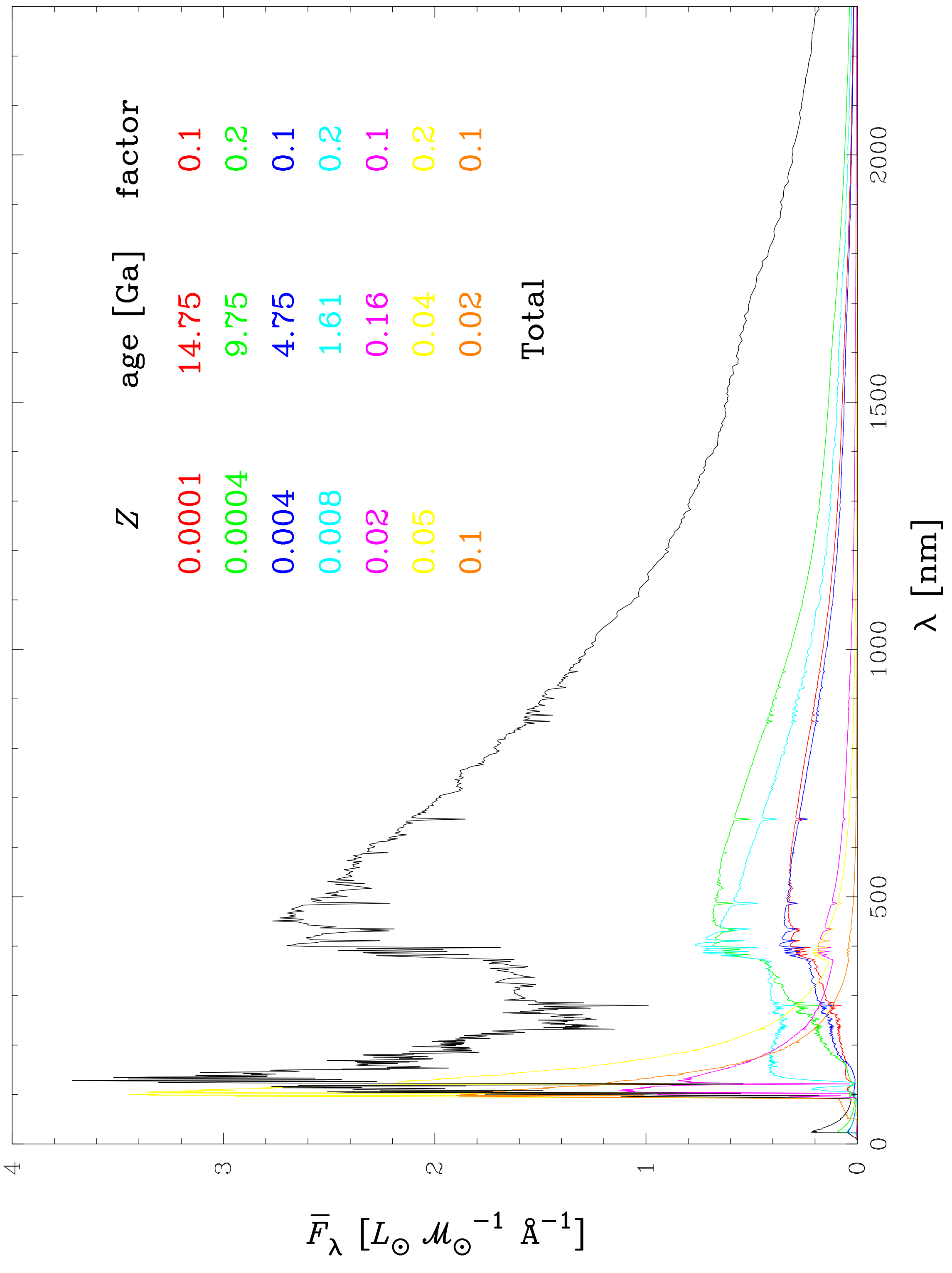

Figure 5.11: The total spectrum composed of 7 normalized subpopulations each at another age, another metallicity, and with different proportionality factors (contributions to the total spectrum).

list the 10 most probable parameter combinations. According to Section 4.2 m_0 is the estimated standard deviation of unit weight (indicating the "goodness of fit" here), p are the proportionality factors, and m_x is the estimated standard deviation of an individual model parameter.

First we can state, that the method developed in Subsection 4.3.2 works because we were able to recover all the proportionality factors correctly and all the standard deviations were zero for the first solution. Moreover we have seen in Subsection 5.1.1 above that all the populations have unique spectra. If we look at the spectra as vectors the condition of linear independence is fulfilled. So the method will work for any other population in BLoIS.

Then we can see in Table 5.6 that there are negative proportionality factors in 4 cases. In the context of deriving subpopulations, these solutions are nonsensical because no population can have a negative contribution to the total spectrum. Thus these solutions have to be rejected. However, a negative factor close to zero could indicate that the corresponding subpopulation does not contribute to the total spectrum. In this case the "negative" population has to be excluded before restarting the programme.

At this point we'd like to mention what happens if a proportionality factor of a subpopulation is set to zero, i.e., if the corresponding subpopulation does not exist: the programme indicates all ages for that population as correct. In analogy to the case with small negative factors just mentioned the corresponding subpopulation must be excluded and the programme has to be restarted.

The 4 youngest subpopulations were all correctly derived in the first 10 solutions. This is due to the fact that the differences amongst older populations are smaller compared to younger populations which can easily be seen in Figure 5.11. As a consequence the values for m_x are smaller at younger ages.

A remarkable result is that for the non rejected solutions the proportionality factors do not scatter a lot. This means that we are able to recover the contributions of the subpopulations quite well, which adds to the statement made in Subsection 4.3.2 that the metallicity characterizes a spectrum in a unique way.

We made the same calculations as above for the integrated colours using the programme "COLSUBPOP". The only differences were that the values for m_0 became smaller (factor ≈ 0.5) and the values for m_x larger (factor ≈ 5). So all the statements made for the spectra case hold true for the colours. Here, we have to repeat the warning made in Subsection 4.3.2: *the programme should use colour magnitudes instead of integrated colours*. But this doesn't matter if we just want to know, whether the method works for 24 colour values (instead of 1 221 flux values).

As a further test of the method we composed a similar spectrum as above using the programme "evochem" from the GISSEL software (see Subsection 2.6, Figure 2.11, and Appendix A). The corresponding input parameters are in **Table 5.7**. Note that the proportionality factors to be recovered can't be set; so all the SFRs are identical. This time we allowed for 20 different ages while running "SPECSUBPOP". The 10 best fit solutions are shown in **Table 5.8**. Although the values for m_0 are quite near to each other, the one with the lowest m_0 has the largest number of correct ages. If we look at the proportionality factors, we can see, that they are not listed in an increasing order. This was not expected because the youngest subpopulation ($Z = 0.1$) should provide the largest contribution to the total spectrum, and the SFR was the same for all subpopulations.

m_0	Z	**age** [Ga]	p	m_x	m_0	Z	**age** [Ga]	p	m_x
0.0000	0.0001	14.75	0.100	0.0000	0.0044	0.0001	9.75	0.085	0.0031
	0.0004	9.75	0.200	0.0000		0.0004	9.75	0.260	0.0031
	0.004	4.75	0.100	0.0000		0.004	1.61	−0.150	0.0027
	0.008	1.61	0.200	0.0000		0.008	1.61	0.396	0.0023
	0.02	0.16	0.100	0.0000		0.02	0.16	0.111	0.0008
	0.05	0.04	0.200	0.0000		0.05	0.04	0.196	0.0010
	0.1	0.02	0.100	0.0000		0.1	0.02	0.102	0.0005
0.0010	0.0001	14.75	0.080	0.0009	0.0051	0.0001	14.75	0.191	0.0043
	0.0004	9.75	0.229	0.0010		0.0004	14.75	0.143	0.0045
	0.004	9.75	0.050	0.0002		0.004	1.61	−0.038	0.0021
	0.008	1.61	0.239	0.0004		0.008	1.61	0.317	0.0021
	0.02	0.16	0.102	0.0002		0.02	0.16	0.080	0.0009
	0.05	0.04	0.200	0.0002		0.05	0.04	0.215	0.0012
	0.1	0.02	0.100	0.0001		0.1	0.02	0.092	0.0006
0.0018	0.0001	9.75	0.053	0.0010	0.0052	0.0001	14.75	0.187	0.0042
	0.0004	9.75	0.234	0.0013		0.0004	14.75	0.128	0.0049
	0.004	4.75	0.141	0.0009		0.004	4.75	0.043	0.0024
	0.008	1.61	0.164	0.0009		0.008	1.61	0.258	0.0025
	0.02	0.16	0.110	0.0003		0.02	0.16	0.079	0.0009
	0.05	0.04	0.194	0.0004		0.05	0.04	0.216	0.0012
	0.1	0.02	0.104	0.0002		0.1	0.02	0.092	0.0006
0.0020	0.0001	9.75	0.034	0.0010	0.0052	0.0001	4.75	−0.144	0.0032
	0.0004	9.75	0.270	0.0013		0.0004	4.75	0.422	0.0042
	0.004	9.75	0.065	0.0004		0.004	4.75	0.217	0.0024
	0.008	1.61	0.223	0.0007		0.008	1.61	0.097	0.0028
	0.02	0.16	0.110	0.0003		0.02	0.16	0.109	0.0009
	0.05	0.04	0.194	0.0004		0.05	0.04	0.198	0.0012
	0.1	0.02	0.103	0.0002		0.1	0.02	0.102	0.0006
0.0029	0.0001	14.75	0.143	0.0025	0.0056	0.0001	14.75	0.174	0.0045
	0.0004	9.75	0.195	0.0026		0.0004	14.75	0.145	0.0052
	0.004	1.61	−0.087	0.0097		0.004	9.75	0.012	0.0012
	0.008	1.61	0.352	0.0008		0.008	1.61	0.282	0.0019
	0.02	0.16	0.095	0.0006		0.02	0.16	0.077	0.0010
	0.05	0.04	0.204	0.0007		0.05	0.04	0.219	0.0012
	0.1	0.02	0.097	0.0003		0.1	0.02	0.090	0.0007

Table 5.6: The 10 most probable solutions for derived subpopulations with the method developed in Subsection 4.3.2 (m_0 estimated standard deviation of unit weight, p proportionality factors, m_x estimated standard deviation of the individual model parameters).

t [Ga]	**SFR** $[\mathcal{M}_\odot/\mathrm{a}]$	Z
5.25	1.0	0.0001
10.25	1.0	0.0004
15.25	1.0	0.004
18.39	1.0	0.008
19.84	1.0	0.02
19.96	1.0	0.05
19.98	1.0	0.1

Table 5.7: Input parameters for the GISSEL programme "evochem".

Nevertheless, we can consider this test as a success, too. As for the first test we can state for the second test that the values for m_0 of the 10 most probable solutions do not show a large scatter and that the results are close to the composed spectrum.

Here are the conclusions for the method of deriving subpopulations:

- The least-squares adjustment method is able to recover the contributions of different model subpopulations correctly.
- The method still succeeds with as less as 24 colour values.
- Care has to be taken with subpopulations of low or no contributions.

5.4 Monte Carlo Simulations

One step towards the comparison of BLoIS to observations is the fitting of model spectra and colours to artificially disturbed model spectra and colours. In this section we'll answer the questions: How high is the probability of finding the correct spectrum depending on the noise level and what are the parameters of the wrong findings? For this we have written versions of "SPECFIT" and "COLFIT" performing Monte Carlo simulation (see Subsection 4.3.1).

First we treat the effects of the accuracy of a measured spectrum on the fitting process. For this we took the low resolution spectrum of the SSP population defined in (5.2), i.e. population 2, at ages 0.1, 2, and 15 Ga to simulate 100 observations per run. As explained in Subsection 4.3.1 we can enter the percentage which corresponds to a relative one sigma error, so we don't simulate the errors but the actual observations by adding noise to the flux values. This percentage p can be transformed to a signal-to-noise value by $\mathrm{S/N} = 100/p$.

In **Figure 5.12** we present the recovery probability calculated from the number of correct recoveries of the "observed" SSP spectrum (e.g., 50 correct recoveries lead to a recovery probability of 0.5) using the programme "SPECFITSIM". Apart from the correct observation (at $Z = 0.008$) the 6 populations with different metallicities (Padova 1994) entered the model matrix, too (see Equation 4.23). Taking more models into account would have been computationally too expensive. The results in Figure 5.12 show again, that older

m_0	Z	age [Ga]	p	m_x	m_0	Z	age [Ga]	p	m_x
0.0073	0.0001	14.75	0.113	0.0060	0.0074	0.0001	14.75	0.259	0.0057
	0.0004	9.75	0.033	0.0057		0.0004	14.75	−0.155	0.0066
	0.004	4.75	0.363	0.0013		0.004	4.75	0.420	0.0021
	0.008	0.51	0.156	0.0030		0.008	0.51	0.088	0.0027
	0.02	0.51	0.071	0.0024		0.02	0.51	0.119	0.0021
	0.05	0.06	0.213	0.0009		0.05	0.06	0.241	0.0007
	0.1	0.02	0.051	0.0004		0.1	0.00	0.027	0.0002
0.0073	0.0001	14.75	0.173	0.0057	0.0075	0.0001	14.75	0.260	0.0058
	0.0004	14.75	−0.033	0.0066		0.0004	14.75	−0.155	0.0067
	0.004	4.75	0.375	0.0021		0.004	4.75	0.420	0.0021
	0.008	0.51	0.144	0.0029		0.008	0.51	0.087	0.0027
	0.02	0.51	0.079	0.0023		0.02	0.51	0.120	0.0022
	0.05	0.06	0.212	0.0009		0.05	0.06	0.241	0.0007
	0.1	0.02	0.050	0.0004		0.1	0.00	0.027	0.0002
0.0073	0.0001	14.75	0.115	0.0064	0.0076	0.0001	14.75	0.260	0.0058
	0.0004	7.25	0.028	0.0055		0.0004	14.75	−0.155	0.0067
	0.004	4.75	0.368	0.0013		0.004	4.75	0.420	0.0021
	0.008	0.51	0.156	0.0032		0.008	0.51	0.088	0.0027
	0.02	0.51	0.070	0.0026		0.02	0.51	0.120	0.0022
	0.05	0.06	0.213	0.0009		0.05	0.06	0.241	0.0007
	0.1	0.02	0.051	0.0004		0.1	0.00	0.027	0.0002
0.0073	0.0001	14.75	0.175	0.0080	0.0076	0.0001	12.25	0.088	0.0057
	0.0004	4.75	−0.025	0.0065		0.0004	9.75	0.046	0.0061
	0.004	4.75	0.361	0.0019		0.004	4.75	0.373	0.0016
	0.008	0.51	0.140	0.0034		0.008	0.51	0.168	0.0029
	0.02	0.51	0.086	0.0033		0.02	0.51	0.059	0.0023
	0.05	0.06	0.219	0.0009		0.05	0.06	0.213	0.0009
	0.1	0.02	0.050	0.0004		0.1	0.02	0.052	0.0004
0.0074	0.0001	14.75	0.140	0.0065	0.0076	0.0001	14.75	0.259	0.0058
	0.0004	12.25	0.006	0.0069		0.0004	14.75	−0.156	0.0067
	0.004	4.75	0.365	0.0018		0.004	4.75	0.421	0.0021
	0.008	0.51	0.149	0.0030		0.008	0.51	0.088	0.0027
	0.02	0.51	0.076	0.0024		0.02	0.51	0.119	0.0022
	0.05	0.06	0.213	0.0008		0.05	0.06	0.241	0.0007
	0.1	0.02	0.051	0.0004		0.1	0.00	0.027	0.0002

Table 5.8: The 10 most probable solutions for derived subpopulations for a spectrum composed by ”evochem” (compare Figure 5.11).

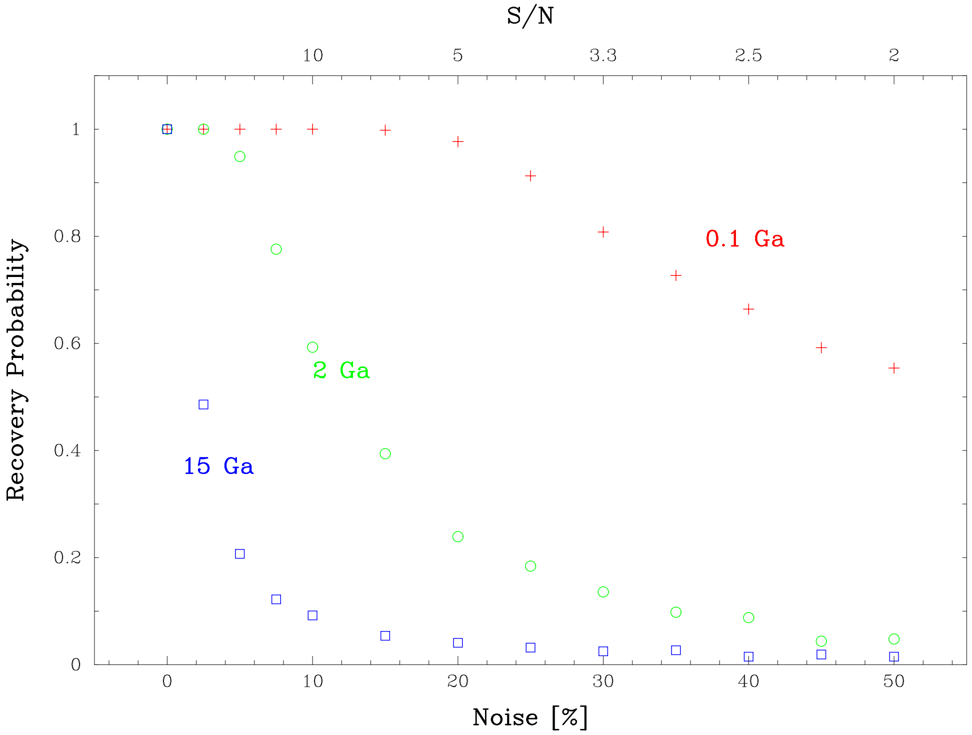

Figure 5.12: Recovery probabilities for SSP spectra. Relative noise has been added to the flux values to simulate 100 observations of the same test spectrum at 3 indicated ages.

populations are harder to distinguish than younger populations, e.g., 10 % noise (S/N = 10) leads to a recovery probability of 1.0 at 0.1 Ga, 0.6 at 2 Ga, and 0.1 at 15 Ga. Although the age spacing for younger populations is narrower compared to older populations (see chapter "The GISSEL User Manual") the spectral evolution is obviously faster at younger ages.

To compare these results with integrated colours we took the same population as above and did the same simulation at the same 3 ages using the programme "COLFITSIM". Here we don't introduce a relative but an absolute one sigma error in magnitudes (see Subsection 4.3.1). In analogy to Figure 5.12 we show the recovery probabilities for the colours in **Figure 5.13**. We can see the same pattern as for the spectra; older populations are harder to distinguish than younger.

In **Figure 5.14** and **Figure 5.15** we show the same investigation just made but for a Composite Stellar Population, i.e., for population 1 from (5.2). If we compare these figures with Figures 5.12 and 5.13, we can state that the recovery probabilities for CSPs are even lower compared to the SSP case. Quite amazing is the fact that the probabilities for the CSP spectrum are higher at 2 than at 0.1 Ga. We can't see this effect while looking at the colours of the CSP. So except for this case, we can confirm that older populations are harder to recover than younger.

Now we want to have a closer look at the incorrect findings and their parameters. A similar investigation (without disturbing the "observation") has been done in Subsection 5.1.2. Here, too, we took population 1 at ages 0.1, 2, and 15 Ga. Then we used the programme "SPECFITSIM", adding 10 % relative noise to the 3 spectra, and performed

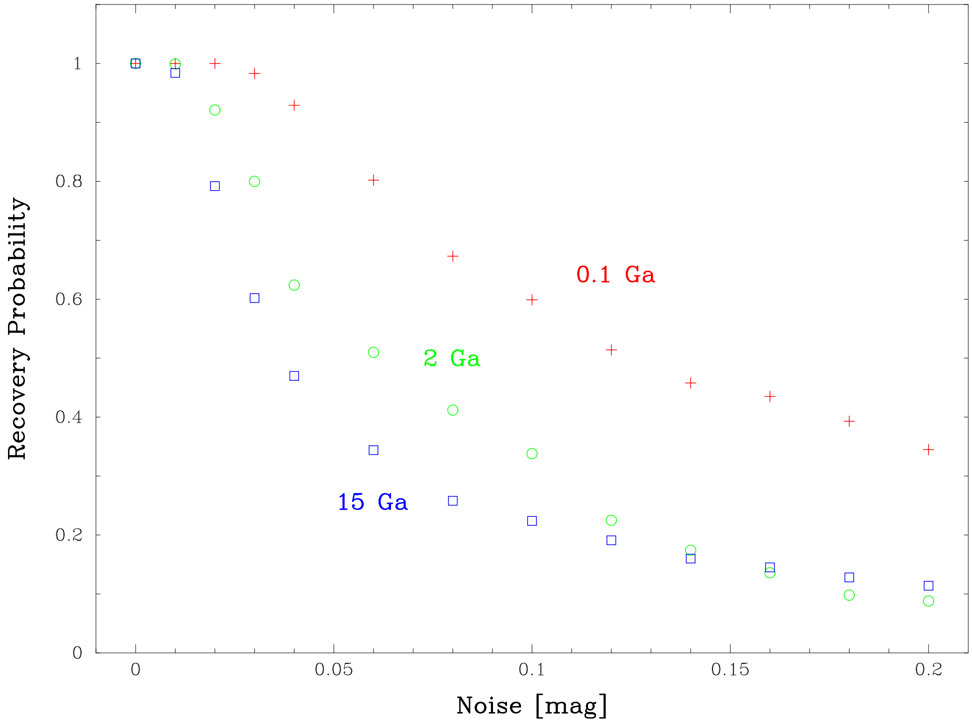

Figure 5.13: Same as Figure 5.12 but for colours. Absolute noise has been added to the colour values.

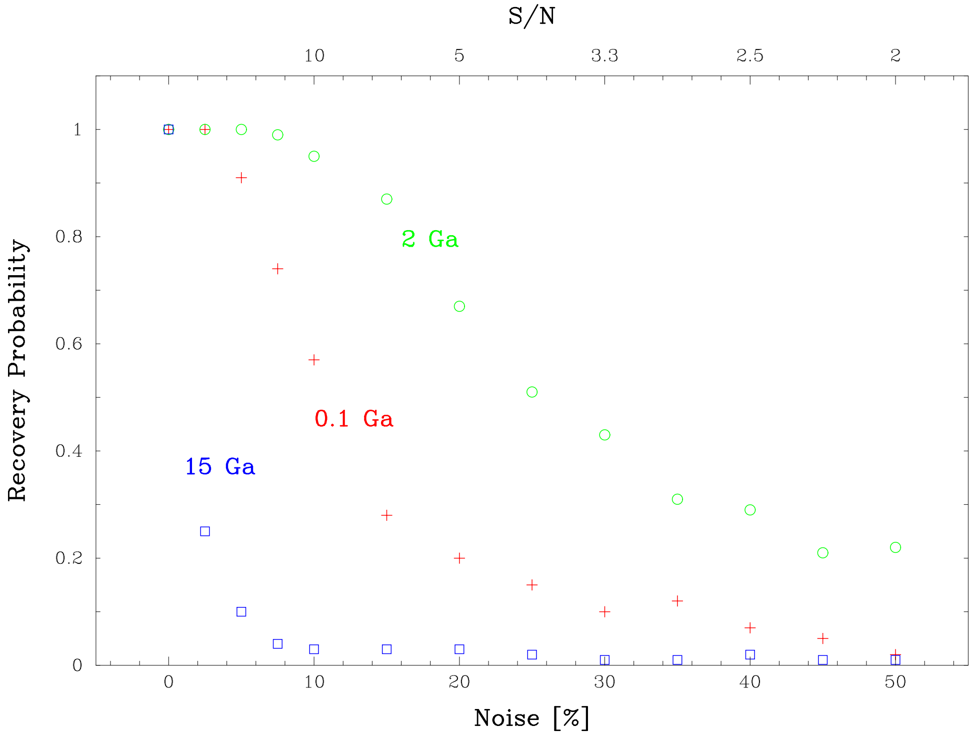

Figure 5.14: Recovery probabilities for CSP spectra (compare Figure 5.12).

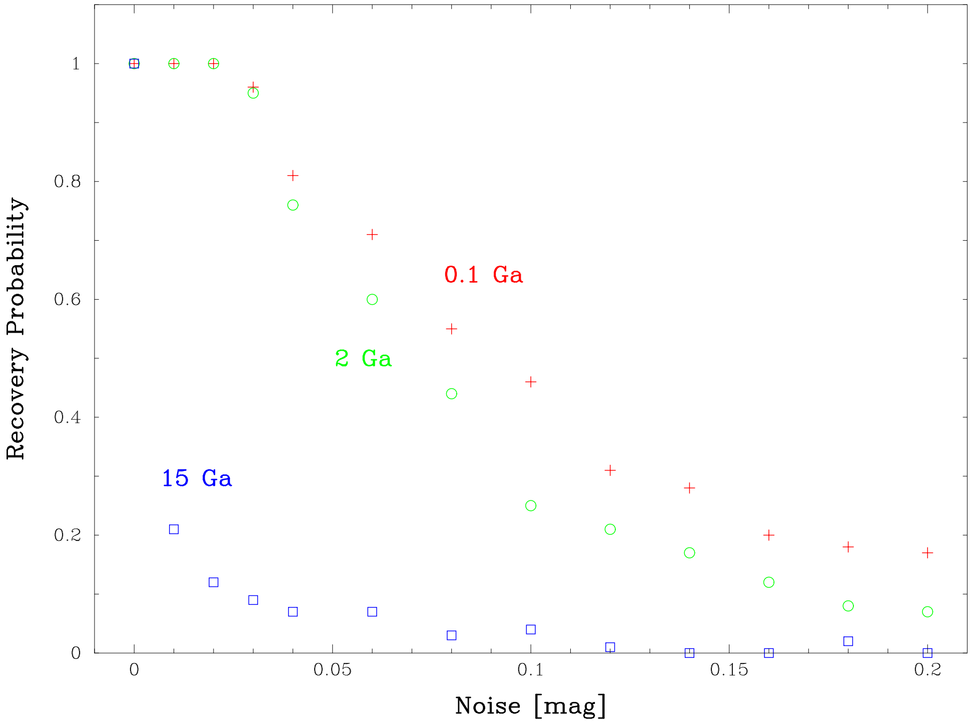

Figure 5.15: Same as Figure 5.14 but for colours (compare Figure 5.13).

100 simulation runs. This time we allowed all the 1 155 model populations. Analogously to Subsection 5.1.2, we then made the statistics of how many times the correct and the incorrect parameters have been found.

The results are shown in **Figure 5.16** for the low resolution case. As we can see in Figure 5.14 the probability of finding the correct population at 2 Ga is more than 0.9. Thus, it's no surprise that for nearly all the 100 simulation runs the 5 parameters have been recovered correctly. The 0.1 Ga spectrum has a peak at 0.15 Ga with a scattering of ± 0.1 Ga. The metallicity is recovered correctly nearly every time, whereas the IMF slope is only correct for about 60 runs. The SFRs are nearly all at the same level, thus badly recovered. The IMF mass range, however, has the most number of best fits at the correct value. The peak for the spectrum at 15 Ga is slightly offset to 14 Ga with a scattering of ± 3 Ga. As for the 0.1 Ga case the metallicity is very well and the IMF slope quite well recovered. The SFR is comparable to the 2 Ga case, whereas the IMF mass range is similar to the 0.1 Ga case.

In **Figure 5.17** we show the results for the high resolution spectra. Compared to Figure 5.16 we can state that there are no substantial differences, except that, in general, the parameters are better recovered.

We did the same investigation just mentioned for the case of integrated colours, with an absolute noise of 0.1 mag. The results are shown in **Figure 5.18**. Over all, we can state that the parameters have been less well recovered compared to the spectra case. At 2 Ga all the parameters peak at the correct value but the scattering is larger compared to the spectra case. The 0.1 Ga colours show a maximum at 0.2 Ga with a scatter of ± 0.2 Ga. All the other parameters, too, never peaked at the correct values. For the colours at 15 Ga the maximum is at 20 Ga. The scattering around the correct value is about ± 5 Ga.

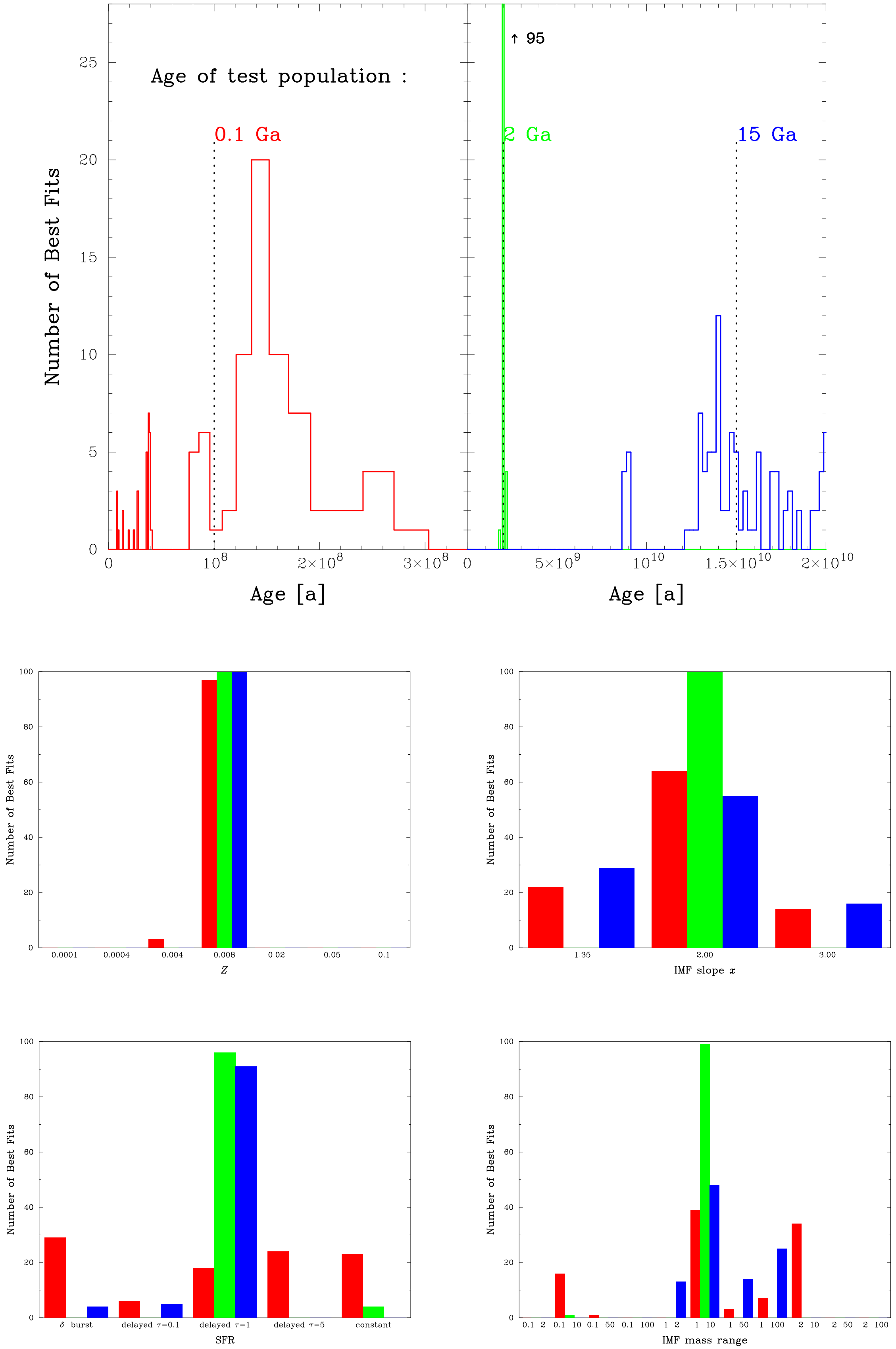

Figure 5.16: Recovery probabilities for low resolution spectra at 0.1, 2, and 15 Ga.

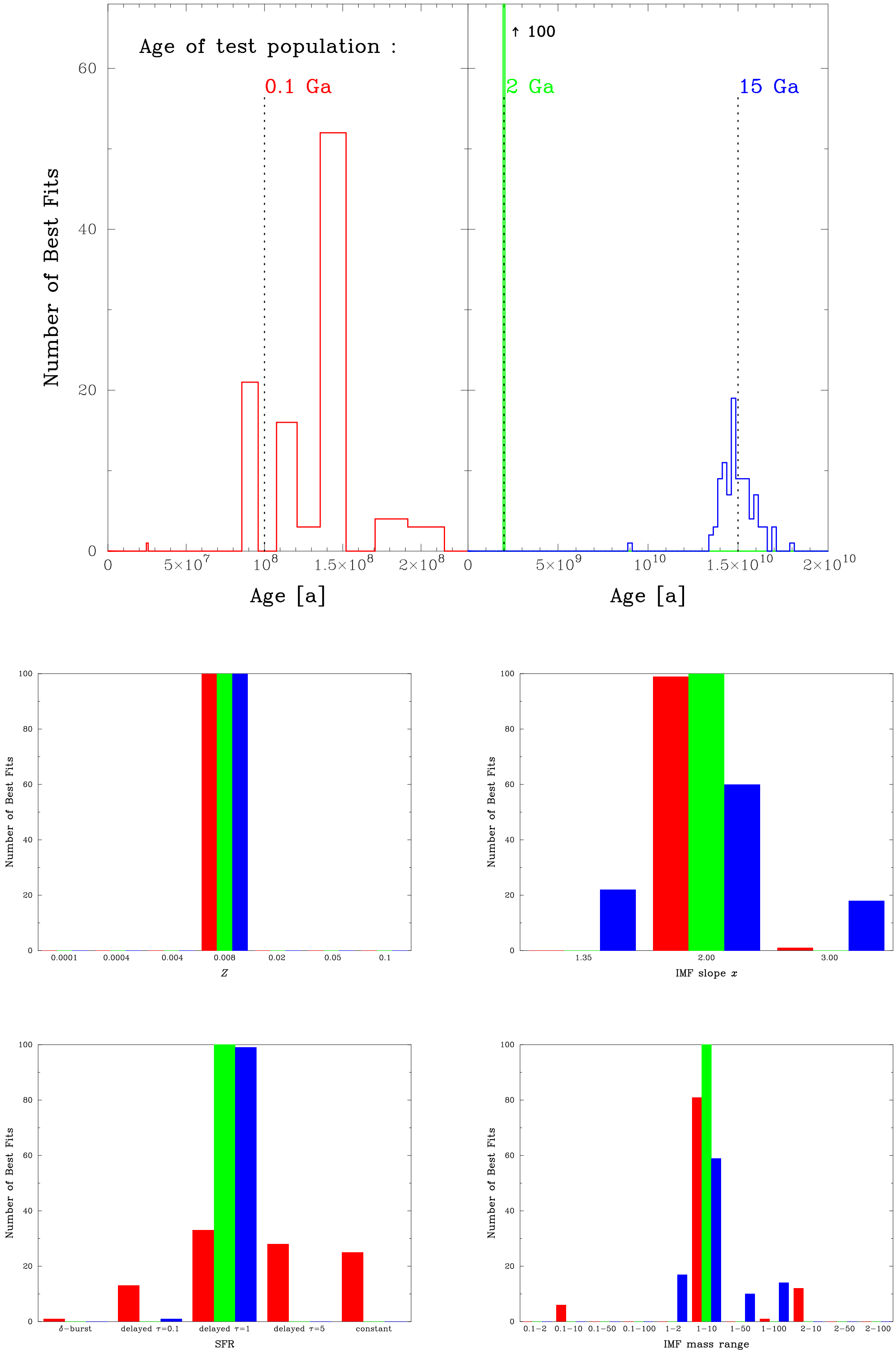

Figure 5.17: Same as Figure 5.16 but for high resolution spectra.

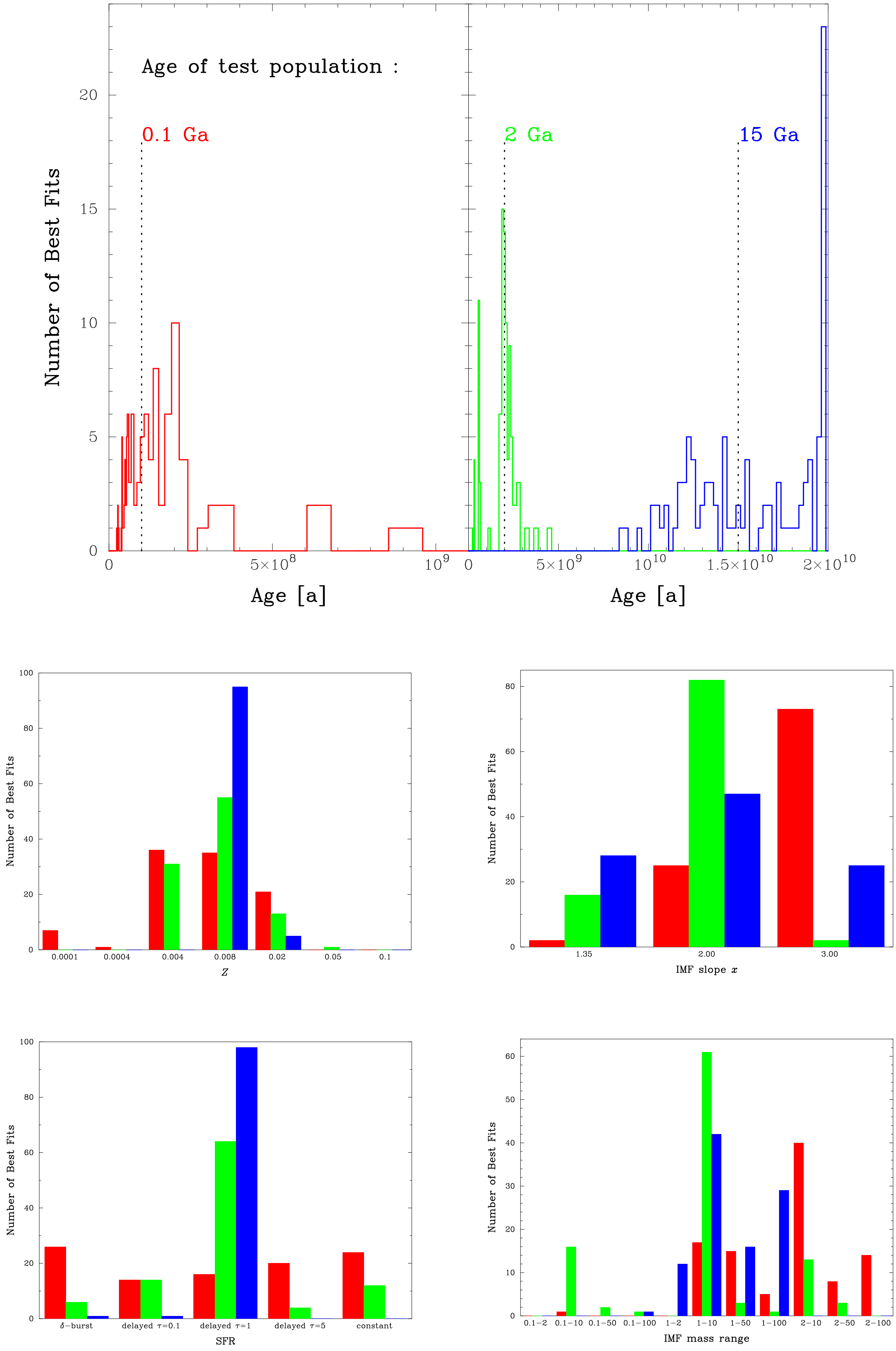

Figure 5.18: Same as Figure 5.16 but for colours.

All the other parameters peaked at the correct values, but (as in general) with a higher scatter compared to the spectra case.

So for the Monte Carlo simulations we can conclude:

- For low resolution SSP spectra and SSP colours younger populations are easier to distinguish than older.
- At intermediate age (2 Ga) low resolution CSP spectra are easier recovered compared to younger (0.1 Ga) and older (15 Ga) ages.
- For CSP colours older populations are harder to distinguish than younger.
- At S/N of 10 for CSP spectra all the parameters can be recovered correctly except for the youngest (0.1 Ga) and the oldest age (15 Ga), and the SFR at young age.
- For CSP colours with a noise level of 0.1 mag the correct values of all the parameters of the youngest population can't be recovered. Except from the age of the oldest population, all the parameters of the intermediate and the old aged population can be recovered correctly.

6 Summary, Conclusions, Outlook

The last chapter is dedicated to the compilation of the results and the discussion. The first goal of this thesis was the study of the effects of the input parameters to the evolutionary synthesis algorithm on the integrated properties. This has been achieved during the establishing of an integrated stellar spectral library called BLoIS. The second goal of this thesis was the analysis of BLoIS, i.e., the treating of the uniqueness of the model populations and their parameter sensitivity, the age-metallicity degeneracy, the deriving of subpopulations from composed model populations, and the constraints on observations by means of Monte Carlo simulations.

Effects of Input Parameters

Between 0 and 2 the slope of the IMF has a very small influence on the integrated spectra and the integrated colours. Slope values higher than 2 do produce differences up to 8 mag in colours. Generally, steeper slopes result in redder colours (see Figure 3.2). The upper mass limit of the IMF affects young populations (< 1 Ga) and the lower mass limit old populations (> 1 Ga). While lower values of the upper mass limit result in redder colours (< 1 mag), higher values of the lower mass limit result in bluer colours (< 2 mag). A two segmented IMF population can be derived by combining a full range IMF with a truncated IMF and a bimodal IMF population by putting together IMFs with different mass limits. Beyond doubt, the IMF is a very important property of a stellar population and many astronomers did make great efforts to derive it from observations, resulting in sophisticated IMFs for different kinds of stellar populations. Thus, one could be disappointed by our findings, i.e. rather meagre effects of slopes < 2 on the integrated properties. This is not to say that observers, using evolutionary synthesis methods, should not take attention to the IMF; if one knows the IMF of an observed population one should use it. Furthermore, our study has shown that the mass range of the IMF is as important as the slope, for the cut-offs of the IMF decide on the distribution of the stars in the different mass bins (compare Figure 3.2 and Figure 3.9). Besides, be aware whether you use linear or logarithmic mass intervals when you deal with the IMF.

The different evolutionary tracks used in this work (Geneva, Padova) have quite small effects: 0.5 mag in colours at maximum (see Figures 3.13 and 3.15). On the one hand side this result sounds very optimistic for consistency reasons. On the other hand one has to be aware that there are still a lot of uncertainties in the calculations of the tracks. The recommendation that the older Padova 1994 tracks should be favoured over the newer

Padova 2000 version only adds to this statement. Furthermore, one wishes some kind of information on the accuracy of the tracks, because it's futile to derive e.g. ages of globular clusters on a sub-Ga level (by isochrone– or spectra fitting), if the tracks are only accurate on a Ga level. Finally, the α-enhancement shouldn't be preset in the tracks but a parameter to choose.

Different stellar spectral libraries, too, have small effects of up to 0.5 mag in colours (see Figures 3.17 and 3.19). Again, the builders of these libraries could be disappointed by this statement. But they are not to be discouraged, for it is not much of a surprise that evolutionary synthesis might "smear out" the fine details of elaborated theoretical stellar spectra.

Synthetic populations with a constant SFR have redder colours (< 5 mag) compared to δ-burst populations. All the other SFR types (short burst of finite length, linearly decreasing, exponentially decreasing, and delayed) have similar effects and all lie between the two cases just mentioned.

Characteristics of BLoIS 1.1

If we compare populations we find that they all have different spectra but can have the same colours for some cases (young, SSPs, or high metallicity). Within one particular population the spectra and the colours can be the same for different ages. The uniqueness of the population spectra shows that the input parameter to the evolutionary synthesis (in order to build up BLoIS) were chosen in such a way that redundancies were avoided. Thus, the grids in the parameter space are not too dense and the library itself it not too large. However, one has to be aware that for some parameter combinations the colours of the populations are not unique. This is of particular interest when we think of the least-squares algorithm for deriving subpopulations, because there, we are not allowed to include identical models in the model matrix. On the other hand we have to mention that we have only investigated the 24 default colours. In principle, any known photometric system can be applied. Since the population spectra are unique, it's quite clear that an increase of the number of colours would lead to a decrease of the ambiguities. Finally, we have to mention that we only compared a set of test populations; there is no guarantee that we have found all the ambiguities.

For high and low resolution spectra the IMF mass range is the most sensitive parameter, whereas for the colours it's the SFR. That's because the sensitivity of the parameters depends on the number of data points (number of flux values, number of colours). But the impact of a change of a certain parameter gets biased if only few data points are influenced by this change, e.g., if a change of an input parameter affects the wavelengths around 1 000 nm we shall not see much of a difference in the colours, because in BLoIS there is no filter in this wavelength region. Furthermore, the result that the IMF mass range is the most sensitive parameter is consistent with the statements made above for the effects of the input parameters. If observers derive the IMF, special care has to be taken on the mass ranges.

Age-Metallicity Degeneracy

There is no 100 % degeneracy between age and metallicity in BLoIS spectra, but certain combinations of these parameters can result in very similar spectra. In the age-metallicity plane the similar populations are located at positions that can be approximated by a power law. The slope of this power law depends on the place in the parameter space and can vary from -5 for young to -1 for old populations. The AMD is more pronounced at older ages and looks similar for spectra and colours. Obviously, the term "degeneracy" is not the adequate expression, because neither observations nor models of stellar populations that belong to different combinations of age and metallicity can be strictly identical. On the other hand insufficient observations or models can lead to this degeneracy. In the literature a rule of thumb for the AMD is found: $\frac{\delta \log(\mathrm{age})}{\delta \log(Z)} = -\frac{3}{2}$. Our work showed that for the populations in BLoIS such values hold true only at old ages. At young ages the slope is considerably steeper.

Deriving Subpopulations

The LSA method to recover the contributions of subpopulations to a composed model spectrum works for all spectra in BLoIS, because they are unique. Attention has to be paid on zero or "negative" contributions. As the differences amongst older populations are smaller compared to younger populations the contributions of the latter are more easily recovered than the ones of the former. This statement holds true for the case of integrated colours. The success of the method might surprise at first glance. But it can easily be explained if one thinks of the spectra or colours as vectors and when you assume that these vectors are all linearly independent. And since all population spectra in BLoIS are unique the method has to work.

Nevertheless, there are some limitations. If we assume a closed box model for a stellar population (no infall, no merging etc.) and if we do not allow a higher metallicity to appear before a lower metallicity, the calculation of the contributions of 7 given subpopulations to a composed low resolution spectrum for 20 given ages still takes about half an hour on a 500 MHz Alpha workstation. Now if one likes to decompose a real population spectrum without knowing anything about the possible subpopulations (metallicities, ages, SFRs, IMFs etc.) it will take quite a lot of CPU time.

Monte Carlo Simulations

Here too, we found that old populations are harder to distinguish than younger populations: e.g. the recovery probability for a 15 Ga SSP spectrum is 10 times smaller than the one for a 0.14 Ga spectrum and about 3 times smaller for the colours. Observers should be aware of the fact that BLoIS hasn't been compiled for the comparison to observations. If one wants to fit observations anyway, make sure to properly calibrate them first (systematic errors included). As observations and model spectra are rarely on the same wavelength grid one has to decide on some kind of resolution reduction (FWHM, Gaussian broadening function, interpolations etc.). Galaxies have to be corrected for velocity dispersion, redshift, and all the different absorptions. And, finally, have a look at the statistical errors, because poor astronomy can be made with, e.g., IUE spectra providing absolute flux values with mean standard deviation of about 30 %. As a matter of fact, for old populations like globular clusters, the probability of dealing with the correct model spectrum is only 0.03. Similar caveats arise for observed colours.

To all of the aspects mentioned for the spectra the problem of the photometric system has to be added. We know e.g. that the original Johnson U filter didn't respect the absorption by the atmosphere of the Earth correctly. Although astronomers use terms like "standard Johnson system" one has to be aware that in practice, matching standard systems is very difficult and that there are at least 4 Johnson photometric systems and 30 different U filters available. The next problem are the errors in colours: in spite of the capability of certain instruments to detect colour differences on a level of 0.01 mag, the absolute error can reach 0.2 mag. For an old population you end up with a probability of 0.1 regardless of whether or not you deal with the correct model colours. For such extreme cases the age dating of globular clusters can deliver values from 1 to 20 Ga.

Future Work

If we build up a library of integrated properties of stellar populations by varying all the input parameters in a systematic way (as we have done for BLoIS), the primary applications lie in the theoretical framework, such as the effect of different SFRs on the spectra. The question of how realistic these models are, belongs to a secondary application and is not treated in this thesis. One necessary step towards realistic model spectra of stellar populations is the development of chemo-dynamical galaxy models (e.g. by Markus Samland) which provide model SFRs and model AMRs and not just analytic functions.

Once we have a realistic library of model populations and we want to compare these to observations, one has to test the method of evolutionary synthesis first. The easiest case would be to focus on a globular cluster where not only the integrated spectrum has been observed but also the spectra of as many individual stars as possible. Then we can synthesize the spectrum and compare it to the observations.

A Publications

A.1 The Age of M3

The following proceeding and the corresponding poster presentation stem from a conference on globular clusters:

New Horizons in Globular Cluster Astronomy
24 – 28 June 2002, Padova, Italy
`http://menhir.pd.astro.it/newhorizons/`
Wenger, E., & Buser, R. 2003, ASP Conference Series, Vol. 296, p. 406

It is to be mentioned that the results in from this publications are not valid anymore. After fixing severe software errors the estimated age of M3 became larger than 16 Ga for the spectrum fit. For lack of consistency with the isochrone fit we have to state that we, too, are not able to decide whether the age of M3 is closer to 12 or to 14 Ga.

New Horizons in Globular Cluster Astronomy
ASP Conference Series, Vol. ???, 2002
Giampaolo Piotto, Georges Meylan, George Djorgovski and Marco Riello, eds.

The Age of M3

Erich Wenger

Astronomisches Institut der Universität Basel, Venusstrasse 7, 4102 Binningen, Switzerland

Roland Buser

Astronomisches Institut der Universität Basel, Venusstrasse 7, 4102 Binningen, Switzerland

Abstract. We used the new BaSeL 3.1 spectral library (WESTERA et al. 2002) along with the latest version of the population synthesis code GISSEL (BRUZUAL & CHARLOT 1993) making use of the Padova 2000 tracks (GIRARDI et al. 2000) to generate theoretical isochrones and spectra. The best fits to the empirical CMD (ROOD et al. 1999) were found at $[\mathrm{Fe/H}] = -1.65$ ($Z = 0.0004$), $E(V - I) = 0.00$, and $(m - M)_V = 15.27$. We derived a most probable age of *12.00* Gyr for the isochrone fit and, for comparison, *12.50* Gyr for the fit to the IUE-spectra.

1. Isochrone Fitting

ROOD et al. (1999) presented a CMD of M3 containing a sample of roughly 37'000 stars measured by the HST. The mean ridge line (MS to TRGB only) is represented by the full line in **Figure 1a**. We calculated two sets of isochrones for $[\mathrm{Fe/H}] = -1.65$ ($Z = 0.0004$) and -1.25 ($Z = 0.001$) using the Ferraro IMF (mass-interval: 0.09 to 125 $M_\odot$). Each set consisted of 25 ages from 10 to 16 Gyr. We interpolated two additional sets of isochrones at $[\mathrm{Fe/H}] = -1.51$ ($Z = 0.00055$) and $[\mathrm{Fe/H}] = -1.41$ ($Z = 0.0007$). To generate the isochrones we used the V and I filters as defined by LANDOLT (1992). The best fitting theoretical isochrone (i.e. at 12.00 Gyr and for $[\mathrm{Fe/H}] = -1.65$) is represented by the dotted line in **Figure 1a**.

2. Spectra Fitting

The empirical spectra were taken from the IUE-archive. Two observations (from 115 to 198 nm and from 185 to 335 nm) were combined and binned to one integrated spectrum which is represented by the full line in **Figure 1b**. In order to generate synthetic spectra we again used the GISSEL code along with the same set of input parameters as we assumed for the calculation of the isochrones. The best fitting synthetic spectrum (i.e. at 12.50 Gyr) is represented by the dotted line in **Figure 1b**.

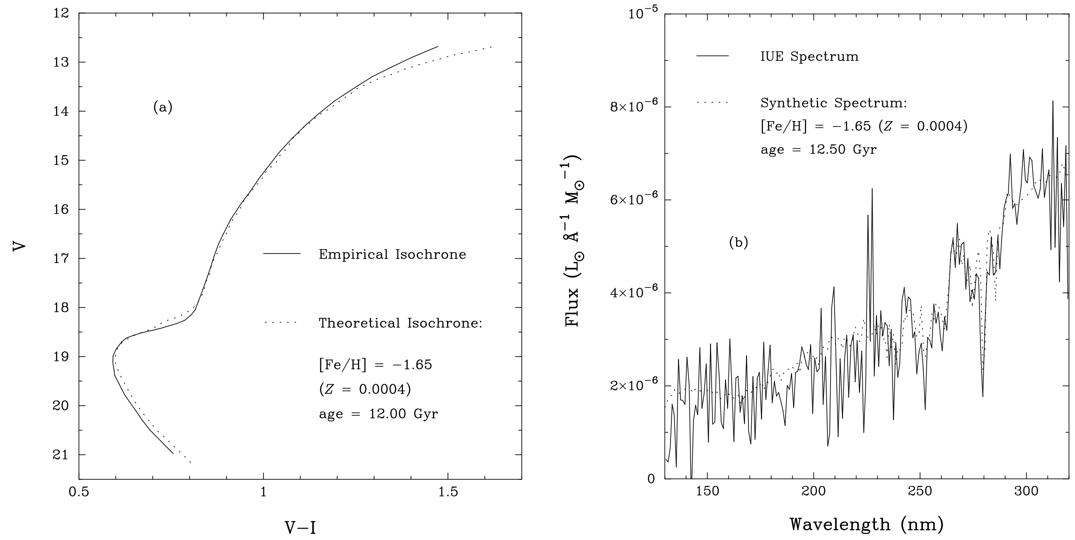

Figure 1. Isochrone Fit (a) and Spectra Fit (b)

3. Conclusions

One big source of uncertainty stems from the assumption of the metallicity. The range of possible values reaches from [Fe/H] = –1.70, ($Z = 0.00036$) to –1.22 ($Z = 0.0011$). Furthermore, the reddening $E(B-V)$ is proposed by different authors from 0.00 to 0.02. Therefore we decided to assume the set of parameters that led to the smallest residuals for the isochrone fit. An extended investigation would consist in respecting other stellar evolutionary phases and in additional observations in other passbands. Nevertheless, our derived age of 12.00 Gyr at [Fe/H] = –1.65 is remarkably consistent with the value of 12.1 Gyr from Salaris & Weiss (2002) calculated at [Fe/H] = –1.66.
Taking only two IUE-observations for the spectra fit represents a data sample of poor value. One would wish to have more observations of the same kind to be combined together. Furthermore, the wavelength-range from 130 to 320 nm is not enough for a meaningful fit.
Due to the relatively good consistency of the two fits we'd like to suggest that *the age of M3 is closer to 12 than to 14 Gyr.*

References

Bruzual, A. G., & Charlot, S. 1993, ApJ, 405, 538

Girardi, L., Bressan, A., Bertelli, G., & Chiosi, C. 2000, A&AS, 141, 371

Landolt, A. U. 1992, AJ, 104, 340

Rood, R. T., Carretta, E., Paltrinieri, B., Ferraro, F. R., Fusi Pecci F., Dorman, B., Chiefi, A., Straniero, O., & Buonanno, R. 1999, ApJ, 523, 752

Salaris, M., & Weiss, A. 2002, A&A, 388, 492

Westera, P., Lejeune, T., Buser, R., Cuisinier, F., & Bruzual, A. G. 2002, A&A, 381, 524

The Age of M3

Fitting isochrones and integrated spectra using the latest BaSeL 3.1 spectral library

Erich Wenger and Roland Buser
Astronomisches Institut der Universität Basel, Switzerland

Abstract

The motivation for this investigation is based on three recent developments: (1) the new BaSeL 3.1 spectral library (Westera et al. 2002), (2) the latest version of the population synthesis code GISSEL (Bruzual & Charlot 1993) using the Padova 2000 tracks (Girardi et al. 2000), and (3) the increasing amount of photometric HST-data of globular clusters. We derived the age of M3 by fitting isochrones to the empirical CMD (Rood et al. 1999) and by fitting integrated IUE-spectra (Rose & Shibing 1999) for comparison. Assuming $E(V-I)=0.02$ two sets of isochrones at [Fe/H] = –1.65 ($Z = 0.0004$) and [Fe/H] = –1.25 ($Z = 0.001$) have been calculated covering the ages from 10 to 16 Gyr. For the same parameter combination we produced two sets of integrated spectra. The results show a most probable age of **12.00** Gyr for the isochrone fit and **12.50** Gyr for the corresponding spectra fit.

Methods

Isochrone fitting

Rood et al. (1999) presented a CMD of M3 containing a sample of roughly 37'000 stars measured by the HST. They transformed these measurements to the standard Johnson V and I system using the Holtzman et al. (1995) recipies. The mean ridge line (MS to TRGB only) is presented in **Figure 1**.

Westera et al. (2002) used the latest Padova stellar evolutionary tracks (Girardi et al. 2000) for a new version of the BaSeL models called the "PADOVA 2000" library. We used the so-called GISSEL code (Galaxy Isochrone Synthesis Spectral Evolution Library) by Bruzual & Charlot (1993) to generate two sets of isochrones for [Fe/H] = –1.65 ($Z = 0.0004$) and –1.25 ($Z = 0.001$) using the Ferraro IMF (mass-interval: 0.09 to 125 $M_\odot$). Each set consisted of 25 ages from 10 to 16 Gyr. We interpolated two additional sets of isochrones at [Fe/H] = –1.51 ($Z = 0.00055$) and [Fe/H] = –1.41 ($Z = 0.0007$). To generate the isochrones we used the V and I filters as defined by Landolt (1983). We adopted a reddening value of $E(B-V) = 0.02$ (Gratton et al. 1999) which is comparable to $E(V-I)$. The comparison of the best fitting calculated isochrones (i.e. at [Fe/H] = –1.65) with the empirical mean ridge line from Rood et al. (1999) is shown in **Figure 1**.

This comparison led to the calculation of residuals which are presented in **Figure 2**. According to the best fit solution at [Fe/H] = –1.65 ($Z = 0.0004$) the most probable age of M3 is **12.00** Gyr.

Figure 1 : Comparison of isochrones

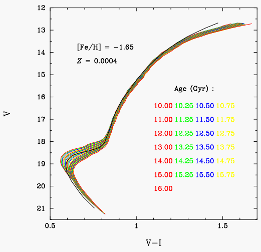

Figure 2 : Residuals of isochrone fit

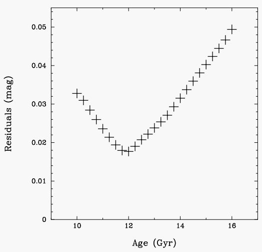

Spectra fitting

The empirical integrated spectral energy distributions (ISEDs) were taken from the IUE-archive (Rose & Shibing 1999). Two observations (from 115 to 198 nm and from 185 to 335 nm) were combined and binned to one integrated spectrum which is shown in **Figure 3**.

In order to generate synthetical ISEDs we again used the GISSEL code along with the same set of input parameters as we assumed for the calculation of the isochrones, i.e. Ferraro-IMF from 0.09 to 125 $M_\odot$, the "PADOVA 2000" stellar SED library, 25 age steps from 10 to 16 Gyr and the metallicity values [Fe/H] = –1.65, –1.51, –1.41 and –1.25 ($Z = 0.0004$, 0.00055, 0.0007 and 0.001). For consistency reasons we present the comparison of the best fitting calculated ISEDs (at [Fe/H] = –1.65, $Z = 0.0004$) with the empirical ISED in **Figure 3**.

Again we calculated the corresponding residuals which are shown in **Figure 4**. Assuming [Fe/H] = –1.65, $Z = 0.0004$ (consistent with the isochrone fit) the most probable age of M3 is **12.50** Gyr.

Figure 3 : Comparison of spectra

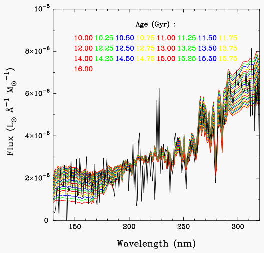

Figure 4 : Residuals of spectra fit

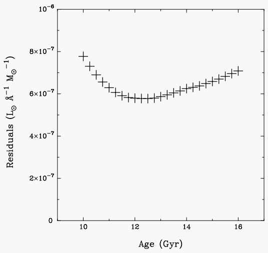

Comments

Isochrone fitting

One of the biggest sources of uncertainty stems from the assumption of the metallicity. The range of possible values reaches from [Fe/H] = –1.70, $Z = 0.00036$ (Buzzoni et al. 1992) to –1.22, $Z = 0.0018$ (Carretta et al. 1997). Furthermore the reddening $E(B-V)$ is proposed by different authors from 0.00 to 0.02. Keeping in mind these uncertainties, we decided to assume the set of parameters that led to the smallest residuals for the isochrone fit.

A more careful investigation would consist in the assumption of many different combinations of parameters and in additional observations in other passbands. This extended search would also lead to the determination of an age range instead of just one most probable value.

Our derived age of 12.00 Gyr at [Fe/H] = –1.65 ($Z = 0.0004$) is in good agreement with the value of 12.1 Gyr from Salaris & Weiss (2002) calculated at a metallicity of [Fe/H] = –1.66 based on Zinn & West (1984).

Spectra fitting

The spectra fit at [Fe/H] = –1.41 ($Z = 0.0007$) resulted in slightly smaller residuals than for [Fe/H] = –1.65 ($Z = 0.0004$), leading to an age of 12.25 Gyr instead of 12.50 Gyr. But for consistency reasons we assumed the same metallicity for both fits.

Taking only two IUE-observations for the spectra fit represents a data sample of poor value. One would wish to have more observations of the same kind to be combined together. Furthermore, the wavelength-range from 130 to 320 nm is not enough for a meaningful fit. Clearly, spectra covering all the important wavelengths are needed. In spite of the poor data the age of 12.25 Gyr is even closer to the value of 12.1 Gyr derived by Salaris & Weiss (2002).

Due to the relatively good consistency of the two fits at [Fe/H] = –1.65 ($Z = 0.0004$) we'd like to suggest that **the age of M3 is closer to 12 than to 14 Gyr**.

References

Bruzual A. G., & Charlot, S. 1993, ApJ, **405**, 538
Buzzoni A., Cacciari C., Fusi Pecci F., Buonanno R., & Corsi C. E. 1992, A&A, **254**, 110
Carretta E., & Gratton R. G. 1997, A&AS, **121**, 95
Girardi L., Bressan A., Bertelli G., & Chiosi C. 2000, A&AS, **141**, 371
Gratton R. G., Fusi Pecci F., Carretta E., Clementini G., Corsi C. E., & Lattanzi M. 1997, ApJ, **491**, 749
Holtzman A. J., Burrows C. J., Casertano S., Hester J., Trauger J. T., & Watson A. M. 1995, PASP, **107**, 1065
Landolt A. U. 1983, AJ, **88**, 439
Rood R. T., Carretta E., Paltrinieri B., Ferraro F. R., Fusi Pecci F., & Dorman B. 1999, ApJ, **523**, 752
Rose J. A., & Shibing D. 1999, AJ, **117**, 2213 R
Salaris M., & Weiss A. 2002, A&A, **388**, 492
Westera P., Lejeune T., Buser R., Cuisinier F., & Bruzual A. G. 2002, A&A, **381**, 524
Zinn R., & West M. J. 1984, ApJS, **55**, 45

A.2 BLoIS: The Basel Library of Integrated Spectra

The following poster presentation was created for a conference on stellar populations:

Stellar Populations 2003
6 – 10 October 2003, Garching, Germany
`http://www.mpa-garching.mpg.de/stelpops/`

Here, too, we have to state, that the contents of this poster does not represent the latest status of the library. The current version incorporates 1 155 populations containing both low and high resolution spectra. These populations are characterized by 5 different SFRs, 3 different IMF slopes, and 11 different IMF mass ranges (see Section 3.4). Besides, one should not use the "Padova 2000" version of the stellar library BaSeL 3.1 anymore (Pieter Westera, private communication). Furthermore, several incapabilities lead to severe data loss. Thus, none of the 15 generated galaxy models of Markus Samland could be implemented in BLoIS.

BLoIS: The Basel Library of Integrated Spectra

The first version of a theoretical library of integrated properties of stellar populations

Erich Wenger • Astronomical Institute • University of Basel • Switzerland

Abstract

We compiled an extensive library of integrated stellar population properties based on the BaSeL stellar libraries (LEJEUNE et al. 1997, WESTERA et al. 2002), the evolutionary synthesis code GISSEL (BRUZUAL & CHARLOT 2003), and the latest chemodynamical galaxy models (SAMLAND 2003). It has been designed for theoretical studies (such as the age-metallicity-degeneracy) as well as for comparison to observations. The first version contains 504 Single Stellar Populations (SSPs), each consisting of integrated spectra for 221 ages between 0 and 20 Ga. We chose 14 different IMFs, varied in slope and shape, as well as 7 different metallicities between $Z = 0.0001$ and 0.1 (corresponding to the Padova 1994 evolutionary tracks). All SSPs for BLoIS 1.0 were created using the latest theoretical BaSeL 3.1 ("Padova 2000") stellar library. Furthermore, 5'544 Composite Stellar Populations (CSPs) were calculated with 3 different types of SFRs and the same 7 metallicities as for the SSPs. The IMF however was not varied. Finally, we generated 1'080 CSPs incorporating not only the SFR but also the chemical evolution as derived from chemodynamical galaxy models by Samland. Apart from the integrated spectra, the library also provides 18 integrated colours, 31 indices, and 23 other properties for each stellar population and for each of the 221 timesteps. BLoIS 1.0 contains 7'128 stellar populations and roughly 1.6 Mio. spectra. It will be made available to the public: **www.astro.unibas.ch/forschung/projects.shtml**

Ingredients

Evolutionary Synthesis

We used the 2003 version of the evolutionary synthesis code GISSEL (Galaxy Isochrone Synthesis Spectral Evolution Library) by BRUZUAL & CHARLOT (2003). As shown in the scheme below, stellar spectra are added up corresponding to the loci of the stars on the theoretical HRD and weighted by the IMF. Once these Simple Stellar Populations are generated one can convolve them with an SFR to get Composite Stellar Populations. Finally, we can account for the chemical evolution by adding up CSPs with different SFRs and metallicities.

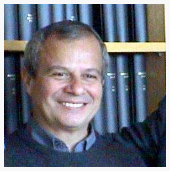

Evolutionary Tracks

Stellar evolutionary codes provide theoretical evolutionary tracks. In the Bruzual & Charlot code the following 3 track types are implemented: Padova 1994, Padova 2000 (GIRARDI et al. 2000), and Geneva 1992 (SCHALLER et al. 2000). These tracks were completed with post-AGB evolution by Bruzual & Charlot. From the tracks we can derive theoretical isochrones which are used for evolutionary synthesis. For BLoIS we selected the Padova 1994 tracks because of their large range in metallicity and their good match to observed galaxy colours.

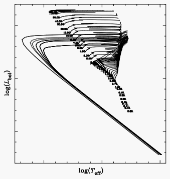

Stellar Spectral Libraries

The Basel group generated stellar spectral libraries called BaSeL (Basel Spectral Energy Distribution Library). LEJEUNE et al. (1997) compiled the first purely theoretical version and the second semi-empirical (colour-calibrated) version, whereas WESTERA et al. (2002) contributed the third semi-empirical (metallicity-calibrated) version. Basically, the theoretical stellar spectra are adjusted to match empirical colours. The next step will be to incorporate empirical high-resolution spectra from the 2003 version of the Bruzual & Charlot code into BLoIS.

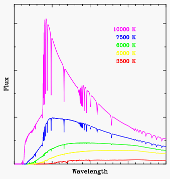

Initial Mass Function IMF

Salpeter was the first to derive an "original mass function" in 1955. Various authors then derived IMFs for various stellar populations. In the GISSEL code 9 different IMFs for solar neighborhood stars, globular culsters, and irregular galaxies are implemented. Soon, 3 more IMFs will be available, including a universal and a present-day IMF. In addition one can enter an arbitrary IMF shape and slope. As far as the evolutionary synthesis code is concerned, the IMF is a time-independent analytical function.

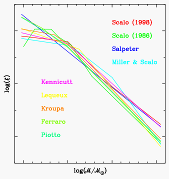

Star Formation Rate SFR

As shown in the panel below, 5 different types of SFRs can be chosen in the Bruzual & Charlot code: an exponentially decreasing, a single burst of finite length (constant first, then dropping instantaneously to zero), a constant, a delayed, and a linearly decreasing SFR. We should mention that the SFR is treated as an analytical function which enters the evolutionary synthesis as an input property. Therefore, it does not contain any physics. Like an arbitrary IMF, one can also apply an arbitrary SFR, thus providing the means to include realistic SFRs.

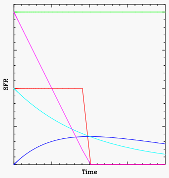

Chemodynamical Evolution

Because the GISSEL code does not account for the chemical evolution of a stellar population in a self-consistent way, we used the chemodynamical galaxy models by SAMLAND (2003). There, the galactic evolution is simulated with a new three-dimensional code, including dark matter, stars, and a multi-phase ISM. These models provide realistic SFRs and realistic age-metallicity-relations, instead of just analytical functions. Of course, the SFR can be calculated not only for the whole population but for each wanted metallicity bin.

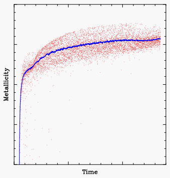

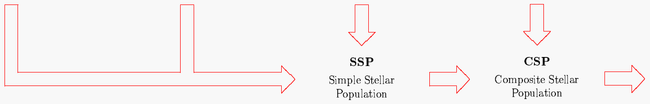

Principle of Evolutionary Synthesis:

SSP
Simple Stellar Population

CSP
Composite Stellar Population

CSP^{++}
Composite Stellar Population^{++}

Properties

General

One population contains 221 spectra between 0 and 20 Ga, whereas one spectrum comes at a resolution of 20 Å (1221 flux values between 91 Å and 160 μm) and 3 Å for the future high-resolution spectra. For each spectrum there are 18 integrated colours, 31 line indices, and 23 other integrated properties.

SSP

We generated 504 SSPs with 3 IMF slopes (1.35, 3.00, and 4.00), 6 upper IMF mass limits (125, 25, 20, 10, 5, and 2 $\mathcal{M}_\odot$), 4 lower IMF mass limits (0.09, 0.8, 1.0, and 2.0 $\mathcal{M}_\odot$), and the Padova 1994 evolutionary tracks at 7 metallicities ($Z = 0.0001 - 0.1$) using the latest theoretical stellar spectral library BaSeL 3.1.

CSP

For the 5'544 CSPs, we have calculated the same general properties as for the SSPs. As far as the SFR is concerned, we took a constant, 5 exponentially decreasing, and 5 bursts of finite length with e-folding time and burst duration time, respectively, of 0.1, 0.5, 1.0, 2.0, and 5.0 Ga.

CSP^{++}

Finally we generated 1'080 CSPs^{++} using 15 different evolution histories, i.e. mean SFR(t) and mean $Z(t)$, by Samland. For these populations we have again calculated the same properties as for the SSPs and the CSPs, except that the timesteps can increase from 221 ages up to several hundreds, depending on the SFR.

Application

Below we can see a chemodynamical galaxy model at age 13.5 Ga provided by Samland, first with all stars of all metallicities and then separated to the 7 stellar subpopulations corresponding to the 7 indicated metallicity ranges. One can clearly recognize the contributions of the different subpopulations, suggesting that *a mean SFR and a mean age-metallicity-relation can't be appropriate enough for a realistic galaxy model.* Furthermore, we can spot the dominance of the stellar subpopulation of roughly solar metallicity and the lack of high metallicity stars for this particular galaxy model.

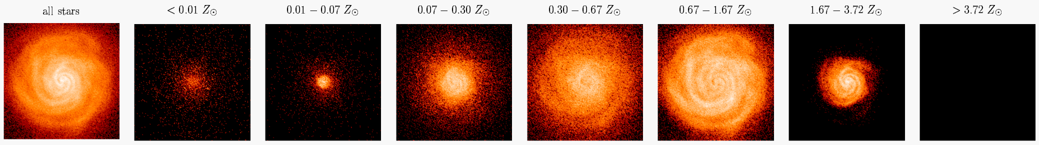
all stars | $< 0.01\ Z_\odot$ | $0.01 - 0.07\ Z_\odot$ | $0.07 - 0.30\ Z_\odot$ | $0.30 - 0.67\ Z_\odot$ | $0.67 - 1.67\ Z_\odot$ | $1.67 - 3.72\ Z_\odot$ | $> 3.72\ Z_\odot$

References

Bruzual A. G., & Charlot, S. 2003, MNRAS, **344**, 1000 B
Girardi L., Bressan A., Bertelli G., & Chiosi C. 2000, A&AS, **141**, 371
Lejeune T., Cuisinier F., & Buser R. 1997, A&AS, **130**, 65
Samland M. 2003, Ap&SS, **284**, 841 S
Schaller G., Schaerer D., Meynet G., & Maeder A. 1992, A&AS, **96**, 269
Westera P., Lejeune T., Buser R., et al. 2002, A&A, **381**, 524

GISSEL User Manual

In our research group many persons made individual contributions. It became necessary to merge all of this on a separate computer account called ”stellarpop”. The following manual does not only contain the description of the GISSEL software by Gustavo Bruzual and Stéphane Charlot but all the other programmes our research group has implemented. Note that the main focus of the manual is on the handling of the programmes and not on the physics. The idea was to ease the initial effort of beginners.

Bibliography

Bruzual, A. G., & Charlot, S. 1993, ApJ, **405**, 538

Bruzual, A. G., & Charlot, S. 2003, MNRAS, **344**, 1000 B

Bruzual, A. G., & Kron, R., G. 1980, ApJ, **241**, 25 B

Buser, R., & Kurucz, R. L. 1992, A&A, **264**, 557

Buzzoni, A. 1990, ApJS, **71**, 817

Chabrier, G. 2001, ApJ, **554**, 1274

Charlot, S., & Bruzual A. G. 1991, ApJ, **367**, 126

Faber, S. M. 1972, A&A, **20**, 361

Ferraro, F. R., Carretta, E., Bragaglia, A., Renzini, A., Ortolani, S. MNRAS, **286**, 1012

Girardi, L., Bressan, A., Chiosi, C., Bertelli, G., Nasi, E. 1996, A&AS, **117**, 113

Kennicutt, R. C. 1983, ApJ, **272**, 54

Kim, Y.-C., Demarque, P., Yi, S., Alexander, D. R. 2002, ApJ S. S., **143**, 499

Kroupa, P. 2001, MNRAS, **322**, 231

Lejeune, T. 1997, Contribution à la synthèse spectrale évolutive d'amas et de galaxies par calibration de bibliothèques stallaires, Ph.D. Thesis, Univ. Strasbourg & Univ. Basel, 334 pp.

Le Borgne, J.-F., Bruzual, A. G., Pelló, R., Lançon, A., Rocca-Volmerange, B., Sanahuja, B., Schaerrer, D., Soubiran, C., Vilichez-Gómez, R. 2003, A&A, **420**, 433

Lejeune, T., Cuisinier, F., Buser, R. 1997, A&A S. S., **125**, 229

Lejeune, T., Cuisinier, F., Buser, R. 1998, A&A S. S., **130**, 65

Lequeux, J. 1979, A&A, **80**, 35

Miller, G. E., & Scalo, J. M. 1979, ApJ S. S., **41**, 513

O'Connell, R. W. 1976, ApJ, **206**, 370

Pickles, A. J. 1998, PASP, **110**, 863

Piotto, G., Cool, A. M., King, I. R. 1997, AJ, **113**, 1345 P

Pritchet, C. 1977, ApJS, **35**, 397

Renzini, A. 1981, AnnPhysFr, **6**, 87

Renzini, A., & Buzzoni, A. 1983, MSAI, **54**, 739

Salpeter, E. E. 1955, ApJ, **121**, 161

Samland, M. 2003, Ap&SS, **284**, 841 S

Sandage, A. 1986, A&A, **161**, 89 S

Scalo, J. M. 1986, IAUS, **116**, 451 S

Scalo, J. M. 1998, ASP Conf. Ser. 142, The Stellar Initial Mass Function (38th Herstmonceux Conference), ed. G. Gilmore & D. Howell (San Francisco: ASP), 201

Schaller, G., Schaerer, D., Meynet, G., Maeder, A. 1992, A&AS, **96**, 269

Spinrad, H., & Taylor, B. J. 1971, ApJS, **22**, 445

Turnrose, B. E. 1976, ApJ, **210**, 33

Westera, P. 2001, The BaSeL 3.1 models: Metallicity calibration of a theoretical stellar spectral library and its application to chemo-dynamical galaxy models, Ph.D. Thesis, Univ. of Basel, 378 pp.

Westera, P., Lejeune, T., Buser, R., Cuisinier, F., Bruzual, A. G. 2002, A&A, **318**, 524

Declaration

I declare that I wrote the thesis "On Spectra and Colours of Synthetic Stellar Populations" with the help indicated and only handed it in to the Faculty of Sciences of the University of Basel and to no other faculty and no other university.

Erich Wenger

Curriculum Vitae

Name:	Erich Wenger
Date of Birth:	2. 9. 1969
Native Place:	Blumenstein BE
Professors:	Prof. Dr. Bruno Binggeli, Prof. Dr. Roland Buser, Prof. Dr. Ortwin Gerhard, Prof. Dr. Eva Grebel, Prof. Dr. Andreas Tammann

1976–1980	Primary School (Hilterfingen BE)
1980–1985	Secondary School (Hünibach BE)
1985–1989	Grammar School (Literargymnasium Bern-Kirchenfeld)
1989–1990	Military Service
1990–1999	Diploma Studies (Astronomical Institute, University of Berne) Courses: Astronomy (main), Physics, Mathematics, and Computer-Science Diploma Thesis: "Weitwinkel-Astrometrie von langsam bewegten Objekten mittels CCD-Mosaik-Aufnahmen" Supervisor: Prof. Dr. Gerhard Beutler
1996–1998	Auxiliary Assistant (Astronomical Institute, University of Berne)
1996–1999	Night Assistant at the Laser- and Astrometry Observatory of Zimmerwald BE (Federal Office of Topography, Wabern BE)
1999	Assistant (Astronomical Institute, University of Berne)
1999	Civil Service
1999–2002	Postgraduate Studies for Grammar School Teacher in Physics (Department of Pedagogy and Didactics, University of Berne)
2000–2005	Doctorate Studies (Astronomical Institute, University of Basel) Supervisor: Prof. Dr. Roland Buser
2004–	Postgraduate Studies in Philosophy (Institute of Philosophy, University of Berne)

Acknowledgements

I'm in debted to the members of the Astronomical Institute of Basel; all of them did help me in one way or the other.

Thanks to Gustavo Bruzual: together with Stéphane Charlot he transformed all the knowledge of evolutionary synthesis into running programmes. These are the tools my thesis is based on.

As far as stellar spectral libraries are concerned, François Cuisinier, Thibault Lejeune, and Pieter Westera contributed a lot to the knowledge just mentioned. Special thanks to Piet for explaining all the programmes and for the experiments out of office.

Markus Samland gave major impulses for the analysis methods and algorithms. I'm also grateful for his coaching and the reading of the manuscript.

Last but not least I'd like to thank my doctoral advisor Roland Buser for giving me the opportunity to write this dissertation, for employing me as an assistant of the Swiss Science Foundation, and for lots of discussions both astronomical and non-astronomical.